UNIVERSIDADE FEDERAL DO RIO GRANDE DO SUL
ESCOLA DE ENGENHARIA
PROGRAMA DE PÓS-GRADUAÇÃO EM ENGENHARIA ELÉTRICA

**JOÃO EDUARDO COSTA GOMES**

# CONTRIBUTIONS TO THE AVERAGE ATTITUDE CONTROL OF NANOSATELLITES

Porto Alegre
2023

**JOÃO EDUARDO COSTA GOMES**

# CONTRIBUTIONS TO THE AVERAGE ATTITUDE CONTROL OF NANOSATELLITES

Master thesis presented to Programa de Pós-Graduação em Engenharia Elétrica of Universidade Federal do Rio Grande do Sul in partial fulfillment of the requirements for the degree of Master in Electrical Engineering.
Area: Control and Automation

ADVISOR: Prof. PhD. Aurélio Tergolina Salton

CO-ADVISOR: Prof. Dr. Daniel Coutinho

Porto Alegre
2023

**JOÃO EDUARDO COSTA GOMES**

# CONTRIBUTIONS TO THE AVERAGE ATTITUDE CONTROL OF NANOSATELLITES

This master thesis was considered adequate for obtaining the degree of Master in Electrical Engineering and approved in its final form by the Advisor and the Examination Committee.

Advisor: _____
Prof. PhD. Aurélio Tergolina Salton, UFRGS
Doutor pela Universidade de Newcastle - Newcastle, Australia

Examination Committee:

Prof. Dr. João Manoel Gomes da Silva Jr., UFRGS
PhD from Université Paul Sabatier – Toulouse, France

Prof. Dr. Renato Alves Borges, UnB
PhD from Universidade Estadual de Campinas – Campinas, Brazil

Prof. Dr. Rafael da Silveira Castro, PUCRS
PhD from Universidade Federal do Rio Grande do Sul – Porto Alegre, Brazil

Coordinator of PPGEE: _____
Prof. Dr. Sérgio Luís Haffner

Porto Alegre, May 2023.

# DEDICATION

To my parents, for their love and support, and to Dudi, for being awesome.

# RESUMO

Este trabalho apresenta contribuições no contexto do método de controle médio para o controle de atitude ativa de nanossatélites através do uso de magnetorquers. Os principais conceitos, restrições e limitações devido ao uso desses atuadores são apresentados. Em seguida, com base em um trabalho anterior empregando um ganho adaptativo, uma lei de controle nova, não adaptativa é proposta para diminuir o consumo de energia do sistema como um todo sem perda de estabilidade. Garantias teóricas referentes às fronteiras das trajetórias do sistema de malha fechada são apresentadas por meio do método de controle médio - aplicado a regiões pré-estabelecidas - e teoria de estabilidade de Lyapunov. Diferentes resultados de simulação ilustram a eficácia da abordagem proposta para alcançar a atitude desejada para diferentes configurações de satélite. Uma comparação entre a nova abordagem com a estratégia adaptativa anterior disponível na literatura indica que uma economia considerável de energia pode ser alcançada, com valores chegando a 70 % para alguns casos. A saturação do sinal de controle é considerada em alguns dos cenários simulados, mas não mitigada.

**Palavras-chave: Controle de atitude, Representação por quaternion, Teoria média, Não-linear.**

# ABSTRACT

This work presents contributions with the average control method for the active attitude control of nano-satellites through the use of magnetorquers. Key concepts, constraints, and limitations due to the use of these actuators are presented. Then, based on a previous work employing an adaptive gain, a novel non-adaptive control law is proposed in order to decrease the energy consumption of the overall system without loss of stability. Theoretical guarantees regarding the ultimate bound of closed loop system trajectories are presented through the average method - applied on pre-established regions - and Lyapunov stability theory. Different simulation results illustrate the effectiveness of the proposed approach to achieve the desired attitude for different satellite configurations. A comparison between the new approach to the previous adaptive strategy available in the literature indicates that a considerable energy economy could be reached, with values reaching 70% for some cases. Control signal saturation is considered in some of the simulated scenarios but not mitigated.

**Keywords: Attitude Control, Quaternion representation, Average Theory, Non-linear.**

# LIST OF FIGURES


Figure 1 – Illustration of the frames. . . . . 16
Figure 2 – Earth's magnetic field for a circular Polar orbit at 450 km according with (1). . . . . 17
Figure 3 – Earth's magnetic field for a circular Polar orbit at 450 km according with (4). . . . . 19
Figure 4 – Representation of the axis-angle rotation. . . . . 20
Figure 5 – Representation of cross product between magnetic field $B(t)$ and magnetic moment $m(t)$. . . . . 25
Figure 6 – Illustration of a function saturation at 1. . . . . 26
Figure 7 – Magnetic field $B_r(t)$ seen at the reference using the Dipole model. . . 32
Figure 8 – Magnetic field $B_r(t)$ seen at the reference using the IGRF model. . . 33
Figure 9 – Eigenvalues of $\Gamma_{av}(t)$ for satellite at the reference and using Dipole model. . . . . 34
Figure 10 – Error Quaternion - Upside Down initial condition with Dipole model 42
Figure 11 – Angular Velocity error - Upside Down initial condition with Dipole model . . . . . 43
Figure 12 – Energy used by controllers normalized - Upside Down initial condition with Dipole model . . . . . 43
Figure 13 – Magnetoquer use for Adaptive gain - Upside Down initial condition with Dipole model . . . . . 44
Figure 14 – Magnetoquer use for Fixed gain - Upside Down initial condition with Dipole model . . . . . 44
Figure 15 – Error Quaternion - Upside Down initial condition with IGRF model . 45
Figure 16 – Angular Velocity error - Upside Down initial condition with IGRF model . . . . . 45
Figure 17 – Energy used by controllers normalized - Upside Down initial condition with IGRF model . . . . . 46
Figure 18 – Magnetoquer use for Adaptive gain - Upside Down initial condition with IGRF model . . . . . 47
Figure 19 – Magnetoquer use for Fixed gain - Upside Down initial condition with IGRF model . . . . . 47
Figure 20 – Error Quaternion - Random initial condition with Dipole model . . . 48
Figure 21 – Angular Velocity error - Random initial condition with Dipole model 48
Figure 22 – Energy used by controllers normalized - Random initial condition with Dipole model . . . . . 49
Figure 23 – Magnetoquer use for Adaptive gain - Random initial condition with Dipole model . . . . . 50

Figure 24 – Magnetoquer use for Fixed gain - Random initial condition with Dipole model . . . . . 50
Figure 25 – Error Quaternion - Random initial condition with IGRF model . . . . 51
Figure 26 – Angular Velocity error - Random initial condition with IGRF model . 51
Figure 27 – Energy used by controllers normalized - Random initial condition with IGRF model . . . . . 52
Figure 28 – Magnetoquer use for Adaptive gain - Random initial condition with IGRF model . . . . . 52
Figure 29 – Magnetoquer use for Fixed gain - Random initial condition with IGRF model . . . . . 53
Figure 30 – Error Quaternion - Upside Down initial condition - 2U CubeSat . . . 54
Figure 31 – Angular velocity error - Upside Down initial condition - 2U CubeSat 55
Figure 32 – Energy used - Upside Down initial condition - 2U CubeSat . . . . . 55
Figure 33 – Magnetoquer use for Weak gain - Upside Down initial condition - 2U CubeSat . . . . . 56
Figure 34 – Magnetoquer use for Strong gain - Upside Down initial condition - 2U CubeSat . . . . . 56
Figure 35 – Error Quaternion - Random initial condition - 2U CubeSat . . . . . 57
Figure 36 – Angular velocity error - Random initial condition - 2U CubeSat . . . 57
Figure 37 – Energy used - Random initial condition - 2U CubeSat . . . . . 58
Figure 38 – Magnetoquer use for Weak gain - Random initial condition - 2U CubeSat . . . . . 58
Figure 39 – Magnetoquer use for Strong gain - Random initial condition - 2U CubeSat . . . . . 59
Figure 40 – Error Quaternion - Upside Down initial condition - 1U CubeSat . . . 61
Figure 41 – Angular velocity error - Upside Down initial condition - 1U CubeSat 61
Figure 42 – Energy used - Upside Down initial condition - 1U CubeSat . . . . . 62
Figure 43 – Magnetoquer use for Weak gain - Upside Down initial condition - 1U CubeSat . . . . . 62
Figure 44 – Magnetoquer use for Strong gain - Upside Down initial condition - 1U CubeSat . . . . . 63
Figure 45 – Error Quaternion - Random initial condition - 1U CubeSat . . . . . 63
Figure 46 – Angular velocity error - Random initial condition - 1U CubeSat . . . 64
Figure 47 – Energy used - Random initial condition - 1U CubeSat . . . . . 64
Figure 48 – Magnetoquer use for Weak gain - Random initial condition - 1U CubeSat . . . . . 65
Figure 49 – Magnetoquer use for Strong gain - Random initial condition - 1U CubeSat . . . . . 65

# LIST OF TABLES


Table 1 – Satellite's initial conditions - Upside Down initial condition. . . . . 41
Table 2 – Satellite's initial conditions - Random initial condition. . . . . 41
Table 3 – Energy used by controllers normalized - Upside Down initial condition with Dipole model . . . . . 43
Table 4 – Energy used by controllers normalized - Upside Down initial condition with IGRF model . . . . . 46
Table 5 – Energy used by controllers normalized - Random initial condition with Dipole model . . . . . 49
Table 6 – Energy used by controllers normalized - Random initial condition with IGRF model . . . . . 52
Table 7 – [Controller parameters - 2U CubeSat]Controller parameters - 2U CubeSat. 54
Table 8 – Energy used on 2U CubeSat - Upside Down initial condition . . . . . 55
Table 9 – Energy used on 2U CubeSat - Random initial condition . . . . . 58
Table 10 – Controller parameters - 1U CubeSat. . . . . 60
Table 11 – Energy used on 1U CubeSat - Upside Down initial condition . . . . . 62
Table 12 – Energy used on 1U CubeSat - Random initial condition . . . . . 65

# LIST OF ABBREVIATIONS

| | |
|---|---|
| IAGA | International Association of Geomagnetism and Aeronomy |
| IGRF | International Geomagnetic Reference Field |
| LEO | Low Earth Orbit |
| PPGEE | Programa de Pós-Graduação em Engenharia Elétrica |
| UFRGS | Universidade Federal do Rio Grande do Sul |
| UFSC | Universidade Federal de Santa Catarina |

# LIST OF SYMBOLS

| | |
|---|---|
| $J$ | Inertia matrix of the satellite |
| $\mathbb{B}$ | Earth's magnetic field |
| $B$ | Earth's magnetic field seen by the satellite |
| $B_r$ | Earth's magnetic field seen at the reference |
| $q$ | Error quaternion |
| $\eta$ | Scalar component of error quaternion |
| $\epsilon$ | Vector component of error quaternion |
| $q_b$ | Satellite quaternion |
| $\eta_b$ | Scalar component of satellite quaternion |
| $\epsilon_b$ | Vector component of satellite quaternion |
| $q_r$ | Reference quaternion |
| $\eta_r$ | Scalar component of reference quaternion |
| $\epsilon_r$ | Vector component of reference quaternion |
| $R$ | Attitude matrix for error quaternion |
| $R_b$ | Attitude matrix for satellite's quaternion |
| $\omega$ | Angular velocity error |
| $\omega_b$ | Angular velocity of the satellite |
| $\omega_r$ | Angular velocity of reference |
| $\omega_o$ | Angular velocity of the orbit |
| $S(\cdot)$ | Skew symmetric matrix |
| $i_m$ | Inclination of the orbit with respect to the geomagnetic equator. |
| $m$ | Magnetic moment |
| $\tau$ | Torque |
| $\bar{\Gamma}$ | Fixed gain matrix |
| $\Gamma_{av}$ | Average gain matrix |

# CONTENTS


**1 INTRODUCTION** . . . . . 12

**2 INSTRUMENTAL TOOLS** . . . . . 15
**2.1 Coordinates** . . . . . 15
**2.2 Earth magnetic field** . . . . . 16
**2.3 Quaternions** . . . . . 20
**2.4 Inertia Matrix** . . . . . 22
**2.5 Magnetorquers dynamics** . . . . . 24
**2.6 Saturation** . . . . . 25
**2.7 Attitude dynamics** . . . . . 26
**2.8 Reference dynamics** . . . . . 27
**2.9 Error dynamics** . . . . . 28
**2.10 Average system** . . . . . 28

**3 SYSTEM CONTROL** . . . . . 30
**3.1 Problem definition** . . . . . 30
**3.2 Adaptive Control Law** . . . . . 32
**3.3 Proposed Control Law** . . . . . 35

**4 NUMERICAL RESULTS** . . . . . 40
**4.1 Controllers comparison** . . . . . 40
**4.2 Fixed controller performance on CubeSats** . . . . . 53

**5 CONCLUSIONS** . . . . . 66

**REFERENCES** . . . . . 68

**APPENDIX A VECTOR MANIPULATION** . . . . . 72

**APPENDIX B MATLAB CODES** . . . . . 75

**APPENDIX C FUTURE PERSPECTIVES** . . . . . 86

# 1 INTRODUCTION

Space has caught humans' imagination and curiosity for centuries but the shift from observation to exploration only started about 70 years ago, with the Soviet satellite Sputnik. Since the beginning of space exploration, the task to send objects to orbit has always been constrained by weight: the bigger (and heavier) the object, the more expensive it is to take it off Earth. For many years, only a few powerful nations had the resources to design, build, launch, and operate spacecraft, the most significant examples being the United States and the former Soviet Union. Considering this restriction, mini, micro, and nanosatellites have become useful platforms for low-orbit scientific research (NASA, 2023), in particular with the very popular CubeSat platform (BOMANI, 2021). Due to their reduced size, these satellites have restrictions regarding batteries, sensors, and actuators. All these limitations can reflect directly on their mission lifetime and successful rate, with a great number of projects lasting only a few months (PANG *et al.*, 2016; MURCIA PIñEROS; DOS SANTOS; PRADO, 2020).

The original idea for CubeSats came in 1999, with professors Jordi Puig-Suari, from California State Polytechnic University and Bob Twiggs, from Stanford University, and aimed to facilitate the design, construction, testing, and operation of satellites with capabilities similar to the pioneer Sputnik by university students (BOMANI, 2021).

The first CubeSat measured 10 cm × 10 cm × 10 cm (JOHNSTONE, 2022) and weighed about 1 kg. These measurements are considered the standard reference for later projects, characterizing a CubeSat basic unit (1U). Projects with different dimensions such as 2U (10 cm x 10 cm x 20 cm), 3U (10 cm x 10 cm x 30 cm) and even 0.5U (10 cm x 10 cm x 2.8 cm) have been successfully developed already. These measurements put CubeSats among Pico (between 0.01 and 1 kilogram) and Nano (between 1 and 10 kilograms) satellite classes, deployed between 500 km and 1,500 km, at Low Earth Orbit (LEO).

The total number of CubeSat-like projects that have been started so far has surpassed 2,000, including Brazilian models such as the NANOSATC-BR (SCHUCH *et al.*, 2019), the AlfaCrux (BORGES *et al.*, 2022) and the FloripaSat-I satellite (MARCELINO *et al.*, 2020). Due to their small dimensions, CubeSats have limited sensor and actuator capa-

bilities, so their attitude control needs to be optimized. Some models choose for passive controls, involving magnets or gravitational gradients to achieve the desired attitude. FloripaSat-I is an example of a standard 1U dimension CubeSat nanosatellite designed with passive attitude control. Passive attitude systems can achieve good results but they are unable to act in any unforeseen attitude correction. On these occasions, only active attitude control can act.

Despite the dimension and sensor restrictions, active attitude control of nanosatellites can be implemented. Among the possible actuator types that can be used, one should mention plasma jet thrusters (RAYBURN *et al.*, 2000; LING *et al.*, 2020; YANG *et al.*, 2023), reaction wheels (SINCLAIR; GRANT; ZEE, 2007; KASIRI; SABERI, 2019; HELMY; HAFEZ; ASHRY, 2022), radiometric actuators (NALLAPU; TALLAPRAGADA; THANGAVELAUTHAM, 2017), magnetorquers (TORCZYNSKI; AMINI; MASSIONI, 2010; JOVANOVIC *et al.*, 2021), and even solar sails (RUKHAIYAR *et al.*, 2021). Among these, magnetorquers are a common choice for LEO applications due to their fixed, compact structures and the stronger influence of Earth's magnetic field. They are powered by batteries (that can be recharged in flight, through solar panels), allowing their activation several times (if necessary). However, the same power source is shared between the actuators and other equipment in the satellite, making energy usage distribution an important aspect of the mission.

Furthermore, magnetorquers also depend on Earth's magnetic field acting on the satellite, which becomes a challenge on its own. Earth's magnetic field varies according to several factors such as the orbit's altitude, path, and time of the year (ALKEN; THéBAULT; BEGGAN, 2021). Studies about the magnetic field and its characteristics have been conducted for several years, even before the beginning of space exploration. Despite its complexity, there exists a variety of models for Earth's magnetic field which can be used to simulate and assess different systems and models (National Centers for Environmental Information (NCEI), 2023). These magnetic field models are more accurate and are updated frequently, making them very useful to estimate the magnetic influence in LEO spacecraft.

This work seeks to design an active attitude control for a CubeSat-type nanosatellite by means of magnetorquers. The control law proposed uses values of the magnetic field at the expected orbit to establish a fixed gain. This fixed approach aims to reduce onboard calculations and reduce energy consumption when compared to the adaptive approach proposed by (LOVERA; ASTOLFI, 2006) while maintaining the stability of the system.

This work evaluates the satellite model and attitude control developed through simulations in the software MATLAB. Even though the space environment where nanosatellites operate has plenty of disturbances, none was considered for this work. These disturbances should be considered in the development of a real attitude control system. Restrictions on control input (specifically saturation of the magnetorquer action) were considered for

some, but not all, simulations. The satellite dimensions used in this work were taken from the literature to better compare the results and assess the viability of the proposed approach. No practical model has been developed.

After this introduction, the dissertation presents the following structure. Chapter 2 presents the necessary concepts used to determine the attitude of a nanosatellite with regard to an inertial frame fixed on Earth. It also presents the basic operation of magnetorquers and their physical restrictions while operating in orbit. Two models for Earth's magnetic field are described, along with their characteristics. The chapter ends with the concepts of stability of average systems.

Chapter 3 defines the attitude control problem and introduces the different active attitude control approaches. The first approach was presented in (LOVERA; ASTOLFI, 2006) and its operations are shown here. The second approach is an original contribution, aimed toward a reduction of energy consumption and complexity of the active system, without the loss of stability and viable to work in LEO assuming that all the parameters of the reference trajectory are known *a priori*.

After that, chapter 4 brings the results obtained through simulation. Initially, the different controllers are evaluated for the same satellite model, in two different attitude initial conditions. Even though this first model is larger than a CubeSat satellite, it was chosen in order to better compare the results of the proposed controller against the adaptive gain controller. For each initial condition, two Earth's magnetic field models were used: a simpler model to verify the controller approach and a more complex one to assess the controller performance. After that, the fixed gain controller is tested using CubeSat dimensions models and actuators, in these same attitude initial conditions. Comparison, analysis, and discussions of all the results are done here.

Chapter 5 concludes this work with a summary of the results and an assessment of what was accomplished. Ideas for future perspectives are suggested. The codes used for the simulations, as well as the bases for a novel (switched-based) attitude control law with some preliminary results, are presented in the appendices.

# 2 INSTRUMENTAL TOOLS

Prior to developing any attitude control for satellites, it is necessary to establish some concepts regarding attitude representation; satellite configuration and dynamics; actuator configuration and dynamics; magnetic field models; and average theory. In this section, the main concepts related to designing and simulating attitude control approaches are presented.

## 2.1 Coordinates

In order to better describe the positioning and orientation of an orbiting satellite with respect to the Earth, it is necessary to establish some coordinate systems. For this work, 3 coordinate systems were determined: one fixed at the center of the Earth, one positioned in orbit and set as the desired orientation (reference), and one fixed in the satellite‘s center of mass. Figure 1 illustrates all three coordinate frames being used.

### 2.1.1 *Earth-Centered Inertial Frame ($\mathcal{F}_i$)*

The first coordinate system to be determined consists of a cartesian coordinate system whose origin coincides with the center of the Earth. The $X_i$ axis is tangent to the Earth's orbit around the Sun, in the same direction as the translation. The $Z_i$ axis points to the geographic north pole and the $Y_i$ axis is positioned on the ecliptic plane, pointing towards the Sun at the vernal equinox, so that the axes form an orthogonal coordinate system by the right-hand rule. The vernal equinox is the moment when Earth's rotation axis is directly perpendicular to the Sun-Earth line, tilting neither toward nor away from the Sun.

### 2.1.2 *Reference Frame ($\mathcal{F}_r$)*

The second coordinate system is placed at the satellite's center of mass, with its axes positioned according to a desired orientation, and following the right-hand rule. Generally, the Local Vertical/Local Horizontal configuration is used. For this configuration the $X_r$ axis is chosen as being tangent to the satellite's orbit around the Earth, with the same translational direction. The $Z_r$ axis points to the center of the Earth, in a direction

Figure 1 – Illustration of the frames.

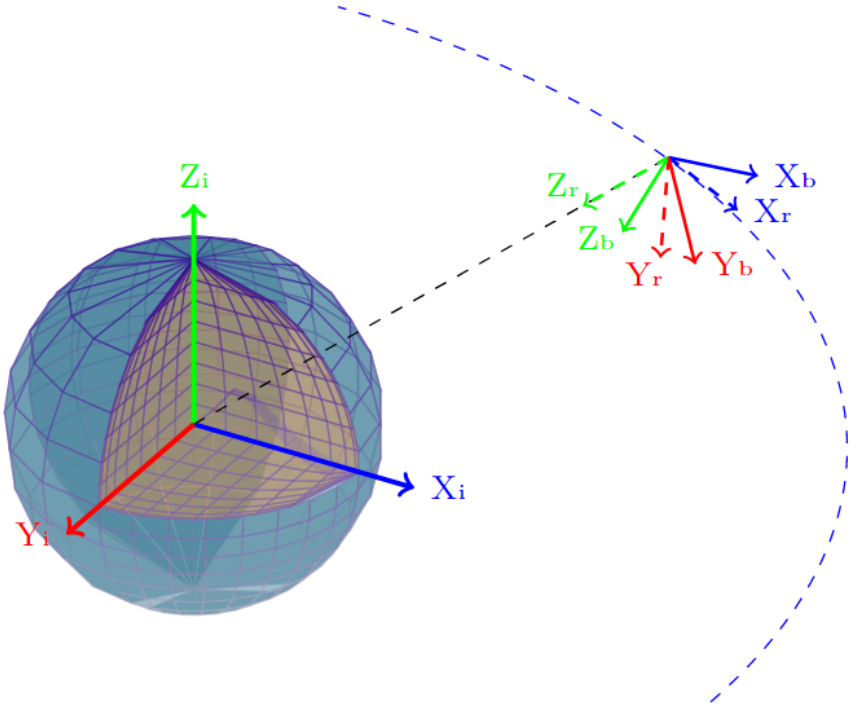


Source: The author.

called *nadir*, and the $Y_r$ axis completes the coordinate system by the right-hand rule. The *Reference* frame establishes the ideal position and orientation (reference) for the satellite, so it is often determined according to the *Satellite Body Frame* ($\mathcal{F}_b$) and the mission's objectives. The quaternion $q_r$ will describe this orientation with respect to $\mathcal{F}_i$.

### 2.1.3 *Satellite Body Frame* ($\mathcal{F}_b$)

The third coordinate system is positioned at the satellite's center of mass and chosen according to the satellite geometry. It is positioned on the satellite structure so that the satellite faces are in the desired position when the coordinate axes coincide with the coordinate axes of the *Reference Frame* ($\mathcal{F}_r$). A common choice during the project phase is to choose the *Satellite Body Frame*($\mathcal{F}_b$) as the principal axes.

## 2.2 Earth magnetic field

The magnetic field of Earth $\mathbb{B}$ varies according to some parameters including the altitude, latitude, longitude, and even the day on which it is measured. When considering an XYZ frame, oriented like the *Earth-Centered Inertial Frame* ($\mathcal{F}_i$), the magnetic field $\mathbb{B}$ can be described by a three-dimensional vector field, with its value decomposed into components on each axis. There are several models to estimate its value, varying its complexity and accuracy.

When considering a satellite describing a Polar orbit starting at the Equator, a useful

simplification of Earth's magnetic field can be given by:

$$\mathbb{B}(t) = \frac{\mu}{{R_o}^3} \begin{bmatrix} 2sin(\omega_o t)sin(i_m) \\ cos(\omega_o t)sin(i_m) \\ cos(i_m) \end{bmatrix} \tag{1}$$

where $\mu$ is the strength of the magnetic dipole and is set as $7.9 \times 10^{15} Wbm$, $R_o$ is the average radius of the orbit (given in meters), $\omega_o$ is the orbital velocity of the satellite and $i_m$ is the inclination of the orbit with respect to the geomagnetic equator. It is important to note that (1) considers a circular orbit, at a fixed altitude as well as a fixed frame orientation.

This model has been adopted by several works (LOVERA; ASTOLFI, 2006; KAPLAN, 2006; STRAY, 2010; SUTHERLAND; KOLMANOVSKY; GIRARD, 2019) with little modifications in its form and order of components, depending on the orientation of the frames adopted by the authors. It is commonly known as *Dipole model* in the literature and this nomenclature will be adopted in this work. Figure 2 illustrates the results of model (1) for a three axes frame, following the same orientation of $\mathcal{F}_i$, with no rotation, positioned at a circular orbit path with 450 km of altitude, for a period of 5 orbits. The inclination $i_m$ was set as $87^o$ and $\omega_o$ was set as $0.0011$ rad/s (relative to 15 translations/-day). The values of $B_X$, $B_Y$, and $B_Z$ represent the intensity of the magnetic field in each of the three axes of the chosen frame. This model does not approximate correctly for low inclinations and can even be deficient for some inclinations close to Polar.

Figure 2 – Earth's magnetic field for a circular Polar orbit at 450 km according with (1).

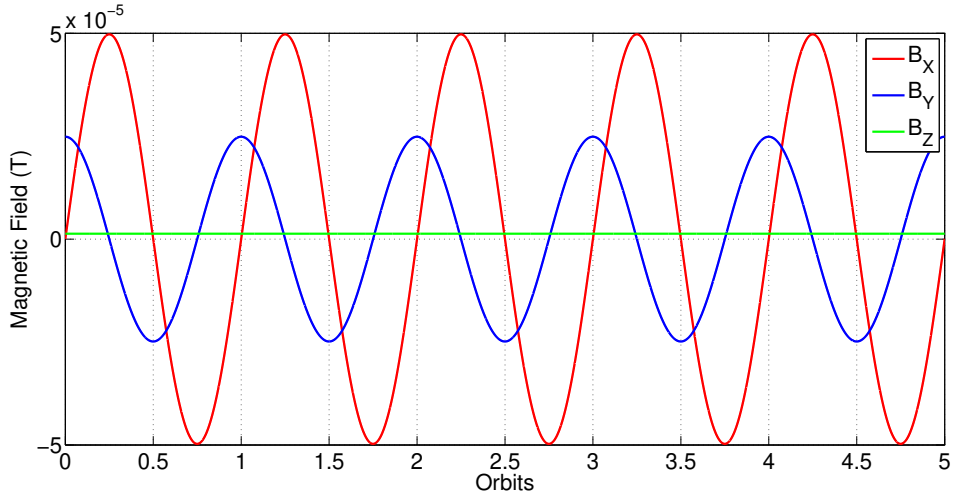


Source: The author.

A more complex and accurate model can be found in the International Geomagnetic Reference Field (IGRF) model. The IGRF model is developed and updated by the International Association of Geomagnetism and Aeronomy (IAGA) since 1965. It is a model currently in its 13th version (ALKEN *et al.*, 2021) and is constantly used in the literature

(KAPLAN, 2006; STRAY, 2010; VÁZQUEZ, 2013; VAN DE HENGEL, 2018) to simulate the behavior of the magnetic field on orbit. The IGRF model describes the magnetic field $\mathbb{B}$ as the gradient of the scalar potential function:

$$V(R,\theta_R,\lambda_R) = R_e \sum_{n=1}^{k} \left(\frac{R_e}{R}\right)^{n+1} \sum_{m=0}^{n} (g_n^m cos(m\lambda_R) + h_n^m sin(m\lambda_R) P_n^m(cos(\theta_R)) \quad (2)$$

where $R_e$ is the equatorial radius of the Earth (in meters), $g_n^m$ and $h_n^m$ are Gaussian coefficients and $R$, $\theta_R$ and $\lambda_R$ are the geocentric distance, the co-elevation and East longitude from Greenwich which define any point on and above Earth's surface.

The term $P_n^m$ is the Schmidt Normalized Associated Legendre Polynomials defined in (ALKEN; THéBAULT; BEGGAN, 2021) and can be calculated by:

$$P_n^m = \frac{(1-x^2)^{m/2}}{2^n n!} \frac{\delta^{n+m}}{\delta x^{n+m}} \left(x^2-1\right)^n \quad (3)$$

The magnetic field is given by

$$\mathbb{B} = -\nabla V \quad (4)$$

In order to obtain (4), first we make the partial derivatives of $V$, which might not be trivial. (YANG ZHONG YAN-WU GUAN, 2020) demonstrates the necessary steps to obtain the elements of $\mathbb{B}$ which are summarized below:

$$U_R = -\frac{\partial V}{\partial R} = \sum_{n=1}^{k} (n+1) \left(\frac{R_e}{R}\right)^{n+1} \sum_{m=0}^{n} (g_n^m cos(m\lambda_R) + h_n^m sin(m\lambda_R)) P_n^m(cos(\theta_R) \quad (5)$$

$$U_\theta = -\frac{\partial V}{\partial \theta_R} = -R_e \sum_{n=1}^{k} \left(\frac{R_e}{R}\right)^{n+1} \sum_{m=0}^{n} (g_n^m cos(m\lambda_R) + h_n^m sin(m\lambda_R)) \frac{\partial P_n^m(cos(\theta_R)}{\partial \theta_R} \quad (6)$$

$$U_\lambda = -\frac{\partial V}{\partial \lambda} = -R_e \sum_{n=1}^{k} \left(\frac{R_e}{R}\right)^{n+1} \sum_{m=0}^{n} (-g_n^m sin(m\lambda_R) + h_n^m cos(m\lambda_R)) P_n^m(cos(\theta_R) \quad (7)$$

The magnetic field components can be determined by:

$$\begin{aligned} B_x &= -\frac{1}{R} U_\theta \\ B_y &= \frac{1}{R sin(\theta_R)} U_\lambda \\ B_z &= U_r \end{aligned} \quad (8)$$

Although the IGRF model demands more calculations than the Dipole model shown before, it has a broad acceptance in the scientific community. It is not difficult to find computer routines that calculate their values for the user. Also, the Dipole model loses quality for orbits with low elevation, making the choice for the IGRF model more attractive to a range of different simulations.

Considering the same circular Polar orbit with an inclination of $87^o$, starting at the Equator, with an altitude of 450 km, and considering a translation period of 15 orbits per day, the magnetic field $\mathbb{B}$ generated by the IGRF model over a three axes frame, following the same orientation of $\mathcal{F}_i$, with no rotation and positioned on the orbit path can be seen in Figure 3. Note that, similarly to Figure 2, this result shows that the values of the magnetic field at each axis are periodic even though their overall shape does not look like a sine as the previous model. The most notable difference is the value of $B_Z$, which can vary between positive and negative values instead of a fixed, negative value on the Dipole model.

Figure 3 – Earth's magnetic field for a circular Polar orbit at 450 km according with (4).

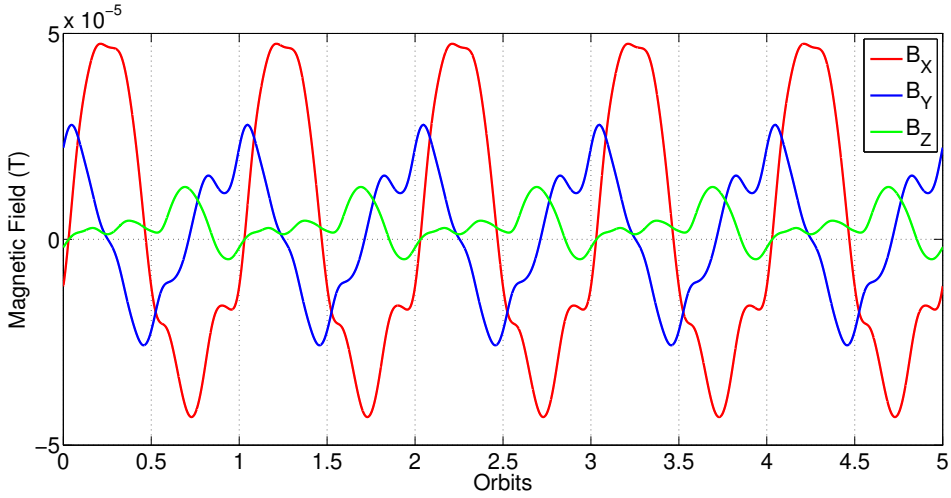


Source: The author.

Regardless of the model being used, another important aspect to consider is the necessity to rotate Earth's magnetic field $\mathbb{B}(t)$ according to the satellite's attitude in order to determine its correct sensor readings and magnetorquer interactions. In other words, it is necessary to rotate the magnetic field to assess its influence on the Satellite Body frame. The magnetic field seen by the satellite $B(t)$ can be obtained by doing:

$$B(t) = R(q_b)\mathbb{B}(t) \tag{9}$$

where $R(q_b)$ is the attitude matrix related to the quaternion $q_b$ which describes the satellite attitude and will be explained in Section 2.3. For now, suffice to state that a rotation is necessary before using the magnetic field $\mathbb{B}(t)$ generated by any model.

## 2.3 Quaternions

When dealing with rotational movements in three-dimensional spaces, it is common to use quaternions to describe the orientation of the body with respect to a reference frame. Quaternions are a useful 4-dimension numeric system that can be described as (SALTON *et al.*, 2017):

$$q = \begin{bmatrix} cos\left(\frac{\gamma}{2}\right) \\ \vec{r}\, sen\left(\frac{\gamma}{2}\right) \end{bmatrix} = \begin{bmatrix} \eta \\ \epsilon \end{bmatrix} = \begin{bmatrix} \eta & \epsilon_1 & \epsilon_2 & \epsilon_3 \end{bmatrix}^\intercal \tag{10}$$

where $\eta \in \mathbb{R}$, $\vec{r}, \epsilon \in \mathbb{R}^3$. The vector $\vec{r}$ describes the direction in which the rotation with the $\gamma$ is performed. When used to describe rotations, a quaternion must have a unitary norm, therefore an attitude parametrization requires that the quaternion values $\eta$ and $\epsilon$ must satisfy the following condition:

$$\|q\| = \sqrt{\eta^2 + {\epsilon_1}^2 + {\epsilon_2}^2 + {\epsilon_3}^2} = 1 \tag{11}$$

Figure 4 – Representation of the axis-angle rotation.

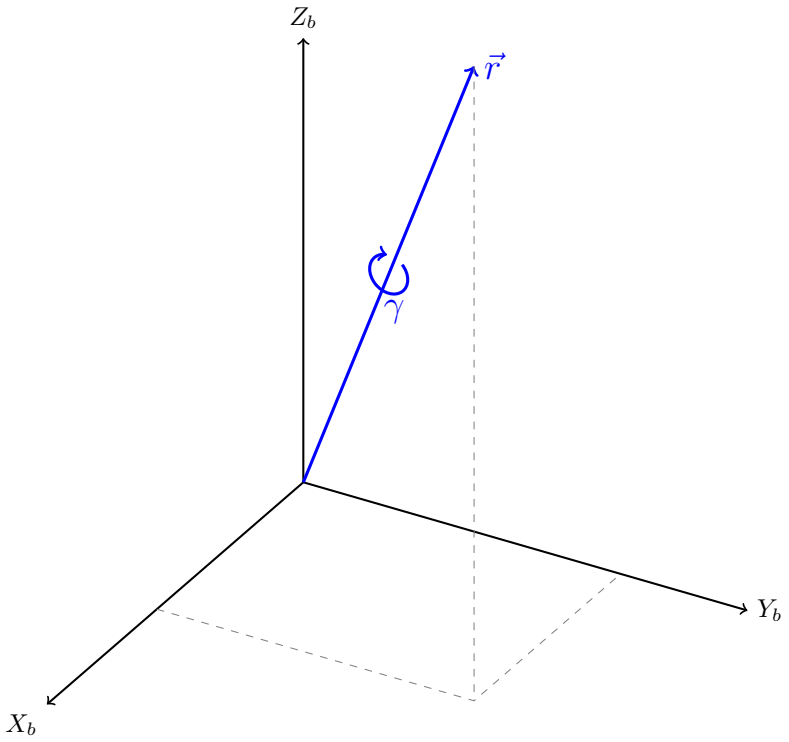


Source: The author.

Once an XYZ coordinate system has been established for the satellite (its body frame $\mathcal{F}_b$ with $X_b$, $Y_b$, and $Z_b$, for example), it is possible to describe any possible orientation for it by establishing the Euler angles $\phi$, $\theta$, and $\psi$ corresponding to the rotations performed by the body with respect to the XYZ axes of reference (a fixed reference frame $\mathcal{F}_i$, for instance) and converting these angles to a quaternion $q_b$. These angles are commonly

associated with *Roll*, *Pitch*, and *Yaw* movements of space and aircraft, and this sequence of rotation follows the Tait-Bryan definition.

The final orientation depends on the sequence of rotation thus, the conversion from Euler angles to quaternion is not always the same. For instance, a possible conversion of Euler angles following a 1-2-3 sequence to a quaternion can be obtained by:

$$q_b = \begin{bmatrix} cos(\phi)cos(\theta)cos(\psi) + sen(\phi)sen(\theta)sen(\psi) \\ sen(\phi)cos(\theta)cos(\psi) - cos(\phi)sen(\theta)sen(\psi) \\ cos(\phi)sen(\theta)cos(\psi) + sen(\phi)cos(\theta)sen(\psi) \\ cos(\phi)cos(\theta)sen(\psi) - sen(\phi)sen(\theta)cos(\psi) \end{bmatrix} \tag{12}$$

When no rotation occurs (i.e. $\phi$, $\theta$, $\psi = 0$), it is evident from (12) that the resulting quaternion is given by:

$$q_b = \begin{bmatrix} 1 & 0 & 0 & 0 \end{bmatrix}^\intercal \tag{13}$$

which is often referred to as the identity quaternion.

In order to obtain the values of the Euler angles $\phi$, $\theta$, and $\psi$ from a given quaternion $q_b$, it is only necessary to do:

$$\begin{aligned} \phi &= arctan2\left(\frac{2(\eta_b\epsilon_{b1} + \epsilon_{b2}\epsilon_{b3})}{1 - 2({\epsilon_{b1}}^2 + {\epsilon_{b2}}^2)}\right) \\ \theta &= arcsen\left(2(\eta_b\epsilon_{b2} - \epsilon_{b3}\epsilon_{b1})\right) \\ \psi &= arctan2\left(\frac{2(\eta_b\epsilon_{b3} + \epsilon_{b1}\epsilon_{b2})}{1 - 2({\epsilon_{b2}}^2 + {\epsilon_{b3}}^2)}\right) \end{aligned} \tag{14}$$

Unlike the $arctan(\cdot)$ function, the $arctan2(\cdot)$ function returns only one possible result as it calculates the value of the corresponding angle taking into account the sign of the terms. Thus, the conversion presented in (14) will be complete.

For a given reference orientation described by the quaternion $q_r$, it is possible to determine the attitude matrix $R(q_r)$ necessary to rotate any other vector to the orientation given by $q_r$. The quaternion representation of the attitude matrix $R(q_r)$ is given by:

$$R(q_r) = ({\eta_r}^2 - {\epsilon_r}^\intercal\epsilon_r)I_3 + 2\epsilon_r{\epsilon_r}^\intercal - 2\eta_r S(\epsilon_r) \tag{15}$$

where $I_3$ is the $3 \times 3$ identity matrix and $S(\epsilon_r) \in \mathbb{R}^{3\times3}$ is the skew-symmetric matrix associated with $\epsilon_r$ and given by:

$$S(\epsilon_r) = \begin{bmatrix} 0 & -\epsilon_{r3} & \epsilon_{r2} \\ \epsilon_{r3} & 0 & -\epsilon_{r1} \\ -\epsilon_{r2} & \epsilon_{r1} & 0 \end{bmatrix} \tag{16}$$

It is also possible to determine an attitude matrix $R$ for the difference between two

attitudes. This matrix can be described in terms of $R_b$ and $R_r$ as follows:

$$R = R_b R_r{}^{\mathsf{T}}. \tag{17}$$

Based on the description on (15), it is possible to deduce that an error quaternion can be defined through

$$R = (\eta^2 - \epsilon^{\mathsf{T}}\epsilon)I_3 + 2\epsilon\epsilon^{\mathsf{T}} - 2\eta S(\epsilon). \tag{18}$$

From (17) and (18), this error quaternion $q$ can be described in terms of $q_b$ and $q_r$ as:

$$\begin{aligned} \eta &= \eta_b\eta_r + \epsilon_b{}^{\mathsf{T}}\epsilon_r, \\ \epsilon &= \eta_r\epsilon_b - \eta_b\epsilon_r + S(\epsilon_b)\epsilon_r. \end{aligned} \tag{19}$$

This error quaternion $q$ follows the same restriction given by (11) and considering the results stated in (13) and (17), when no rotation between $q_b$ and $q_r$ is needed, the attitude matrix $R(q)$ and error quaternion $q$ become:

$$\begin{aligned} q &= \begin{bmatrix} 1 & 0 & 0 & 0 \end{bmatrix}^{\mathsf{T}}, \\ R &= I. \end{aligned} \tag{20}$$

## 2.4 Inertia Matrix

Every physical body that can be rotated has an inertia matrix (also referred to as moment of inertia, inertia tensor, or rotational inertia). This value can be determined by its mass distribution with respect to a chosen point of rotation on a given reference frame, which will describe how the body is rotating. A common choice for a point of rotation when working with satellites and aircrafts is the body center of mass.

When a body is free to rotate in a 3-dimensional space (such is the case of an orbiting satellite), the inertia matrix can be described as a matrix $J \in \mathbb{R}^{3\times3}$ given by:

$$J = \begin{bmatrix} J_{xx} & J_{xy} & J_{xz} \\ J_{yx} & J_{yy} & J_{yz} \\ J_{zx} & J_{zy} & J_{zz} \end{bmatrix} \tag{21}$$

where the elements of the main diagonal respect the triangular inequality property.

For a rigid body, with a continuously distributed mass, i.e. with an homogeneous

mass density, the matrix $J$ is symmetric and its terms can be calculated as

$$\begin{aligned} J_{xx} &= w \int\int\int (y^2 + z^2) dxdydz \\ J_{yy} &= w \int\int\int (x^2 + z^2) dxdydz \\ J_{zz} &= w \int\int\int (x^2 + y^2) dxdydz \end{aligned} \tag{22}$$

$$\begin{aligned} J_{xy} = J_{yx} &= -w \int\int\int (xy) dxdydz \\ J_{xz} = J_{zx} &= -w \int\int\int (xz) dxdydz \\ J_{yz} = J_{zy} &= -w \int\int\int (yz) dxdydz \end{aligned} \tag{23}$$

where the term $w$ is a constant and represents the mass density of the body.

A cubic object with edge $a$ and uniformly distributed mass $W$ has a coincident center of mass and geometric center. Thus, the inertia matrix components of the object given by (22) and (23) can be simplified to:

$$\begin{aligned} J_{xx} = J_{yy} = J_{zz} &= \frac{Wa^2}{6} \\ J_{xy} = J_{xz} = J_{yz} &= 0 \end{aligned} \tag{24}$$

Whenever the body frame axes and the rotation axes coincide, the elements of $J$ different from the main diagonal will be null. Rigid bodies that have an inertia matrix in the form

$$J = \kappa I_3 \tag{25}$$

where $\kappa > 0$, are called spherical top bodies (CLINE, 2021, Section 10.10). This name comes from the fact these bodies have the same symmetry as the inertia tensor about the center of a uniform sphere. An uniform cube has a spherical top body configuration. A less obvious consequence of spherical symmetry is that any orientation of three mutually perpendicular axes about the center of mass of a uniform cube is an equally good principal axis system.

However, if the rigid body has a constant mass density but a cuboid shape different from a cube, the inertia matrix $J$ will be given by:

$$\begin{aligned} J &= \begin{bmatrix} J_{xx} & 0 & 0 \\ 0 & J_{yy} & 0 \\ 0 & 0 & J_{zz} \end{bmatrix}, \\ J_{xx} &\neq J_{yy} \neq J_{zz} \geq 0, \end{aligned} \tag{26}$$

and will be called asymmetric top.

## 2.5 Magnetorquers dynamics

Magnetorquer, or magnetic torquer, is an electromagnet actuator that produces a torque based on the interaction of a magnetic dipole created by its coils and a given magnetic field. When orbiting Earth, the magnetic field used by the magnetorquer is Earth's magnetic field $\mathbb{B}$ itself. The current that flows through its windings produces a magnetic moment $m_{coil}(t)$ according to the following equation (STRAY, 2010):

$$m_{coil}(t) = nAi_{coil}(t) \tag{27}$$

where $n$ is the number of turns of the coils, $A$ is the surface area of the coil, and $i_{coil}(t)$ is the control current used. By alternating the direction and amplitude of the current $i_{coil}$, it is possible to reverse the direction and change the intensity of the magnetic moment generated by the magnetorquer, making it a very useful actuator.

Since the magnetic moment $m_{coil}(t)$ generated by the windings is perpendicular to the surface area $A$, the positioning of the magnetorquers in a satellite is made such that a magnetic moment component coinciding with one of the axes of the *Satellite Body frame ($\mathcal{F}_b$)* can be generated by activating one or more magnetorquers. A common approach is to position each magnetorquer coinciding with one of the axes of the *Satellite Body frame ($\mathcal{F}_b$)*. This way, the orientation given by the quaternion $q_b$ can be used to describe the magnetic moment $m(t)$ generated by the control system.

$$m(t) = \begin{bmatrix} m_{coilx}(t) \\ m_{coily}(t) \\ m_{coilz}(t) \end{bmatrix} = nA \begin{bmatrix} i_{coilx}(t) \\ i_{coily}(t) \\ i_{coilz}(t) \end{bmatrix}. \tag{28}$$

As the orientation of the satellite relative to the inertial frame changes, the orientation of the magnetic moment $m(t)$ changes in the same way. The torque $\tau(t)$ produced by the magnetorquers results from the cross-product of the magnetic moment $m(t)$ and the Earth's magnetic field seen by the body $B(t)$ as follows:

$$\tau(t) = m(t) \times B(t) = S(B(t))m(t). \tag{29}$$

One property of the cross product operation is that, by breaking up the vector $m(t)$ into two components: $m_{||}(t)$ parallel to the vector $B(t)$ and $m_{\perp}(t)$ perpendicular to the vector $B(t)$ such that

$$m(t) = m_{||}(t) + m_{\perp}(t) \tag{30}$$

Figure 5 – Representation of cross product between magnetic field $B(t)$ and magnetic moment $m(t)$.

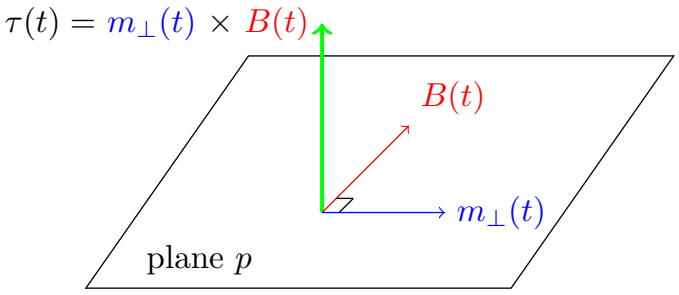


Source: The author.

and the result of (29) will always be the same as

$$\tau(t) = m(t) \times B(t) = m_\perp(t) \times B(t) \tag{31}$$

thus, any energy used to create $m_{||}(t)$ will be useless in generating torque and should be avoided.

It is also valid to notice that, due to the cross product, the magnetic torque $\tau(t)$ is always perpendicular to the plane $p$ created by the magnetic field on the satellite $B(t)$ and the perpendicular component of the magnetic moment created by the magnetorquers $m_\perp(t)$. This creates an important limitation to the direction in which the actuator can effectively apply control in an active system because if the magnetic moment $m(t)$ only has a parallel component to $B(t)$, the value of $\tau(t)$ is null, making it impossible to control in that direction. Figure 5 illustrates the cross product between $m_\perp(t)$ and $B(t)$.

## 2.6 Saturation

Different from simulations and theoretical models, real-life systems and components usually have nonlinear behaviors, with saturation being among the most common of these. Saturation can be understood as physical limitations that confine a signal to a certain range. It is classified as a memoryless, zero memory, or static nonlinearity because it does not depend on previous behaviors (KHALIL, 2002, Section 1.2.7). This limitation in the range can occur due to the component's characteristics – material, dimensions, design specifications (to protect other components) – or due to indirect reasons – power source limitations, for instance.

A generic function $y(t)$ saturating at 1 can be defined as

$$sat(y) = \begin{cases} y(t), & \text{if } |y(t)| \leq 1 \\ -1, & \text{if } y(t) < -1 \\ 1, & \text{if } y(t) > 1 \end{cases} \tag{32}$$

Figure 6 – Illustration of a function saturation at 1.

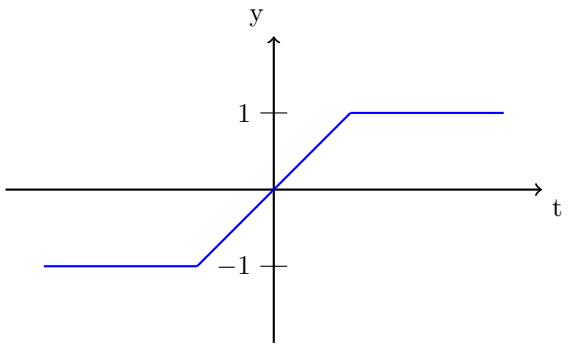


Source: The author.

In the case of magnetorquers, saturation might occur when the magnetic moment required by the control input is the same or above its nominal value. In this case, the control input $m(t)$ required is larger than the actuator's capacity to generate and it cannot achieve the desirable magnetic moment.

## 2.7 Attitude dynamics

The behavior of satellites and spacecraft orbiting Earth can be described as rigid bodies and their attitude dynamics can be summarized by (F. LANDIS MARKLEY, 2014):

$$\dot{\omega_b}(t) = J^{-1}\big( - S(\omega_b(t))J\omega_b(t) + \tau(t)\big) \tag{33}$$

where the matrix $J \in \mathbb{R}^{3\times3}$ is the inertia matrix of the satellite, $\dot{\omega_b}(t) \in \mathbb{R}^3$ is the angular acceleration of the satellite, $\omega_b(t) \in \mathbb{R}^3$ is the angular velocity of the satellite, $\tau(t) \in \mathbb{R}^3$ is the resultant torque applied to the body and $S(\omega_b(t)) \in \mathbb{R}^{3\times3}$ is the skew-symmetric matrix associated with $\omega_b(t)$.

The resulting torque applied in an orbiting satellite can be expressed as the sum of all the active torques being applied along with all the disturbance torques. It might include the aerodynamic torque ($\tau_{aero}$), solar radiation torque ($\tau_{rad}$), gravitational torque ($\tau_{grav}$), residual dipole torque ($\tau_{dip}$) and torque generated by magnetorquers ($\tau_{mag}$) (STRAY, 2010) as defined bellow:

$$\tau = \tau_{aero} + \tau_{rad} + \tau_{grav} + \tau_{dip} + \tau_{mag}. \tag{34}$$

When the center of gravity coincides with the center of mass and the body is symmetrical about this center (as is the case in a theoretical 1U CubeSat), the torques $\tau_{aero}$, $\tau_{rad}$ and $\tau_{grav}$ are null. This type of precision in construction is very difficult to achieve but can be mitigated in the design phase. The residual dipole torque $\tau_{dip}$ is generated by any magnetic field created by the satellite's electronic components and ferromagnetic materials, therefore, unavoidable. For this work, all disturbance torques were disregarded then (34) can be simplified to

$$\tau(t) = \tau_{mag}(t). \tag{35}$$

By determining the satellite's orientation with quaternion

$$q_b = \begin{bmatrix} \eta_b & \epsilon_b \end{bmatrix}^\intercal, \tag{36}$$

the dynamics of the body can be described by:

$$\begin{aligned} \dot{\eta}_b(t) &= -\frac{1}{2}\epsilon_b(t)^\intercal \omega_b(t), \\ \dot{\epsilon}_b(t) &= \frac{1}{2}\big(\eta_b(t) I_3 + S(\epsilon_b(t))\big)\omega_b(t), \\ \dot{\omega}_b(t) &= J^{-1}\big( - S(\omega_b(t)) J \omega_b(t) + \tau(t)\big). \end{aligned} \tag{37}$$

## 2.8 Reference dynamics

Similar to how it was done for the satellite, the desired orientation can be described by a quaternion $q_r$.

$$q_r = \begin{bmatrix} \eta_r & \epsilon_r \end{bmatrix}^\intercal \tag{38}$$

The reference dynamics considered in this work is as follows

$$\begin{aligned} \dot{\eta_r}(t) &= -\frac{1}{2}\epsilon_r(t)^\intercal \omega_r(t), \\ \dot{\epsilon_r}(t) &= \frac{1}{2}\big(\eta_r(t) I_3 + S(\epsilon_r(t))\big)\omega_r, \\ \dot{\omega_r}(t) &= 0, \end{aligned} \tag{39}$$

where $\omega_r \in \mathbb{R}^3$ is the desired angular velocity of the reference. This value is constant and determined according to a circular orbit chosen for the satellite such that the desired face of the satellite always points towards Earth's surface and no unnecessary rotation affects the reference. The reference angular velocity has the same module of the orbital angular velocity and does not suffer any influence from any torque, being determined by the mission and constant for all purposes.

## 2.9 Error dynamics

The error dynamics can be determined based on the attitude and the reference dynamics. First, consider the error quaternion $q$ determined by (19). The satellite's angular velocity and the desired angular velocity can be used to determine the angular velocity error $\omega(t)$ by:

$$\omega(t) = \omega_b(t) - R(q)\omega_r(t). \tag{40}$$

Taking the time derivative of (40), specially the derivative of the term $R(q)\omega_r(t)$ (see, e.g., (ZHAO, 2016)), we obtain:

$$\begin{aligned} \dot{\omega} &= \dot{\omega}_b - \dot{R}(q)\omega_r, \\ \dot{\omega} &= \dot{\omega}_b - S(\omega)R(q)\omega_r. \end{aligned} \tag{41}$$

From the result above and taking $\dot{\omega}_b$ from (37), the error dynamics is determined by:

$$\begin{aligned} \dot{\eta} &= -\frac{1}{2}\epsilon^{\intercal}\omega, \\ \dot{\epsilon} &= \frac{1}{2}(\eta I_3 + S(\epsilon))\omega, \\ \dot{\omega} &= J^{-1}\big(S(\omega_b)J\omega_b + \tau - JS(\omega)R(q)\omega_r\big). \end{aligned} \tag{42}$$

Note that the error dynamics depends on both the satellite's angular velocity $\omega_b(t)$ and the reference angular velocity $\omega_r$.

## 2.10 Average system

The use of magnetorquers and the periodicity of the magnetic field for an orbiting satellite enable the application of the averaging method to design an active control system. This method asserts that it is possible to determine the stability of a system based on the stability of its average system if a few assumptions are respected. Averaging method is explained in detail in (KHALIL, 2002, Section 10.4) but is summarized here to make it easier for the reader to understand the approaches presented.

Consider a system in the form

$$\dot{x} = \varepsilon f(t, x, \varepsilon) \tag{43}$$

where $\varepsilon$ is a positive small scalar and the function $f(t, x, \varepsilon)$ is T-periodic in $t$, i.e., for a period $T > 0$, then

$$f(t + T, x, \varepsilon) = f(t, x, \varepsilon),\ \forall (t, x, \varepsilon) \in [0, \infty) \times D \times [0, \varepsilon_0] \tag{44}$$

with a domain $D \subset \mathbb{R}^n$ and $\varepsilon_0 > 0$.

Consider now an autonomous average system

$$\dot{x} = \varepsilon f_{av}(x) \tag{45}$$

where the average value is obtained by

$$f_{av}(x) = \frac{1}{T}\int_0^T f(\sigma, x, 0)d\sigma. \tag{46}$$

The system (43) can be represented as a perturbation of the autonomous system (45), around the equilibrium point.

**Theorem 1.** *Let $f(t, x, \varepsilon)$ be continuous and bounded and assume it has continuous, bounded partial derivatives up to the second order with respect to $(x, \varepsilon)$ for $(t, x, \varepsilon) \in [0, \infty) \times D_0 \times [0, \varepsilon_0]$, for every compact set $D_o \subset D$, where $D \subset \mathbb{R}^n$ is a domain. Suppose $\varepsilon > 0$ and $f$ is periodic in $t$ for some $T > 0$. Let $x(t, \varepsilon)$ and $x_{av}(\varepsilon t)$ denote solutions for* (43) *and* (45)*, respectively.*

- *If the origin $x = 0 \in D$ is an exponentially stable equilibrium point of the average system* (45)*, then there exist positive constant $\varepsilon^*$ and $\kappa$ such that, for all $0 < \varepsilon < \varepsilon^*$,* (43) *has a unique, exponentially stable, T-periodic solution $\bar{x}(t, \varepsilon)$ with the property $||\bar{x}(t, \varepsilon)|| \leq \kappa\varepsilon$.*

Thus, the averaging method assures that if $f(t, 0, \epsilon) = 0$ and the origin of the average system (45) is exponentially stable, then there exists a $\varepsilon^* > 0$ such that for all $0 < \varepsilon < \varepsilon^*$, the origin of the original system (43) will be exponentially stable as well.

# 3 SYSTEM CONTROL

After presenting the necessary elements to describe the satellite dynamics in orbit, we now present two different active attitude control approaches using only magnetorquers as actuators. The first one represents the state of the art as proposed by (LOVERA; ASTOLFI, 2006) which considers an average model of Earth's magnetic field and an adaptive control law to achieve the control objective. This controller will be used as the benchmark to which the results will be compared.

Then, an alternative modification is proposed to the adaptive control law described previously. This alternative uses a fixed gain instead of an adaptive gain, without loss of stability to the system. The actuators keep generating only perpendicular magnetic moment $m(t)$ relative to the magnetic field $B(t)$ as the first control law. This assures that the system avoids any waste of energy in unnecessary command inputs.

## 3.1 Problem definition

The purpose of an active attitude control system that uses magnetorquers is to use Earth's magnetic field seen at the satellite $B(t)$ and the magnetic moments $m(t)$ created by the actuators to create a magnetic torque $\tau(t)$ to position the satellite according to a desired attitude reference or simply to null the satellite's angular momentum.

A simple attitude reference choice is to keep one of the satellite's sides always facing the surface of the Earth and one side always perpendicular to the trajectory orbit. In this way, a satellite can maintain an observation instrument always pointed to Earth's surface, without any undesired lateral rotation. The control input also needs to consider the satellite restrictions and mission purposes. Therefore, it should be as efficient as possible regarding battery use otherwise it might achieve the desired attitude but might not be able to perform its mission.

By establishing the orbital trajectory of the satellite (its altitude, inclination, and orbital velocity), it is possible to determine Earth's magnetic field $\mathbb{B}$ using any given model, such as presented in Section 2.2. For illustration purposes, consider a circular Polar orbital trajectory (i.e. inclination of $87^o$ with respect to the equatorial plane) beginning at

the Equator, with a constant altitude of 450 km, and that completes 15 orbits in one day. The magnetic field values for the Dipole model and for the IGRF model are shown in Figure 2 and 3, respectively.

Considering the attitude of the satellite given by $q_b$ and the desired attitude given by $q_r$, it is possible to determine the attitude error $q$ using Equation (19) as seen bellow:

$$\begin{aligned} \eta(t) &= \eta_b(t)\eta_r(t) + \epsilon_b(t)^\intercal \epsilon_r(t), \\ \epsilon(t) &= \eta_r(t)\epsilon_b(t) - \eta_b(t)\epsilon_r(t) + S(\epsilon_b(t))\epsilon_r(t). \end{aligned} \tag{47}$$

Another important variable for the problem is the angular velocity error between the satellite's attitude and the reference given by:

$$\omega(t) = \omega_b(t) - R(q)\omega_r(t). \tag{48}$$

The main objective of the active control system is to set the satellite's attitude equal to the reference's attitude. In other words, it is to obtain

$$\begin{aligned} \lim_{t\to\infty} \|\epsilon(t)\| &= 0, \\ \lim_{t\to\infty} \|\omega(t)\| &= 0, \end{aligned} \tag{49}$$

regardless of the orbital trajectory and attitude reference.

In order to achieve that, a control law might be written in the form

$$\tau(t) = -K_p\epsilon(t) - K_v\omega(t) \tag{50}$$

where $K_p$, $K_v \in \mathbb{R}$ are positive control gains. Taking the torque equation given in (29), a straightforward idea would be to define the magnetic moment input as

$$m(t) = -S(B(t))^{-1}\big(K_p\epsilon(t) + K_v\omega(t)\big) \tag{51}$$

such that

$$\begin{aligned} \tau(t) &= S(B(t))m(t) \\ \tau(t) &= -S(B)S(B)^{-1}\big(K_p\epsilon(t) + K_v\omega(t)\big) \\ \tau(t) &= -K_p\epsilon(t) - K_v\omega(t) \end{aligned} \tag{52}$$

Unfortunately, the matrix $S(B(t))$ does not have full rank, making it impossible to find its inverse as suggested by (52). It is necessary to use some other technique to bypass this problem and create a control input $m(t)$ that achieves the control objectives.

Consider the orbital path previously described and a desired reference configured as:

$$\begin{aligned} q_r &= \begin{bmatrix} 1 & 0 & 0 & 0 \end{bmatrix}^\intercal, \\ \omega_r &= \begin{bmatrix} 0 & 0.0011 & 0 \end{bmatrix}^\intercal, \end{aligned} \tag{53}$$

at the beginning of the suggested orbit. The magnetic field $B_r(t)$ can be calculated by:

$$B_r(t) = R(q_r)\mathbb{B}(t) \tag{54}$$

Figure 7 shows the magnetic field $B_r(t)$ calculated by (54) and seen by the reference using the Dipole model of the magnetic field $\mathbb{B}(t)$.

Figure 7 – Magnetic field $B_r(t)$ seen at the reference using the Dipole model.

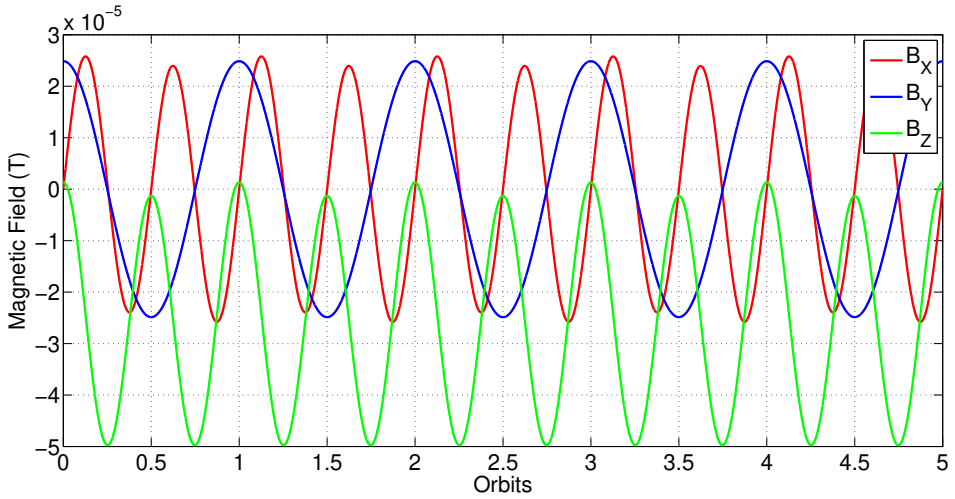


Source: The author.

The equivalent result for the IGRF model is presented in Figure 8. In both cases, it can be seen that the magnetic field $B_r(t)$ calculated by (54) is periodic for this reference. This indicates that averaging theory can be an alternative to the lack of invertibility of the matrix $S(B(t))$, when dealing with the magnetic field seen by the body. Note that the periodicity of $B(t)$ would come after the body starts following the reference.

## 3.2 Adaptive Control Law

Considering the problem that the matrix $S(B(t))$, with the magnetic field seen by the body, does not have full rank and considering the control objectives given in Equation (49), it is possible to consider a magnetic moment $m_a(t)$ in the form

$$m_a(t) = \frac{S(B(t))^\intercal}{||B(t)||^2} u(t) \tag{55}$$

Figure 8 – Magnetic field $B_r(t)$ seen at the reference using the IGRF model.

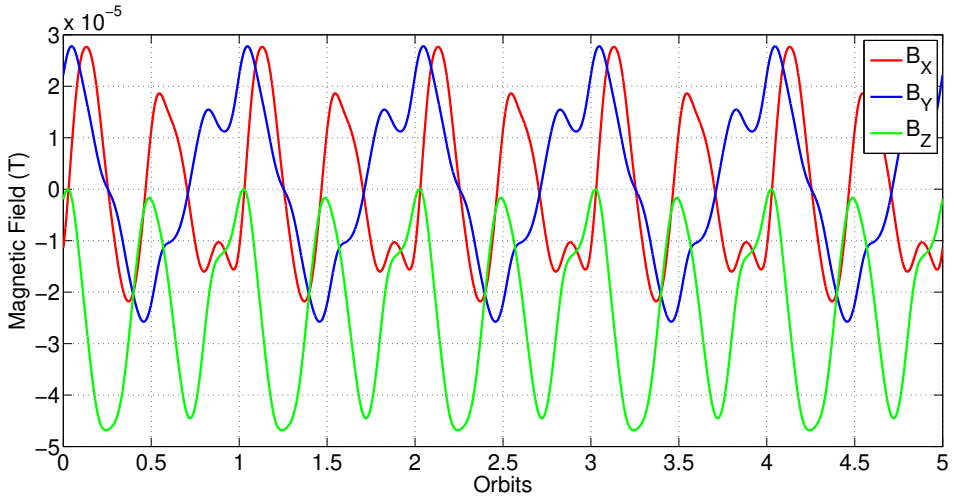


Source: The author.

where $u(t)$ is a control signal input. For this case, the magnetic torque $\tau(t)$ becomes

$$\tau(t) = S(B(t))\frac{S(B(t))^{\intercal}}{||B(t)||^2}u(t) \tag{56}$$

The motive to generate a magnetic moment $m_a(t)$ with the term $S^T(B(t))u(t)$ might not be clear at first sight. The explanation is that this product makes all components of $m_a(t)$ perpendicular to the magnetic field $B(t)$, thus avoiding any waste of energy while using the magnetorquers. Consider then a matrix $\Gamma(t)$ in the form:

$$\Gamma(t) = \frac{S(B(t))S(B(t))t}{||B(t)||^2} \tag{57}$$

Similar to the matrix $S(B(t))$, the matrix $\Gamma(t)$ given in (57) cannot be inverted. However, due to the periodic nature of Earth's magnetic field $\mathbb{B}(t)$ and the values for a high elevation orbit, it is possible to create an average value matrix $\Gamma_{av}(t)$ that has full rank, thus, is invertible. For orbits with low elevation, might reach singularity. The authors suggested to calculate $\Gamma_{av}(t)$ through the following differential equation system: :

$$\begin{aligned} \dot{\Gamma}_{av}(t) &= \frac{1}{t}\Gamma(t) - \frac{1}{t}\Gamma_{av}(t) \\ \Gamma_{av}(0) &= \Gamma(0) \end{aligned} \tag{58}$$

Next, the authors define a control input in the form:

$$\begin{aligned} u(t) &= -K_v\omega(t), && t \leq \bar{t} \\ u(t) &= -\Gamma_{av}^{-1}(t)\big(K_p\epsilon(t) + K_v\omega(t)\big), && t > \bar{t} \end{aligned} \tag{59}$$

where $\bar{t}$ is an arbitrary moment in time. At first, the control law acts as a classic *B-dot* control algorithm (LOVERA, 2015) to minimize the angular velocity error. The second part introduces an attitude correction part, along with the matrix $\Gamma_{av}(t)$.

Over time, after $t > \bar{t}$, by applying (59) into (56), the following result is obtained:

$$\lim_{t\to\infty} \tau(t) = -\big(K_p\epsilon(t) + K_v\omega(t)\big) \tag{60}$$

This result is obtained through the application of the averaging method presented in Section 2.10. At the equilibrium point, the error system becomes

$$\lim_{T\to\infty} \frac{1}{T}\int_t^T \Gamma(t)\Gamma_{av}(t)^{-1}dt = I \tag{61}$$

It is possible to verify matrix $\Gamma_{av}(t)$ invertibility by looking at its eigenvalues. Figure 9 shows the eigenvalues of $\Gamma_{av}(t)$ for a satellite following a reference when analyzing the magnetic field $B(t)$ given by the Dipole model and the same orbit configuration as determined for Figure 7. As can be seen, the values vary significantly at the first few orbits but decrease their variation considerably at later orbits. Therefore, the value of the adaptive gain $\Gamma_{av}(t)$ tends towards a single value.

Figure 9 – Eigenvalues of $\Gamma_{av}(t)$ for satellite at the reference and using Dipole model.

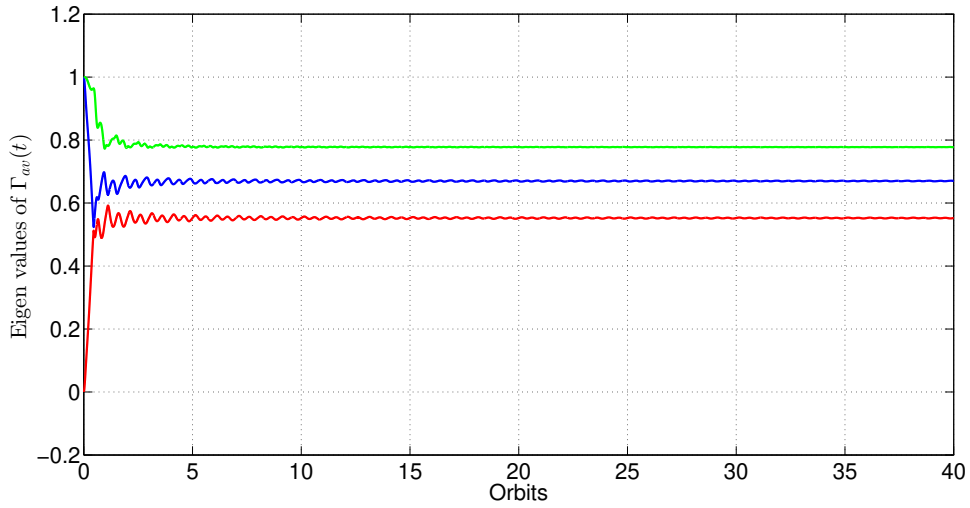


Source: The author.

The authors of (LOVERA; ASTOLFI, 2006) did not explain how to determine the transition moment $\bar{t}$ that should be used to switch the dynamic of $u(t)$ but the variation of the eigenvalues might be used as a criterion. For example, the control input switch might happen when the values of the eigenvalues vary less than a certain amount, indicating that the matrix is going through smaller changes and can be better used to determine the control input.

## 3.3 Proposed Control Law

Considering the adaptive gain controller presented previously, an alternative is proposed. Consider a satellite orbiting a fixed path, with the torque $\tau(t)$ being applied in (37) entirely from the magnetorquers through (29). As mentioned before, the cross-product in (29) limits the control torques to be perpendicular to both the magnetic field seen at the body $B(t)$ and the magnetic moment generated by the magnetorquers $m(t)$, effectively canceling any other control signal.

In other words, any control effort component of $m(t)$ that is parallel to the magnetic field seen at the body will consume energy but will not generate torque. Thus, the best alternative is to limit the control inputs to be always perpendicular to $B(t)$. Therefore, consider a magnetic moment $m_f(t)$ defined in the same way as $m_a(t)$ in (55)

$$m_f(t) = \frac{S(B(t))^\intercal}{||B(t)||^2} u(t), \tag{62}$$

where $u(t)$ is the new control signal determined by the proposed controller. Then the control torque becomes,

$$\tau(t) = S(B(t))m_f(t) = \Gamma(t)u(t), \tag{63}$$

with $\Gamma(t)$ determined as in (57). As stated before, the product $\Gamma(t)u(t)$ will be a vector perpendicular to $B(t)$ and all energy used by the magnetorquers will be converted into torque by the actuators. Consider the following assumption:

**Assumption 1.** *The satellite's trajectory in orbit, as well as the magnetic field $\mathbb{B}(t)$, are known and periodic at the reference.*

Given assumption 1, an average value of $\Gamma(t)$ can be computed around the reference trajectory

$$\bar{\Gamma} = \frac{1}{T}\int_0^T \Gamma(t)dt \tag{64}$$

where $T$ corresponds to the period of one orbit of the satellite around Earth.

Notice, in view of (57), that the matrix $\bar{\Gamma}$ is positive definite for a high elevation orbit. Consider now a control input $u(t)$ in the form

$$u(t) = -\varepsilon^2 k_p y(t) - \varepsilon k_v \omega(t), \tag{65}$$

where $\varepsilon$ is a parameter related to the average model of (42) with (65) and

$$y(t) = \bar{\Gamma}^{-1}\epsilon(t). \tag{66}$$

Since the value of Earth's magnetic field on the satellite $B(t)$ along the satellite's orbit

and for a reference that always keeps one of its surfaces towards the surface constitutes a periodic system as indicated by (1) and illustrated in Figure 7, it is possible to apply the averaging method to obtain a controllable model of the system. To do so, let us introduce the following variable transformations,

$$z = \frac{\omega}{\varepsilon},\ z_b = \frac{\omega_b}{\varepsilon},\ z_r = \frac{\omega_r}{\varepsilon}, \tag{67}$$

with $\varepsilon$ being a sufficiently small positive scalar. Then, the average closed-loop error system can be defined as follows,

$$\begin{aligned} \dot{\eta} &= -\frac{1}{2}\varepsilon\epsilon^{\intercal}z, \\ \dot{\epsilon} &= \frac{1}{2}\varepsilon\big(\eta I_3 + S(\epsilon)\big)z, \\ \dot{z} &= J^{-1}\left(\varepsilon S(z_b)Jz_b + \frac{\bar{\Gamma}}{\varepsilon}u - \varepsilon JS(z)R(q)z_r\right). \end{aligned} \tag{68}$$

From (KHALIL, 2002, Section 10.4), there exists $\varepsilon^* > 0$ such that for any $\varepsilon \in (0, \varepsilon^*)$ the stability of (68) implies the stability of the original closed-loop system as defined in (42). The following result shows that the trajectories of system (68) are globally ultimate bounded in closed-loop.

**Proposition 1.** *For any $\varepsilon > 0$, $k_p > 0$ and $k_v > 0$, the trajectories of system* (68) *with $u(t)$ as given in* (65) *satisfy the following as $t \to \infty$*

- $\|z(t)\| \to 0$*;*
- $\|\epsilon(t)\| \leq c$*; and*
- $\sqrt{1-c^2} \leq |\eta(t)| \leq 1$.

*where*

$$c = \frac{1}{k_p}\ \sup\ \|S(R(q)z_r)JR(q)z_r\|. \tag{69}$$

*Moreover, when the satellite has a spherical top configuration (i.e. $J = hI_3$, $h > 0$), then $\|\eta(t)\| \to 1$ and $\|\epsilon(t)\| \to 0$ as $t \to \infty$.*

*Proof.* Consider the following Lyapunov function candidate:

$$V = \frac{1}{2}\Big(z^{\intercal}Jz + z_r^{\intercal}\big(J - R(q)^{\intercal}JR(q)\big)z_r + 4k_p(1-\eta)\Big) \tag{70}$$

with $k_p$ being sufficiently large such that $V > 0$ for all $z \neq 0$ and $\eta \neq 1$. In addition, notice that $V \to 0$ as $z \to 0$ and $\eta \to 1$, since $R(q) \to I_3$.

In order to evaluate the stability of the satellite's equilibrium point, it is necessary to consider the time-derivative of $V$. The terms $z_r^{\intercal}Jz_r$ and $4k_p$ are constants and the

derivative of $\eta$ can be taken from (68). By applying the derivative to the other terms, the derivative of (70) along the trajectories of the closed loop system (68) is given by:

$$\dot{V} = z^{\intercal} J\dot{z} - z_r^{\intercal} R(q)^{\intercal} J\dot{R}(q) z_r + \varepsilon k_p \epsilon^{\intercal} z. \tag{71}$$

Now, from the expression of $\dot{z}$ in (68) along with (41) and (67), we obtain

$$\begin{aligned} \dot{z} &= J^{-1}\big(\varepsilon S(z_b) J z_b + \tfrac{\bar{\Gamma} u}{\varepsilon} - \varepsilon J S(z) R(q) z_r\big) \\ &= \varepsilon J^{-1} S(z_b) J z_b + \tfrac{J^{-1}\bar{\Gamma} u}{\varepsilon} - \varepsilon S(z) R(q) z_r. \end{aligned} \tag{72}$$

Taking angular velocity error stated in (40) and applying the variable transformation (67), we obtain that

$$z_b = z + R(q) z_r. \tag{73}$$

Applying this value of $z_b$ into (72), it becomes

$$\begin{aligned} \dot{z} &= \varepsilon J^{-1} S(z + R(q)z_r) J (z + R(q) z_r) \\ &\quad + \tfrac{J^{-1}\bar{\Gamma} u}{\varepsilon} - \varepsilon S(z) R(q) z_r \\ &= \varepsilon J^{-1} S(z) J z + \varepsilon J^{-1} S(z) J (R(q) z_r) \\ &\quad + \varepsilon J^{-1} S(R(q) z_r) J z \\ &\quad + \varepsilon J^{-1} S(R(q) z_r) J R(q) z_r \\ &\quad + \tfrac{J^{-1}\bar{\Gamma}}{\varepsilon} u - \varepsilon S(z) R(q) z_r. \end{aligned} \tag{74}$$

By replacing the input $u$ from (65) into (74), the time derivative of $V$ can be cast as

$$\begin{aligned} \dot{V} =& \varepsilon z^{\intercal} S(z) J z + \varepsilon z^{\intercal} S(z) J R(q) z_r \\ &+ \varepsilon z^{\intercal} S(R(q) z_r) J z + \varepsilon z^{\intercal} S(R(q) z_r) J R(q) z_r \\ &- \varepsilon k_p z^{\intercal} \bar{\Gamma} y - \varepsilon k_v z^{\intercal} \bar{\Gamma} z - \varepsilon z^{\intercal} J S(z) R(q) z_r \\ &- \varepsilon z_r^{\intercal} R(q)^{\intercal} J S(z) R(q) z_r + \varepsilon k_p z^{\intercal} \bar{\Gamma} y. \end{aligned} \tag{75}$$

Since knowing that $z^{\intercal} S(z) = 0$, rearranging the terms of (75) gives

$$\begin{aligned} \dot{V} = & \varepsilon z^{\intercal} S(R(q) z_r) J z - \varepsilon z^{\intercal} J S(z) R(q) z_r \\ &+ \varepsilon z^{\intercal} S(R(q) z_r) J R(q) z_r \\ &- \varepsilon z_r^{\intercal} R(q)^{\intercal} J S(z) R(q) z_r \\ &- \varepsilon k_v z^{\intercal} \bar{\Gamma} z. \end{aligned} \tag{76}$$

Given two arbitrary vectors $a$ and $b$, it is possible to verify that $S(a)^{\intercal} b = S(b) a$. Since the inertia matrix $J$ is symmetric, i.e., $J = J^{\intercal}$, the first two terms of (76) are equivalent

as shown below

$$\begin{aligned}
\varepsilon z^{\intercal} S(R(q)z_r)Jz &= \varepsilon z^{\intercal} JS(z)R(q)z_r \\
z^{\intercal} S(R(q)z_r)Jz &= z^{\intercal} JS(z)R(q)z_r \\
(z^{\intercal} S(R(q)z_r)Jz)^{\intercal} &= z^{\intercal} JS(z)R(q)z_r \\
z^{\intercal} J^{\intercal} S(R(q)z_r)^{\intercal} z &= z^{\intercal} JS(z)R(q)z_r \\
z^{\intercal} JS(z)R(q)z_r &= z^{\intercal} JS(z)R(q)z_r
\end{aligned} \tag{77}$$

In a similar way, the third and fourth terms of (76) are also equivalent

$$\begin{aligned}
\varepsilon z^{\intercal} S(R(q)z_r)JR(q)z_r &= \varepsilon z_r^{\intercal} R(q)^{\intercal} JS(z)R(q)z_r \\
z^{\intercal} S(R(q)z_r)JR(q)z_r &= z_r^{\intercal} R(q)^{\intercal} JS(z)R(q)z_r \\
(z^{\intercal} S(R(q)z_r)JR(q)z_r)^{\intercal} &= z_r^{\intercal} R(q)^{\intercal} JS(z)R(q)z_r \\
z_r^{\intercal} R(q)^{\intercal} J^{\intercal} S(R(q)z_r)^{\intercal} z &= z_r^{\intercal} R(q)^{\intercal} JS(z)R(q)z_r \\
z_r^{\intercal} R(q)^{\intercal} JS(z)R(q)z_r &= z_r^{\intercal} R(q)^{\intercal} JS(z)R(q)z_r
\end{aligned} \tag{78}$$

By canceling the analogous terms, the time derivative of $V$ becomes

$$\dot{V} = -\varepsilon k_v z^{\intercal} \bar{\Gamma} z < 0, \forall z \neq 0 \tag{79}$$

which implies that $z(t) \to 0$ as $t \to \infty$ (since by assumption $\bar{\Gamma} \succ 0$, $\varepsilon > 0$ and $k_v > 0$).

Next, it is shown that $\epsilon(t)$ and $\eta(t)$ are ultimately bounded. To this end, for a sufficiently large $t$, assume that $\dot{z} = z = 0$, that is, $z_b = z_r$. Then, from (72) with the proposed control law (65), the following is obtained:

$$\epsilon = \frac{1}{k_p} S(R(q)z_r)JR(q)z_r. \tag{80}$$

Taking into account that, by definition, $q^{\intercal} q = 1$ and the fact that $z_r$ is a constant vector, there exists a $c$ as defined in (69) such that $\|\epsilon\| \leq c$. The fact that $\sqrt{1-c^2} \leq |\eta| \leq 1$, with $0 \leq c \leq 1$, follows from the definition presented in Section 2.3.

Finally, when the satellite has a spherical top configuration, with $J = hI_3$, the equation stated in (80) becomes

$$\epsilon = \frac{h}{k_p} S(z_b)z_b = 0,$$

since $z \to 0$, $z_b = R(q)z_r$ and $S(z_b)z_b = 0$. Then, $\eta = 1$ follows from $\eta^2 = 1 - \epsilon^{\intercal}\epsilon$ which completes the proof. □

**Remark 1.** *Notice in view of* (80) *that* $\|\epsilon\|$ *can be made arbitrarily small for a sufficiently large* $k_p$*, at the cost of large control signals. The resulting magnetic moment* $m(t)$ *might be limited by saturation and not be achievable.*

**Remark 2.** *Differently from the adaptive gain suggested by (LOVERA; ASTOLFI, 2006), we assumed that* $\bar{\Gamma}$ *is computed* a priori *from the knowledge of the satellite's reference orbit. As a result, we do not need to implement either a detumbling phase – because a factor for the angular velocity error is always present in the control input – or to continuously calculate the gain* $\Gamma_{av}(t)$ *which led to smaller energy consumption as shown in Chapter 4. When the control gain* $\bar{\Gamma}$ *has to be computed online, we can apply the control law defined in* (65) *by redefining* $y = \bar{\Gamma}^{\imath}(t)\epsilon(t)$*, for* $t \in [0, T)$*, where* $\bar{\Gamma}^{\imath}$ *stands for the pseudo inverse of* $\bar{\Gamma}$*, which could be used on the initial moments.*

Thus, by knowing the satellite orbit and with the aid of a magnetic field model, a fixed controller gain $\bar{\Gamma}$ can be established for the system, without the need to continuously update its value.

# 4 NUMERICAL RESULTS

Once the necessary parameters that govern the satellite dynamics in orbit were established and the proposed controller was validated, it is possible to simulate and assess its efficiency when dealing with different initial conditions and different types of satellites. In order to evaluate how the proposed fixed controller performs compared to the adaptive controller, a satellite with an asymmetrical top configuration, similar to the one used by (LOVERA; ASTOLFI, 2006) was chosen. Although it does not consist of a CubeSat specification, this type of satellite is not uncommon in the literature, e.g. (WISNIEWSKI, 1997).

Using this configuration, two initial attitude conditions were tested and, for both conditions, two different magnetic field models were used. After these four comparisons, the fixed controller was evaluated with two CubeSat configurations based on parameters found in the literature and with magnetorquer parameters found in commercial, out-of-the-shelf products. Even though both the adaptive and the fixed controller proposed utilize the average model given in (68) to formulate their parameters, the numerical results presented were obtained using the satellite model given in (37) and the error dynamics given in (42). All satellites configurations simulated belong to a fixed, circular orbit set in a polar orbit configuration, with an $87^o$ inclination with respect to the equatorial plane, beginning at the Equator, at an altitude of 450 km from Earth's surface, and completing 15 orbits in one day.

## 4.1 Controllers comparison

Along with the orbital parameters given previously, it is necessary to determine the satellite parameters in order to perform a simulation. Following the hypothetical satellite presented by (LOVERA; ASTOLFI, 2006), the inertia matrix chosen was given by (81). Note that the second element of the inertia matrix is much smaller than the other two. That configuration aims to represent a satellite with a long gravity gradient boom along the y axis, similar to projects like the Ørsted satellite (WISNIEWSKI, 1997). However, this configuration cannot be physically achieved since the elements of the diagonal do not

respect the triangular inequality.

$$J = \begin{bmatrix} 60 & 0 & 0 \\ 0 & 5 & 0 \\ 0 & 0 & 70 \end{bmatrix} kgm^2. \tag{81}$$

For this satellite model, two initial conditions were tested: the first consists of the satellite oriented “upside down" from its desired orientation and with a small angular velocity; the second situation consists of the satellite with a random orientation and a higher angular velocity than before. The aim of these scenarios is to investigate the efficiency of the control laws in: (a) targeting the desired attitude; (b) addressing the detumbling phase; (c) achieving tracking in the presence of large initial velocities; and (d) saving energy consumption.

In order to make it easier for the reader, the initial attitudes are determined with *roll*, *pitch*, and *yaw* angles, which were converted to quaternion using a 1-2-3 sequence of rotation. Both conditions are shown in Tables 1 and 2, respectively. To simplify these initial conditions will be referred to as *Upside Down* and *Random*, respectively.

Table 1 – Satellite’s initial conditions - Upside Down initial condition.

| Axis (local frame) | Reference initial Attitude | Reference initial Angular Velocity $\omega_r$ (rad/s) | Satellite initial Attitude | Satellite initial Angular Velocity $\omega_b$ (rad/s) |
|---|---|---|---|---|
| X | 0 | 0 | 0 | 0.0011 |
| Y | 0 | 0.0011 | $\pi$ | 0.0011 |
| Z | $\pi$/2 | 0 | $\pi$/2 | 0.0011 |

Table 2 – Satellite’s initial conditions - Random initial condition.

| Axis (local frame) | Reference initial Attitude | Reference initial Angular Velocity $\omega_r$ (rad/s) | Satellite initial Attitude | Satellite initial Angular Velocity $\omega_b$ (rad/s) |
|---|---|---|---|---|
| X | 0 | 0 | $-\pi$/4 | -0.01 |
| Y | 0 | 0.0011 | $\pi$/8 | 0.01 |
| Z | $\pi$/2 | 0 | $-\pi$/16 | 0.005 |

For both conditions, the objective is to make the error quaternion becomes $q = \begin{bmatrix} 1 & 0 & 0 & 0 \end{bmatrix}^\intercal$ while the angular velocity error $\omega = \begin{bmatrix} 0 & 0 & 0 \end{bmatrix}^\intercal$. The controller parameters chosen were $\epsilon = 0.0001$, $K_p = 500$, and $K_v = 200$, in order to use the same gain values as (LOVERA; ASTOLFI, 2006). The fixed gain matrix $\bar{\Gamma}$ depends only on the magnetic field $B_r(t)$ seen at the desired reference frame. For the Dipole model, its value was determined as:

$$\bar{\Gamma} = \begin{bmatrix} 1.4996 & 0 & -0.0470 \\ 0 & 1.2860 & 0 \\ -0.0470 & 0 & 1.8033 \end{bmatrix}, \tag{82}$$

For the IGRF model, $\bar{\Gamma}$ was determined as:

$$\bar{\Gamma} = \begin{bmatrix} 1.4393 & 0.0997 & 0.0681 \\ 0.0997 & 1.2874 & 0.0794 \\ 0.0681 & 0.0794 & 1.9383 \end{bmatrix}. \tag{83}$$

### 4.1.1 Upside Down Initial Condition

Among all possible initial attitudes on a satellite, the worst case would be for it to be "upside down" from its desired orientation. In this case, the attitude system has to rotate the satellite half turn around one of its axes to get the correct orientation. Along with that, the angular velocity might not be the same as the reference, requiring the satellite to slow down (or speed up), accordingly. Table 1 set what will be called Upside Down initial condition for the experiments. In order to emphasize the rotation effort demanded to the controller, the initial angular velocity $\omega_b(t)$ chosen was similar to the desired angular velocity of the reference $\omega_r$.

#### *4.1.1.1 Dipole Model*

For the first simulation of the Upside Down initial condition, the Dipole model for the magnetic field was used. Both controllers were simulated for a total of six orbits and the Fixed controller used (82). Figures 10 and 11 show the results obtained for this case.

Figure 10 – Error Quaternion - Upside Down initial condition with Dipole model: Adaptive controller (red dashed line) and Fixed controller (blue solid line).

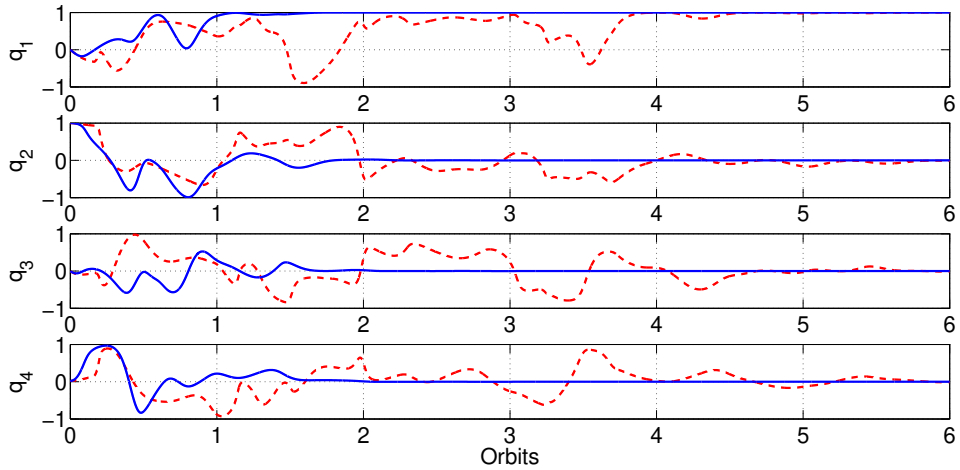


Source: The author.

The error quaternion and the angular velocity error graphics indicate that both controllers achieved the targeted objective, although the Adaptive controller seems to reach it much closer to the end of the six orbits while the Fixed controller achieves that in about two orbits. In order to better compare the results, the amount of energy used by the controllers was recorded and normalized, using the Adaptive controller result as the base.

Figure 11 – Angular Velocity error - Upside Down initial condition with Dipole model: Adaptive controller (red dashed line) and Fixed controller (blue solid line).

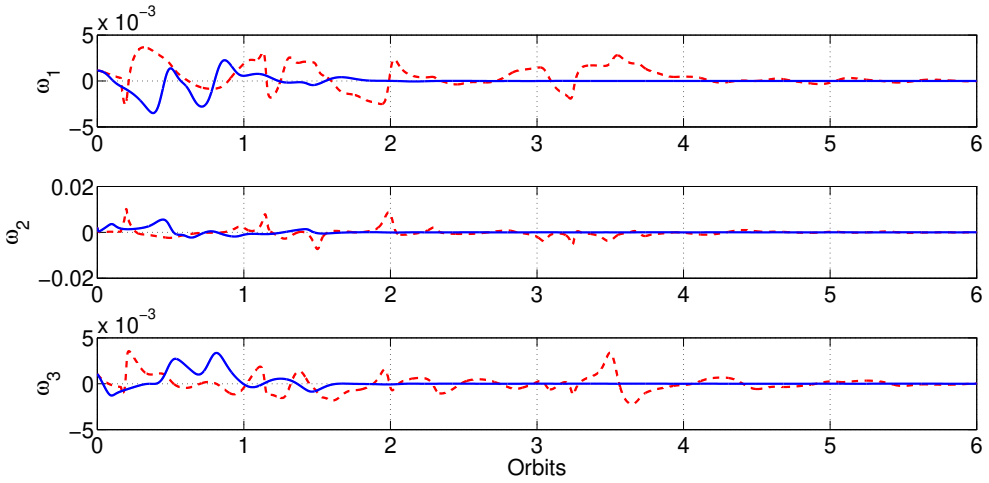


Source: The author.

The result for the energy used is summarized in Table 3. A graphic visualization of the energy used throughout the simulation can be seen in Figure 12. Both the table and the graphic shows that the Fixed controller proposed had a better result.

Figure 12 – Energy used by controllers normalized - Upside Down initial condition with Dipole model: Adaptive controller (red dashed line) and Fixed controller (blue solid line).

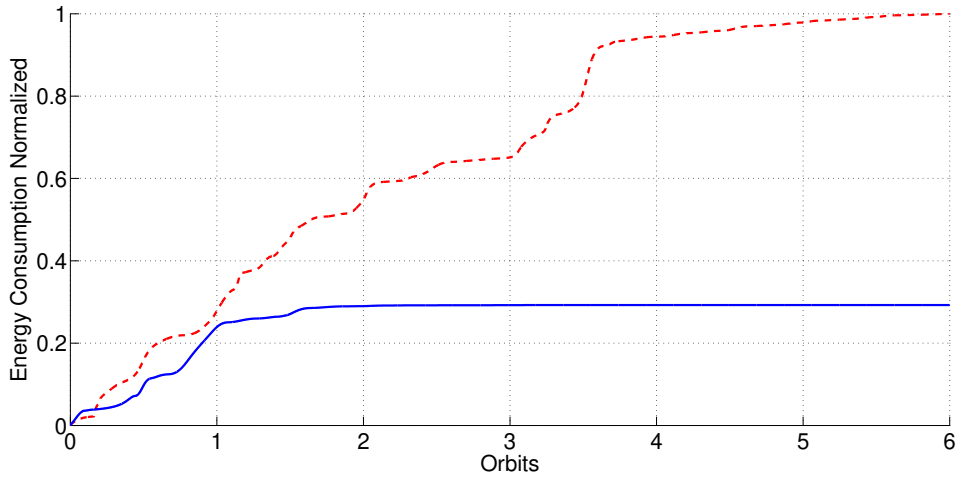


Source: The author.

Table 3 – Energy used by controllers normalized - Upside Down initial condition with Dipole model.

| Controller | Energy (normalized) |
|---|---|
| Adaptive | 1 |
| Fixed | 0.292564 |

The individual use of each magnetorquer is illustrated in Figures 13 and 14. For these

initial simulations, no saturation was considered. It can be seen that the magnetorquer use by the Fixed gain controller basically stops after the second orbit as indicated by the Energy used graphic as well.

Figure 13 – Magnetoquer use for Adaptive gain - Upside Down initial condition with Dipole model.

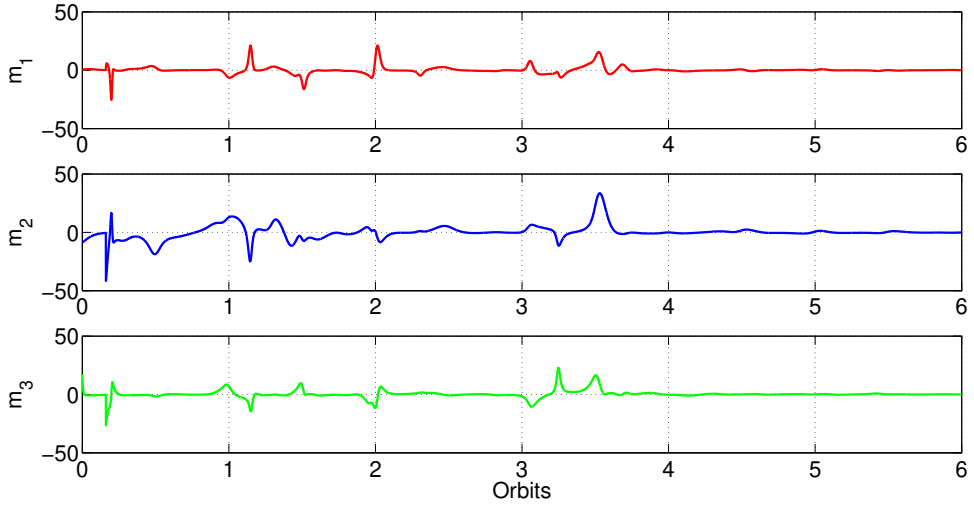


Source: The author.

Figure 14 – Magnetoquer use for Fixed gain - Upside Down initial condition with Dipole model.

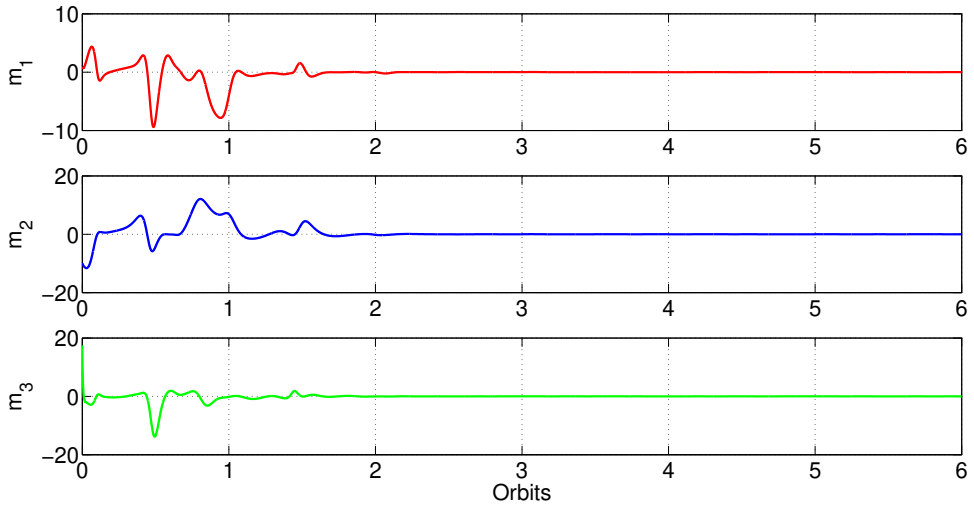


Source: The author.

#### *4.1.1.2 IGRF Model*

For the second simulation of the Upside Down initial condition, the IGRF model for the magnetic field was used. Both controllers were simulated for a total of six orbits and the Fixed controller used (83). Figures 15 and 16 show the results obtained for the simulation.

Figure 15 – Error Quaternion - Upside Down initial condition with IGRF model: Adaptive controller (red dashed line) and Fixed controller (blue solid line).

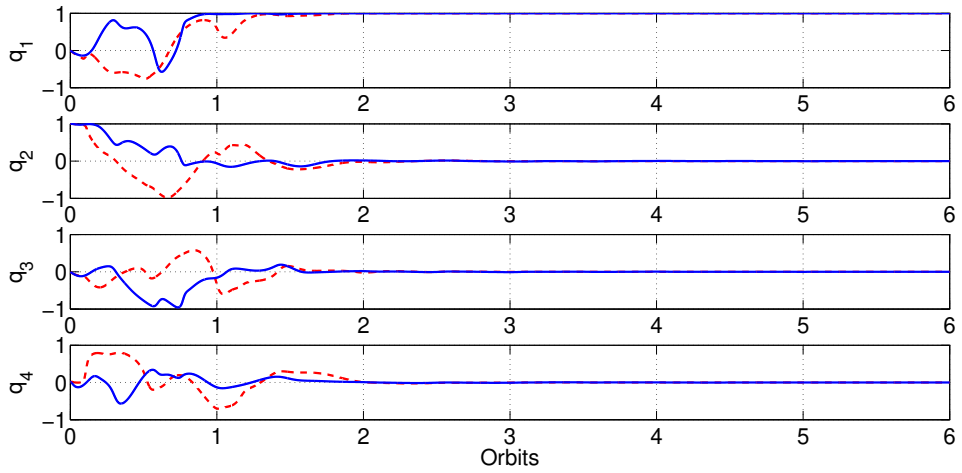


Source: The author.

Figure 16 – Angular Velocity error - Upside Down initial condition with IGRF model: Adaptive controller (red dashed line) and Fixed controller (blue solid line).

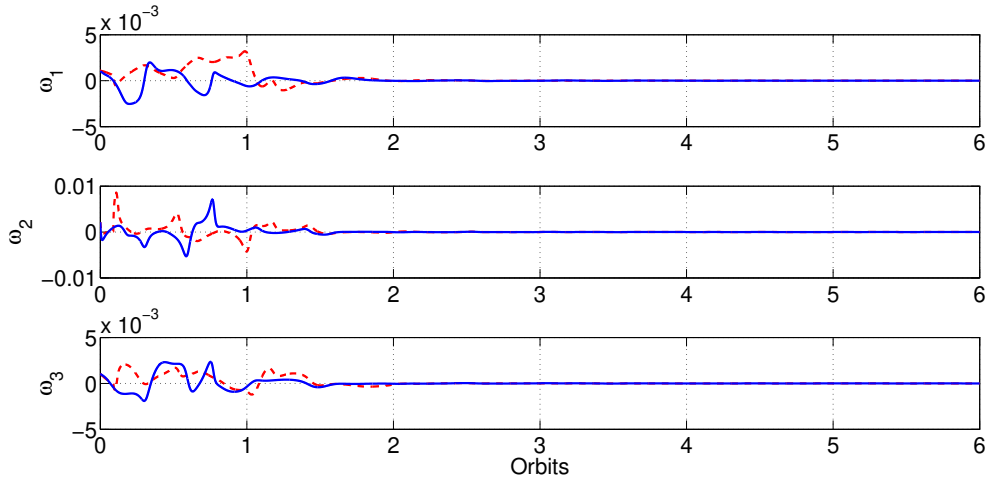


Source: The author.

After the change in the magnetic field model, the error quaternion and angular velocity error graphics indicate that both controllers achieved the objective in about two orbits. These results indicate that both controllers have similar effectiveness in achieving the objective. The analysis of the amount of energy used by the controllers can be used as a tiebreaker. Once again, the energy was recorded and normalized, using the Adaptive controller result as the base. The result for the energy used can be seen in Table 4.

Table 4 – Energy used by controllers normalized - Upside Down initial condition with IGRF model.

| Controller | Energy (normalized) |
|---|---|
| Adaptive | 1 |
| Fixed | 0.766543 |

Once again, the Fixed controller utilized less energy to achieve the objective, indicating that it is a better alternative. A graphic visualization of the energy used throughout the simulation can be seen in Figure 17. The graphic indicates that the Fixed controller required more energy on the first orbit but that effort was reduced afterward, opposite to the Adaptive controller which uses a greater amount of energy on the second orbit.

Figure 17 – Energy used by controllers normalized - Upside Down initial condition with IGRF model: Adaptive controller (red dashed line) and Fixed controller (blue solid line).

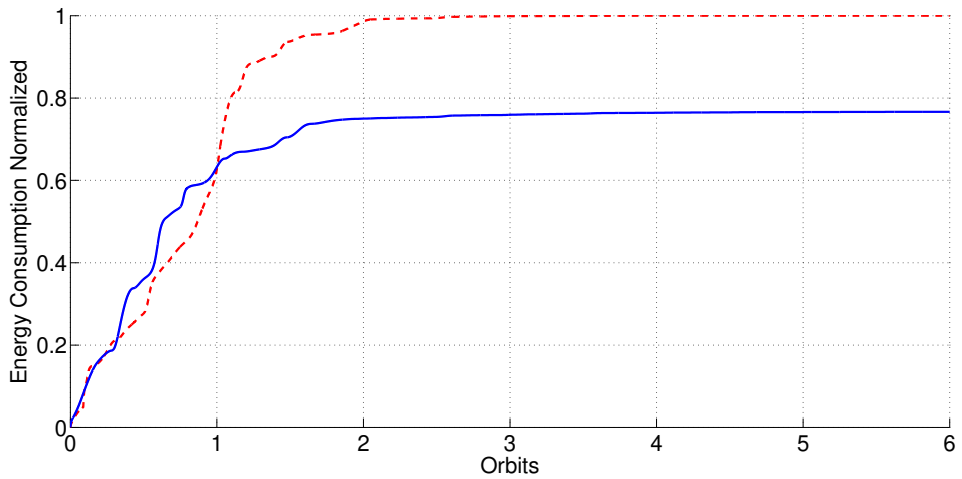


Source: The author.

The individual use of each magnetorquer is illustrated in Figures 18 and 19. Similar to the previous simulation, no saturation was considered on these actuators. It can be seen from the graphics that the magnetorquers stop after the second orbit on both controllers.

Figure 18 – Magnetoquer use for Adaptive gain - Upside Down initial condition with IGRF model.

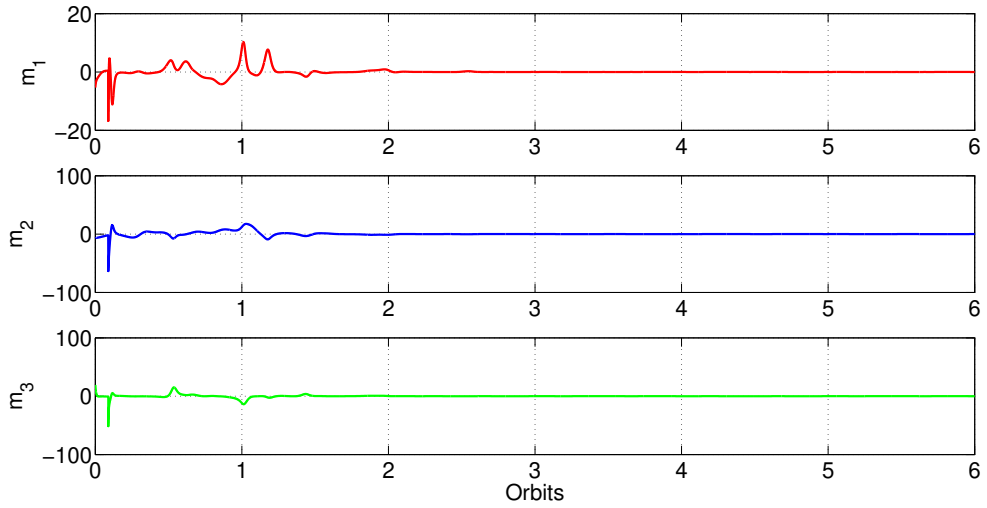


Source: The author.

Figure 19 – Magnetoquer use for Fixed gain - Upside Down initial condition with IGRF model.

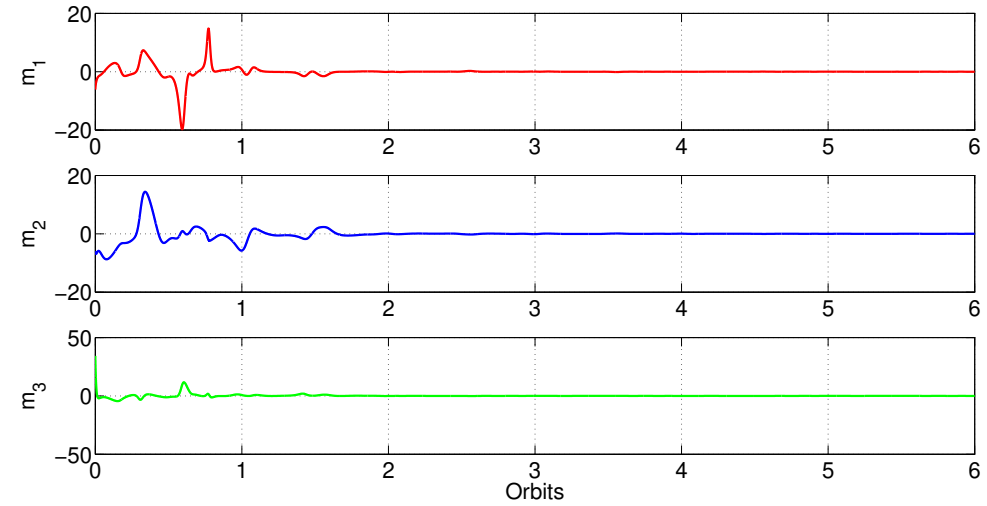


Source: The author.

### 4.1.2 Random Initial Condition

After the satellite leaves the delivery platform, it ideally would have the correct orientation and angular velocity or at least some attitude closer to it. However, initial conditions in orbit depend on the satellite deployer configuration and settings and any sort of unpredictable event might happen. Consequently, the satellite might start with a very different attitude than planned. In this case, the attitude system has to identify its current attitude and rotate the satellite to achieve the correct orientation. It might be required to slow down (or speed up) the angular velocity to keep the satellite at the desired reference as well. Right after deployment, it is common for satellites to have high angular velocities.

Table 2 set what will be called the Random initial condition for the experiments. Note that the initial angular velocities set were higher than the Upside Down initial condition. This was chosen so a greater effort is put to correct the angular velocity.

#### *4.1.2.1 Dipole Model*

For the first simulation of the Random initial condition, the Dipole model for the magnetic field was used. Both controllers were simulated for a total of six orbits and the Fixed controller used (82). Figures 20 and 21 show the results obtained for this simulation.

Figure 20 – Error Quaternion - Random initial condition with Dipole model: Adaptive controller (red dashed line) and Fixed controller (blue solid line).

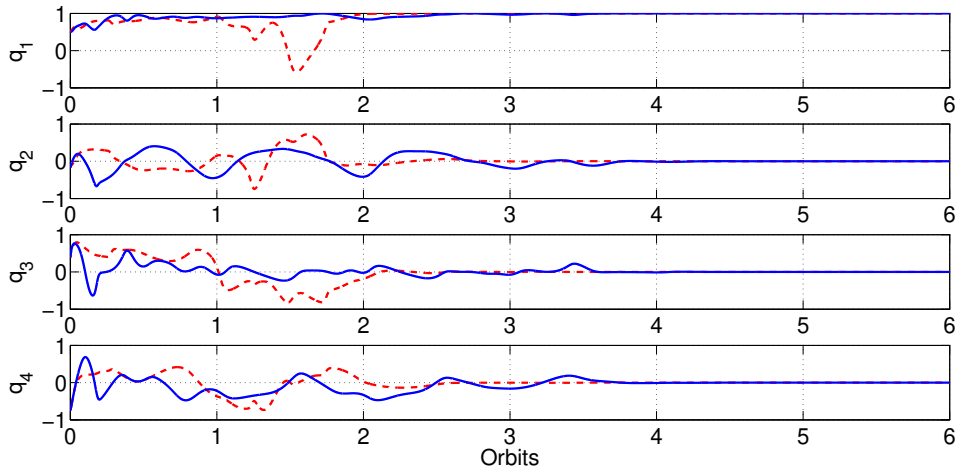


Source: The author.

Figure 21 – Angular Velocity error - Random initial condition with Dipole model: Adaptive controller (red dashed line) and Fixed controller (blue solid line).

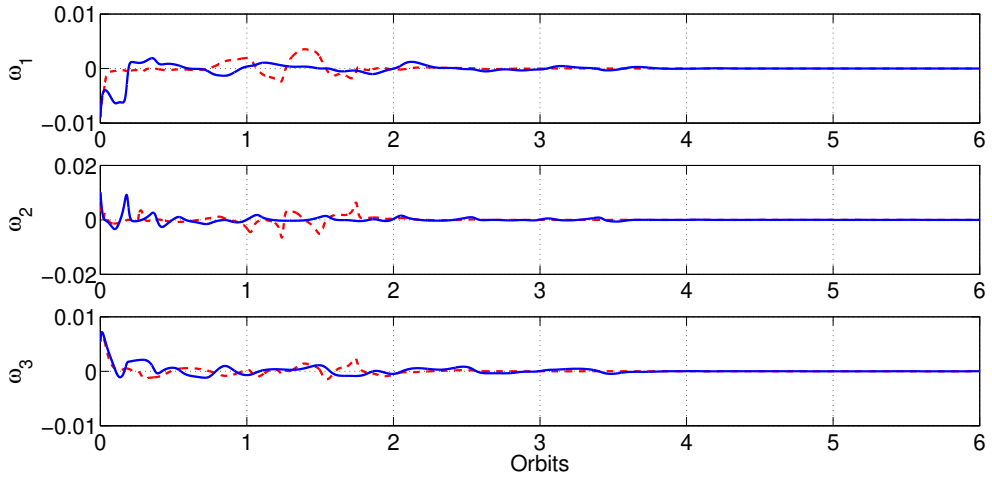


Source: The author.

The error quaternion and angular velocity error graphics indicate that both controllers achieved the objective of aligning the satellite to the reference. The Adaptive controller

reaches the objective in about three orbits while the Fixed controller appears to require four orbits to completely position the satellite to the reference, as the values of error quaternion indicate. In order to complement these results and better compare the efficiency of the controllers, the amount of energy used by each controller was recorded and normalized, using the Adaptive controller result as the base. The result for the energy used can be seen in Table 5.

Table 5 – Energy used by controllers normalized - Random initial condition with Dipole model.

| Controller | Energy (normalized) |
|---|---|
| Adaptive | 1 |
| Fixed | 0.861840 |

A graphic visualization of the energy used throughout the simulation can be seen in Figure 22. The graphic shows clearly that the Fixed controller only completes its effort around the fourth orbit while the Adaptive controller reaches the objective at the third orbit. However, once again, the Fixed controller required less energy to complete the task.

Figure 22 – Energy used by controllers normalized - Random initial condition with Dipole model: Adaptive controller (red dashed line) and Fixed controller (blue solid line).

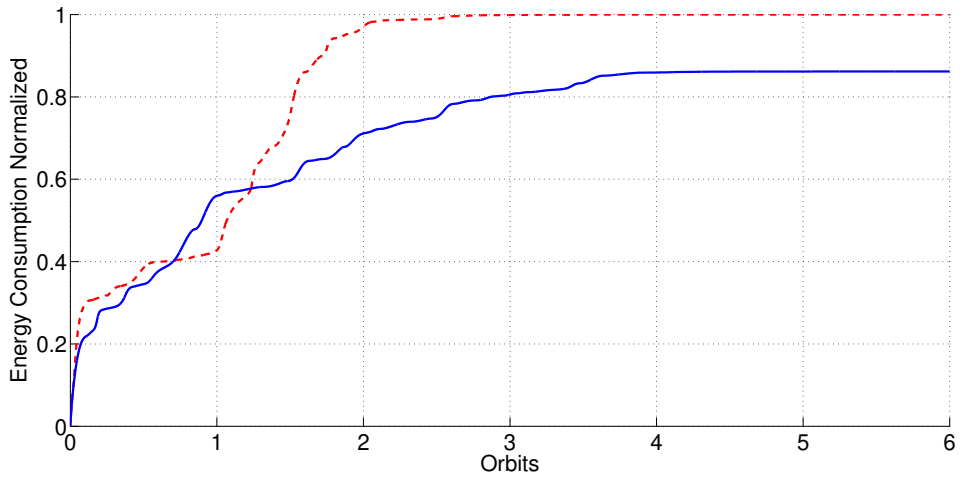


Source: The author.

Figures 23 and 24 show how the magnetorquers were activated on each simulation. Since no saturation was considered, there is a great effort at the beginning to correct the angular velocity followed by some attitude corrections, specially before the second orbit is completed.

Figure 23 – Magnetoquer use for Adaptive gain - Random initial condition with Dipole model.

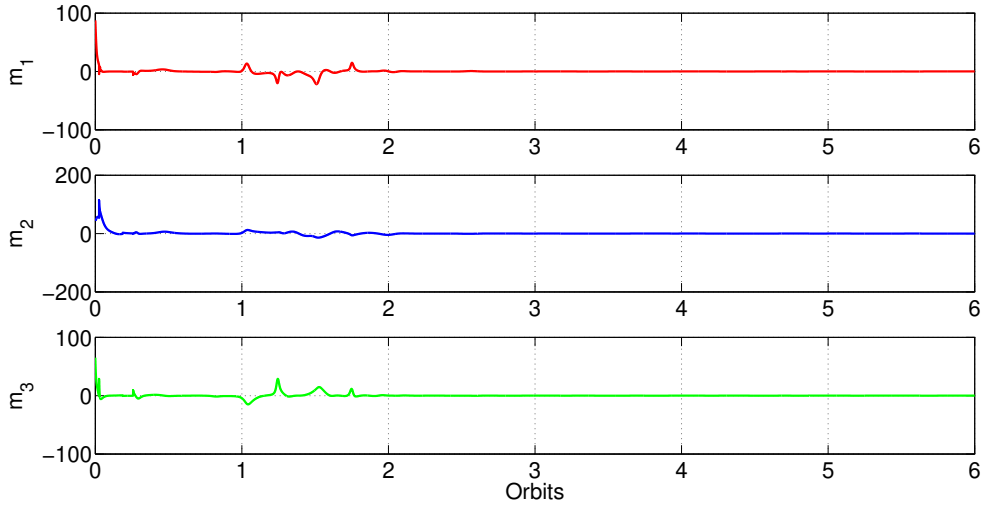


Source: The author.

Figure 24 – Magnetoquer use for Fixed gain - Random initial condition with Dipole model.

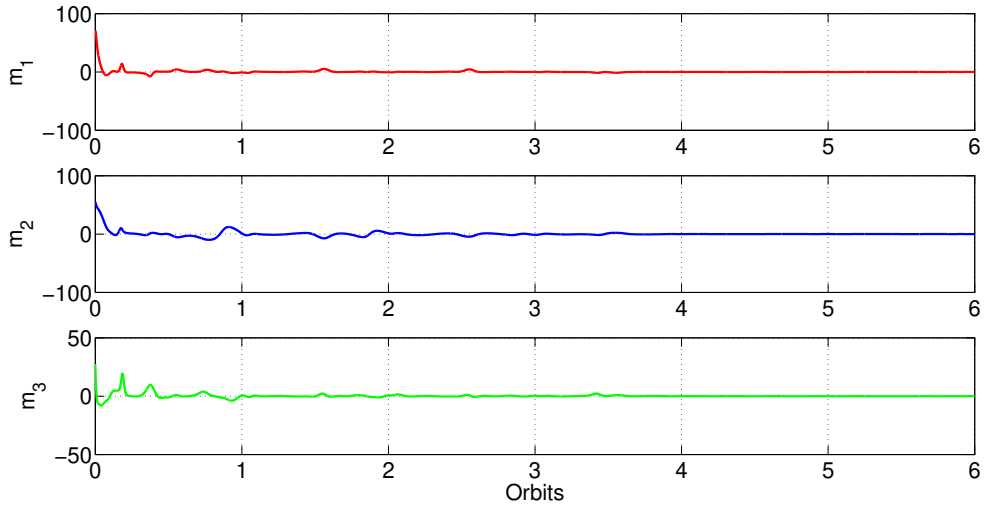


Source: The author.

#### *4.1.2.2 IGRF Model*

For the second simulation of the Random initial condition, the IGRF model for the magnetic field was used. Both controllers were simulated for a total of six orbits and the Fixed controller used (83). Figures 25 and 26 show the results obtained for the simulation.

Figure 25 – Error Quaternion - Random initial condition with IGRF model: Adaptive controller (red dashed line) and Fixed controller (blue solid line).

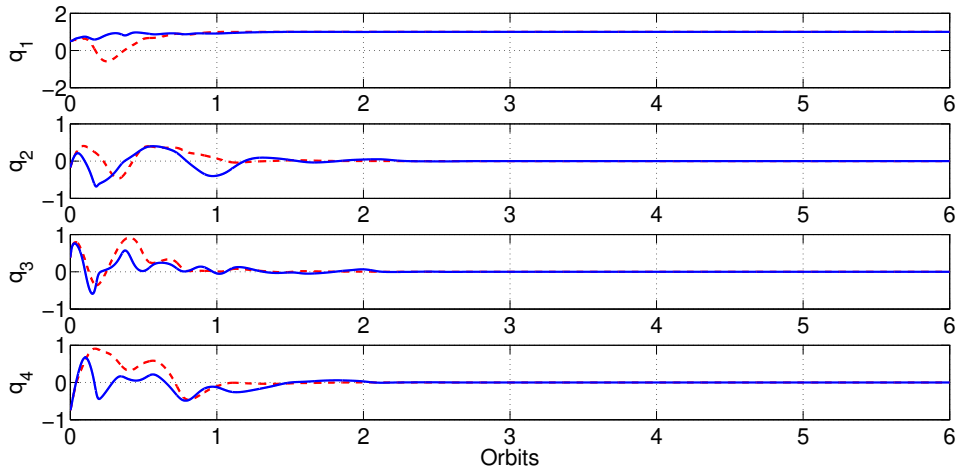


Source: The author.

Figure 26 – Angular Velocity error - Random initial condition with IGRF model: Adaptive controller (red dashed line) and Fixed controller (blue solid line).

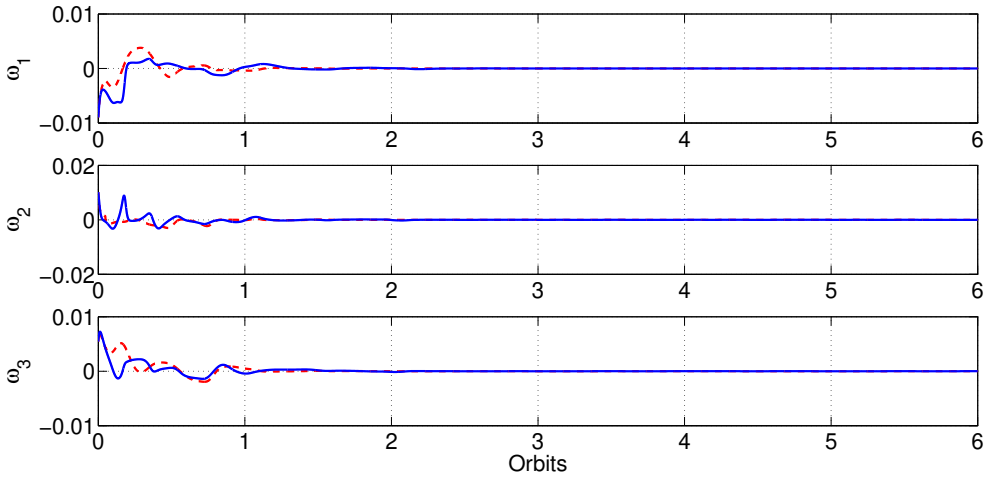


Source: The author.

The error quaternion and angular velocity error graphics indicate that both controllers achieved the objective in about two orbits. For this scenario, it is even harder to determine any difference between performances since both controllers reach the objective around the same moment (despite their different ways).

The amount of energy used by the controllers can be used to determine which controller is more efficient. The recorded energy used was normalized, using the Adaptive controller result as the base, and presented in Table 6. A graphic visualization of the energy used throughout the simulation can be seen in Figure 27. Considering that both controllers achieved the objective at the same time, the table and the graphic shows that the fixed controller had better efficiency in doing so.

Table 6 – Energy used by controllers normalized - Random initial condition with IGRF model.

| Controller | Energy (normalized) |
|---|---|
| Adaptive | 1 |
| Fixed | 0.833924 |

Figure 27 – Energy used by controllers normalized - Random initial condition with IGRF model: Adaptive controller (red dashed line) and Fixed controller (blue solid line).

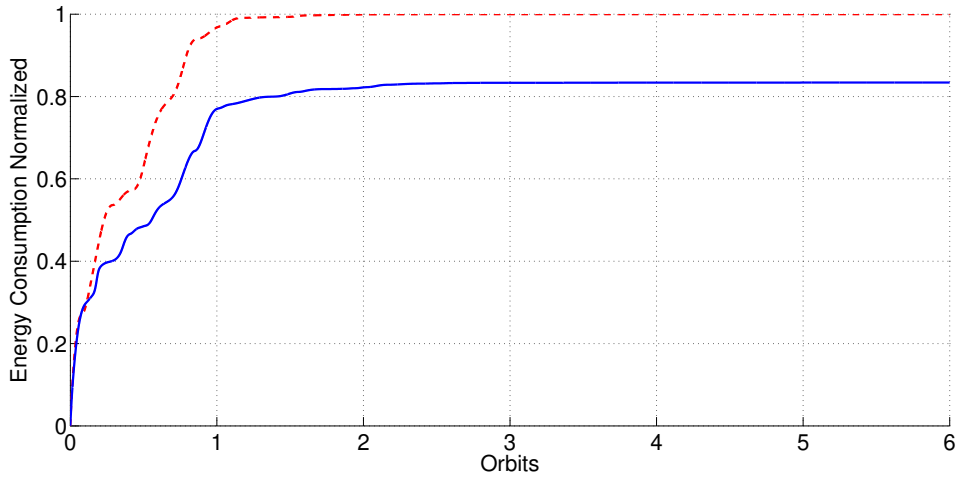


Source: The author.

The individual use of each magnetorquer is illustrated in Figures 28 and 29. As was expected, the magnetorquers are practically not use after the second orbit, on both controllers.

Figure 28 – Magnetoquer use for Adaptive gain - Random initial condition with IGRF model.

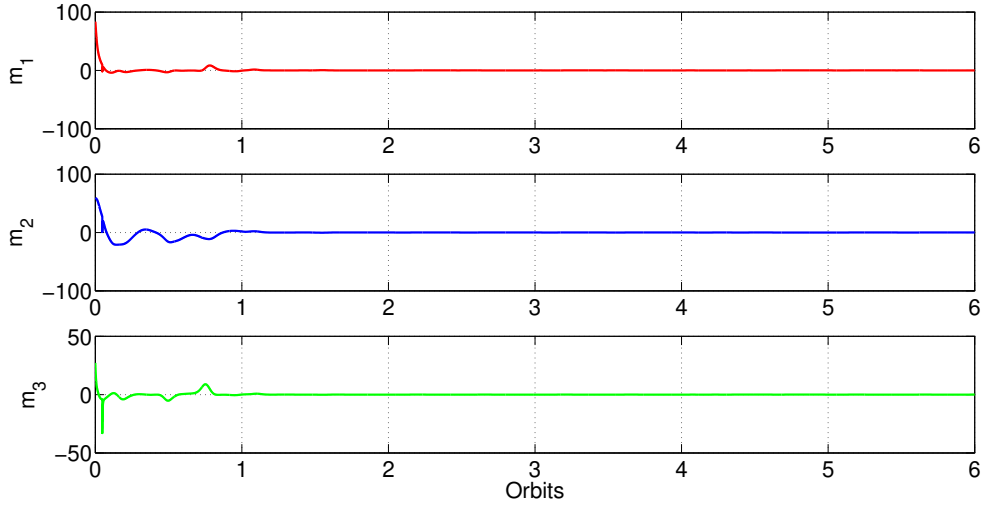


Source: The author.

Figure 29 – Magnetoquer use for Fixed gain - Random initial condition with IGRF model.

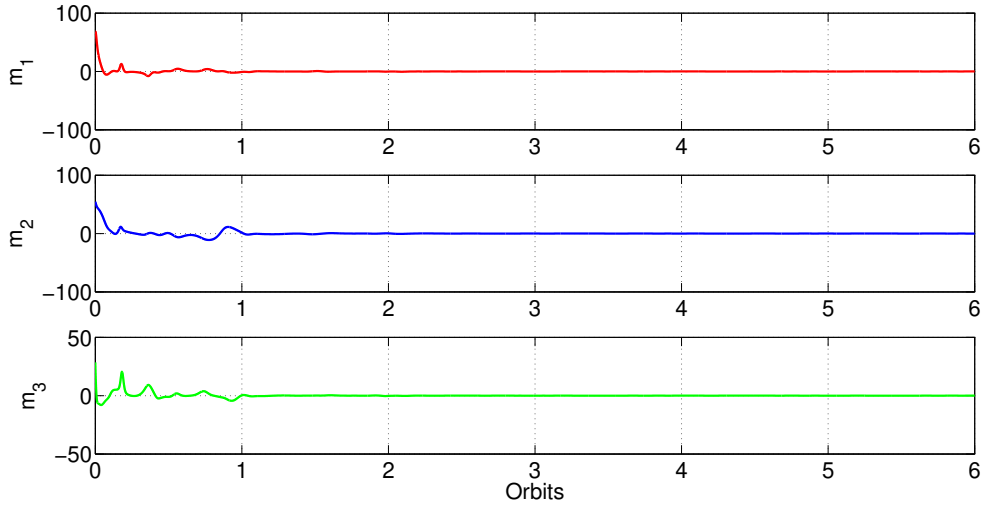


Source: The author.

## 4.2 Fixed controller performance on CubeSats

After comparing the results obtained by the Adaptive and Fixed controllers assessing the same theoretical satellite, the Fixed controller was simulated with two different satellite models, with two inertia matrices based on different CubeSat sizes obtained from the literature. The first inertia matrix is taken from a 2U CubeSat project given in (BAUER, 2021). The second inertia matrix is based on a 1U CubeSat described in (LI; POST; LEE, 2013). The same orbital parameters and the same initial conditions were tested as before.

The only magnetic model used for these simulations was the IGRF model, due to its greater accuracy when compared to the Dipole model. Therefore, the only value used for the gain matrix $\bar{\Gamma}$ was (83). Also, for these satellite models, it was considered that the magnetorquers had a capacity of $0.019\ Am^2$. Thus, for any magnetic moment $m(t)$ stronger than that, the actuator would saturate. This value was chosen based on an *off-the-shelf* magnetorquers available for purchase (MT01: COMPACT MAGNETORQUER, 2023) and estimated values found in the literature (LI; POST; LEE, 2013). The situations which the models went through tried to induce and assess this saturation.

### 4.2.1 2U CubeSat

A 2U Cubesat basically consists of two 1U CubeSat piled together. The value for the inertia matrix $J$ for the 2U CubeSat model was obtained from (BAUER, 2021) and is given by

$$J = \begin{bmatrix} 0.0359 & 0.0014 & 0.0031 \\ 0.0014 & 0.0398 & 0.0024 \\ 0.0031 & 0.0024 & 0.0483 \end{bmatrix} kgm^2. \tag{84}$$

The abovementioned paper used an attitude control system with reaction wheels instead of magnetorquers but the influence of the reaction wheels was disregarded while determining the inertia matrix. Note that this inertia matrix is similar to the previous model in the point of $J_{XX} \neq J_{YY} \neq J_{ZZ}$ but its components are a lot smaller, demanding that the gains $K_p$ and $K_v$ to be reduced as well.

For this model, two different pairs of gains were tested: one pair with smaller values for $K_p$ and $K_v$; another pair with bigger values for $K_p$ and $K_v$. The values for the gains were chosen empirically, based on values used in Section 4.1 and the reduction of scale of $J$. In order to make it easier to read the results, the first pair will be called *Weak gain*, and the second pair will be called *Strong gain* and their values are summarized in table 7.

Table 7 – [Controller parameters - 2U CubeSat]Controller parameters - 2U CubeSat.

| | Gain | Value |
|---|---|---|
| Weak | $K_p$ | 0.1 |
| | $K_v$ | 0.04 |
| Strong | $K_p$ | 0.25 |
| | $K_v$ | 0.1 |

#### *4.2.1.1 Upside Down Initial Condition*

For the first simulation of the 2U CubeSat model, the Upside Down initial condition given by Table 1 was used. The model was simulated for a total of eight orbits for each pair of gains. Figures 30 and 31 show the results obtained for the simulation.

Figure 30 – Error Quaternion - Upside Down initial condition - 2U CubeSat: Strong gain (red dashed line) and Weak gain (blue solid line).

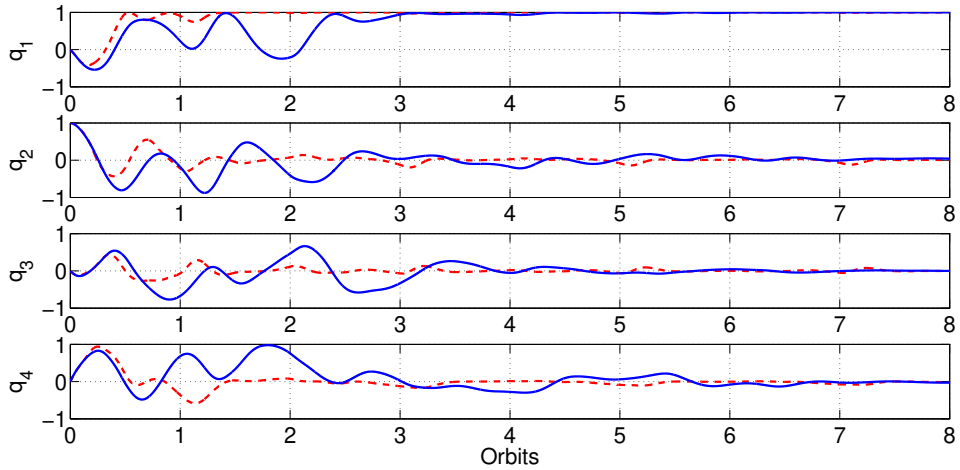


Source: The author.

The error quaternion and angular velocity error graphics indicate that both controllers still generate some attitude adjustments, albeit small, after eight orbits. The graphic visualization and the normalized energy used of these two gain configurations are shown

Figure 31 – Angular velocity error - Upside Down initial condition - 2U CubeSat: Strong gain (red dashed line) and Weak gain (blue solid line).

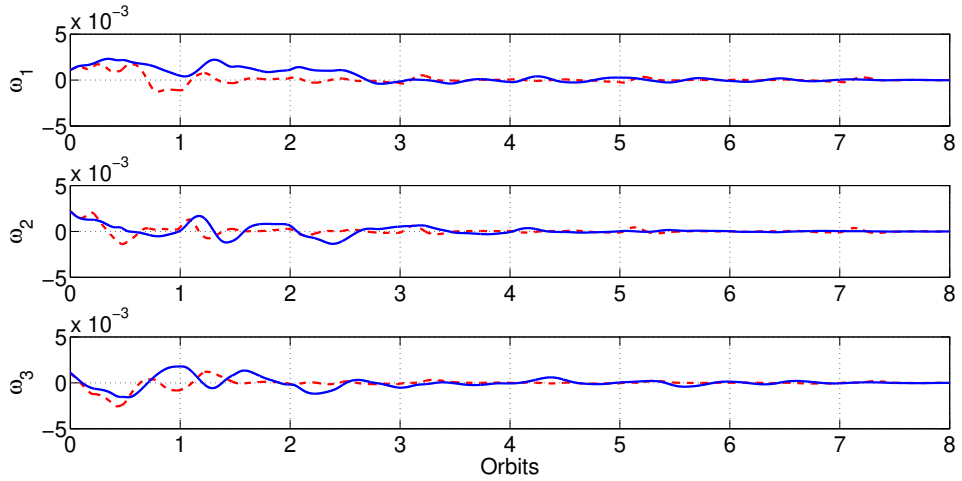


Source: The author.

in Table 8 and Figure 32, respectively. The table indicates that the Weak gain pair consumed less energy at the task while the graphic confirms that the objective was achieved by neither pair since the energy used continues to increase on both lines.

Table 8 – Energy used on 2U CubeSat - Upside Down initial condition.

| Controller | Energy (normalized) |
|---|---|
| Strong gain | 1 |
| Weak gain | 0.494992 |

Figure 32 – Energy used - Upside Down initial condition - 2U CubeSat: Strong gain (red dashed line) and Weak gain (blue solid line).

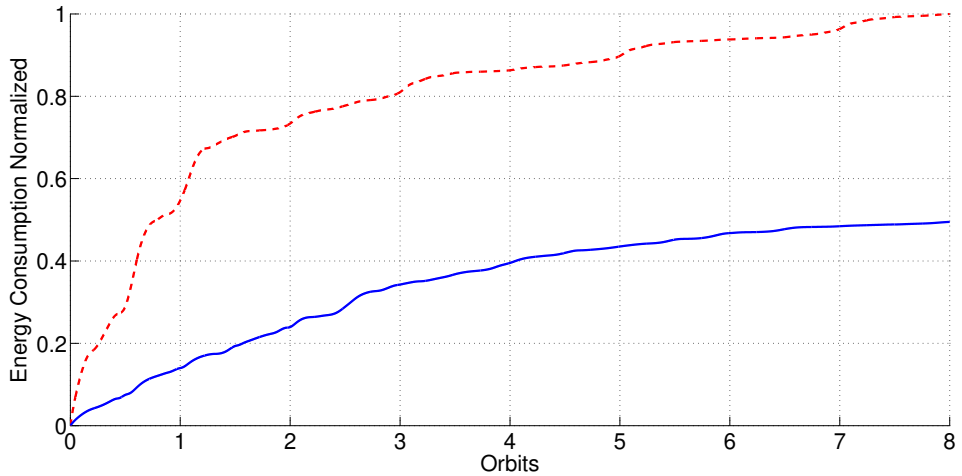


Source: The author.

The individual use of each magnetorquer for each pair of gains is illustrated in Figures 33 and 34. Looking at these graphics, it is possible to notice a relevant difference

between the gain pairs, namely, the Strong gain has saturation on all three magnetorquers at the beginning. These saturations coincide with the steep inclination of the energy used graphic around the first orbit.

Figure 33 – Magnetoquer use for Weak gain - Upside Down initial condition - 2U CubeSat.

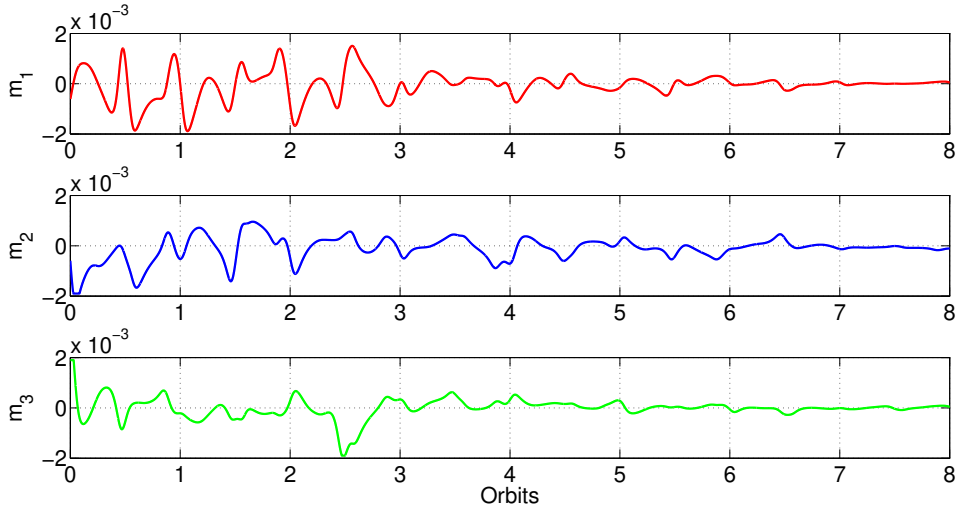


Source: The author.

Figure 34 – Magnetoquer use for Strong gain - Upside Down initial condition - 2U CubeSat.

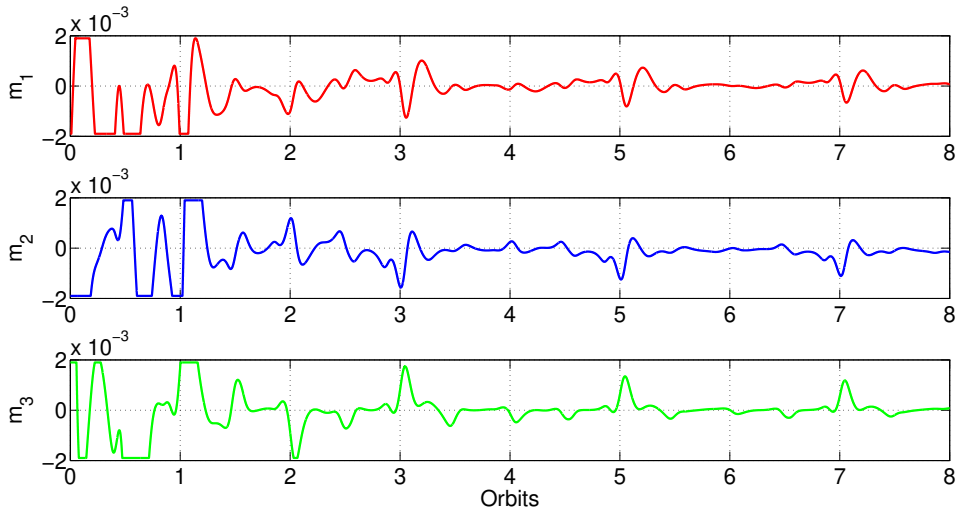


Source: The author.

#### *4.2.1.2 Random Initial Condition*

For the second simulation of the 2U CubeSat model, the Random initial condition given by Table 2 was used. The model was also simulated for a total of eight orbits for each pair of gains. Figures 35 and 36 show the results obtained for this initial condition.

The angular velocity error graphic indicates that both pairs of gains achieved the objective however the error quaternion graphic indicates that both controller configurations

Figure 35 – Error Quaternion - Random initial condition - 2U CubeSat: Strong gain (red dashed line) and Weak gain (blue solid line).

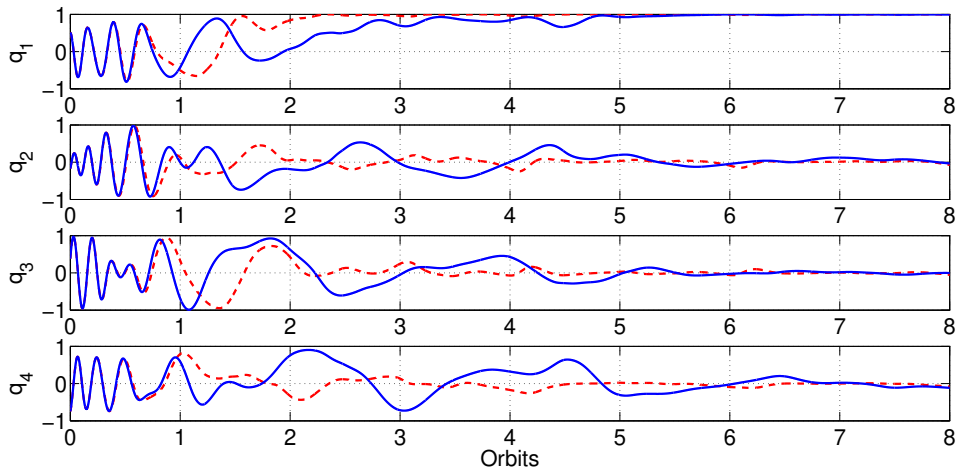


Source: The author.

still generate some attitude adjustments after eight orbits. It is interesting to notice that both configurations presented a very similar result for the first orbit but differ on the following orbits. This is easily explained by observing the magnetorquers use graphics shown in Figure 38 and 39.

Figure 36 – Angular velocity error - Random initial condition - 2U CubeSat: Strong gain (red dashed line) and Weak gain (blue solid line).

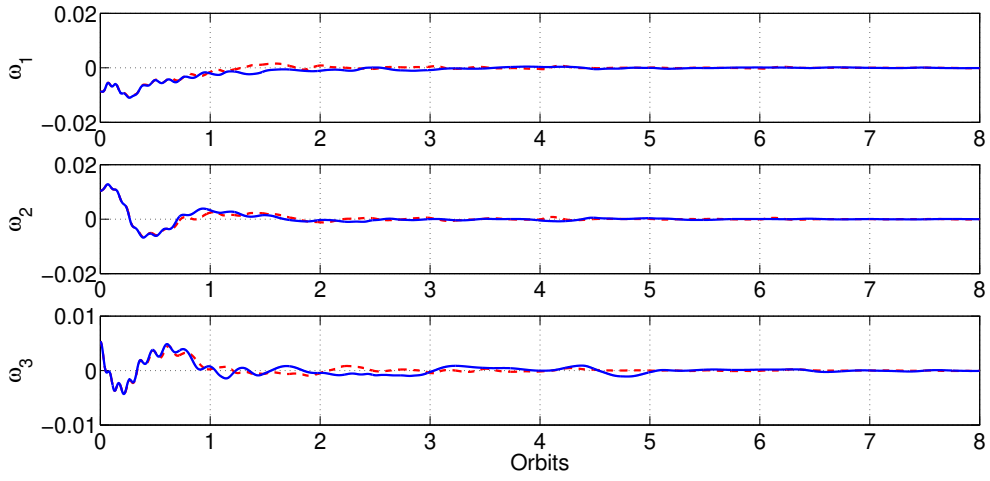


Source: The author.

The graphic visualization and the normalized energy used of these two gain configurations are shown in Table 9 and Figure 37, respectively. Once again, the table indicates that the Weak gain pair consumed a lot less energy at the task while the graphic confirms that the objective was achieved by neither pair since the energy used continues to increase, albeit smoothly, on both lines.

Figure 37 – Energy used - Random initial condition - 2U CubeSat: Strong gain (red dashed line) and Weak gain (blue solid line).

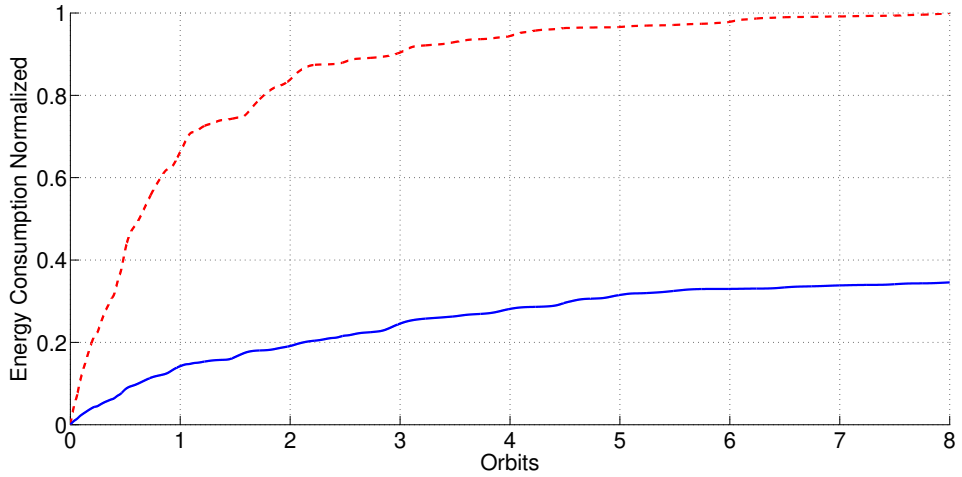


Source: The author.

Table 9 – Energy used on 2U CubeSat - Random initial condition.

| Controller | Energy (normalized) |
|---|---|
| Strong gain | 1 |
| Weak gain | 0.345661 |

The individual use of each magnetorquer for each pair of gains is illustrated in Figures 38 and 39. Looking at these graphics, it is possible to notice a relevant difference from the results obtained for the Upside Down initial condition, namely, both configurations have saturation on the first orbits. This is easily explained by the fact that the Random initial condition demands a bigger effort to slow down the satellite.

Figure 38 – Magnetoquer use for Weak gain - Random initial condition - 2U CubeSat.

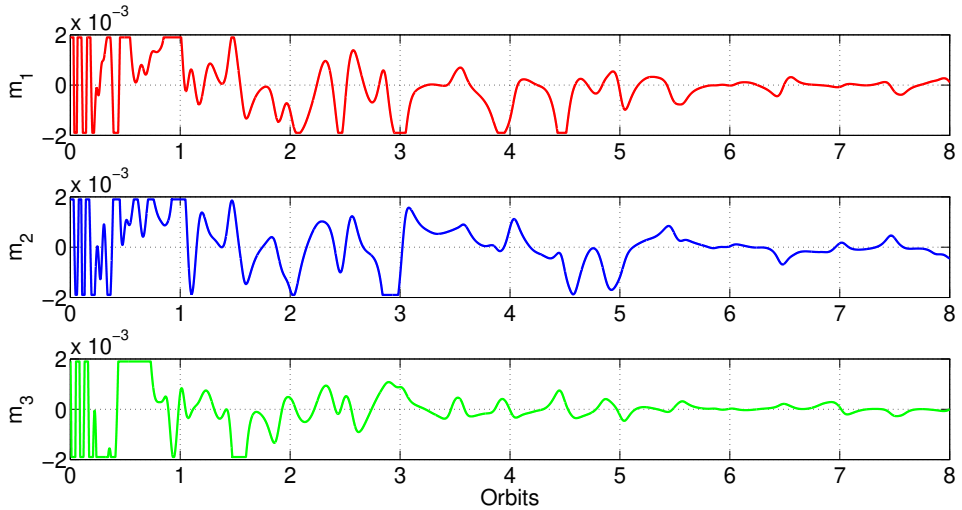


Source: The author.

The resemblance of the error quaternion and angular velocity error presented previously are also explained here. Both configurations presented similar magnetorquer use on the first orbit, resulting in a similar dynamic. The higher presence of saturation on the Strong gain pair after the first orbit explains the higher use of energy. Also, the predominance of saturations on the first orbits coincides with the steep inclination of the energy used graphic, although this is not so evident on the Weak gain curve.

Figure 39 – Magnetoquer use for Strong gain - Random initial condition - 2U CubeSat.

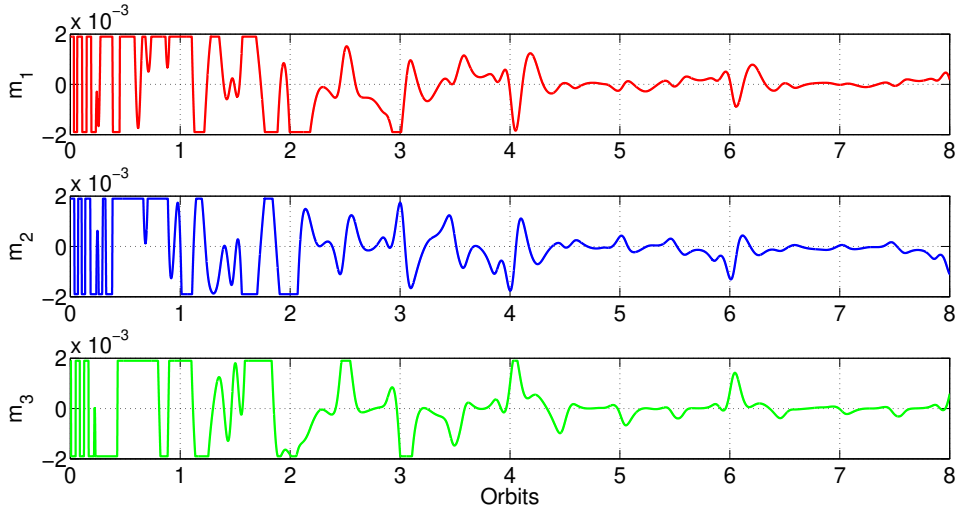


Source: The author.

### 4.2.2 1U CubeSat

A 1U Cubesat is the standard size used as the reference for all the CubeSat-like projects. The value for the inertia matrix $J$ for this satellite model was obtained from (LI; POST; LEE, 2013) and is presented in (85). A similar, although more accurate value, can be obtained from the UWE-3 project described in (BANGERT, 2019), for example.

$$J = \begin{bmatrix} 0.002 & 0 & 0 \\ 0 & 0.002 & 0 \\ 0 & 0 & 0.002 \end{bmatrix} kgm^2. \tag{85}$$

A valid observation is that this inertia matrix is a spherical top, which means that the Coriolis effect on the satellite becomes null since the product $S(\omega_b)J\omega_b = 0$. Therefore,

the angular velocity error will change from (42) and become just

$$\dot{\omega} = J^{-1}\big(\tau - JS(\omega)R(q)\omega_r\big). \tag{86}$$

Note that the angular velocity error given in (42) will vary only due to the applied torque and the term due to the reference. When the system reaches $\omega = 0$, there will not be necessary to apply torque to correct the system's angular velocity. This allows the Fixed controller to make the system asymptotically stable, both for the attitude as well as for the angular velocity since the torque $\tau$ is defined by the control system and (86) becomes

$$\dot{\omega} = J^{-1}\tau. \tag{87}$$

Similar to the 2U CubeSat model, the 1U CubeSat demands that the gains $K_p$ and $K_v$ have to be adjusted. Thus, for this model, two different pairs of gains were tested, following the same idea as before: one pair with smaller values for $K_p$ and $K_v$; and another pair with bigger values for $K_p$ and $K_v$. Once again, in order to make it easier to read and differentiate the results, the first pair will be called *Weak gain*, the second pair will be called *Strong gain* and their values are summarized in Table 10.

Table 10 – Controller parameters - 1U CubeSat.

| | Controller Gain | Value |
|---|---|---|
| Weak | $K_p$ | 0.0005 |
| | $K_v$ | 0.0002 |
| Strong | $K_p$ | 0.005 |
| | $K_v$ | 0.002 |

#### *4.2.2.1 Upside Down Initial Condition*

For the first simulation of the 1U CubeSat, the Upside Down initial condition given by Table 1 was used. The model was simulated for a total of 24 orbits for each pair of gains determined in Table 10. Figures 40 and 41 show the error quaternion and angular velocity error results obtained for this scenario.

Figure 40 – Error Quaternion - Upside Down initial condition - 1U CubeSat: Weak gain (blue solid line) and Strong gain (red dashed line).

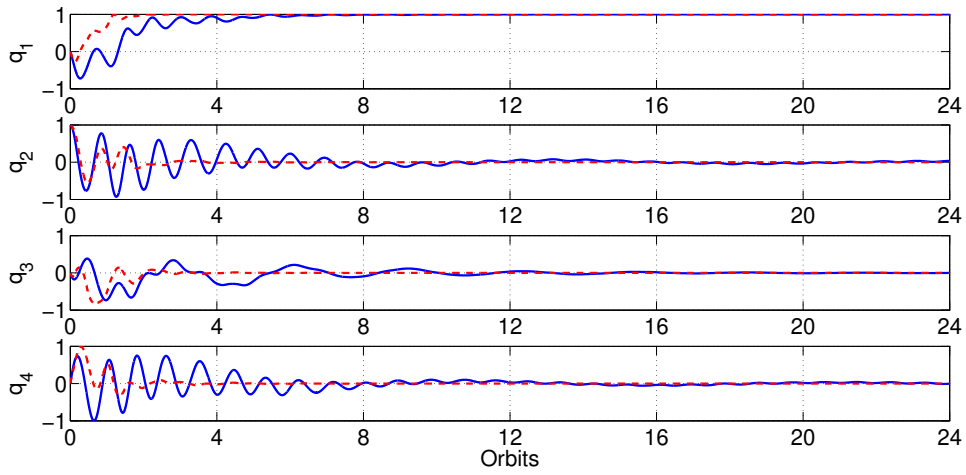


Source: The author.

Figure 41 – Angular velocity error - Upside Down initial condition - 1U CubeSat: Weak gain (blue solid line) and Strong gain (red dashed line).

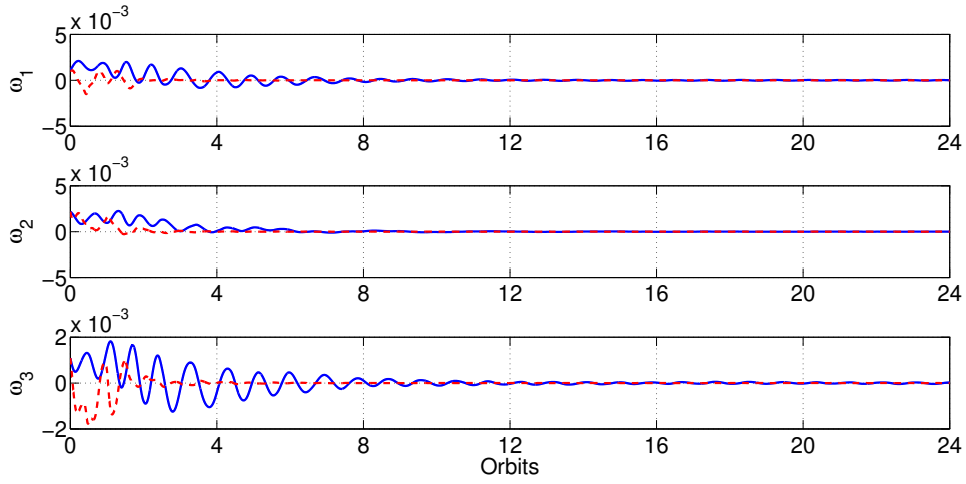


Source: The author.

The error quaternion and angular velocity error graphics indicate that the Strong gain seems to have achieved the objective after eight orbits while the Weak gain takes more orbits to reach it. An oscillatory behavior, both in the attitude and the angular velocity, can be observed in the simulation with the Weak gain. Despite that, the results of the Weak gain setup indicate that it converges to equilibrium.

The normalized energy used for these gain configurations is shown in Table 11 and Figure 42. Both the graphic and the table indicate that the Strong gain used considerably more energy. However, since the Weak gain did not actually achieve the objective in 24 orbits, the actual energy difference wwould require more orbits..

Figure 42 – Energy used - Upside Down initial condition - 1U CubeSat: Weak gain (blue solid line) and Strong gain (red dashed line).

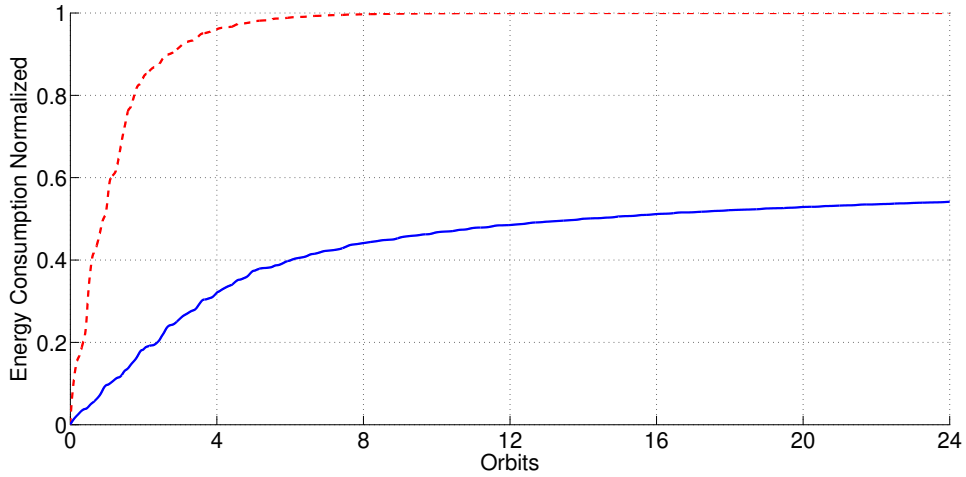


Source: The author.

Table 11 – Energy used on 1U CubeSat - Upside Down initial condition.

| Controller | Energy (normalized) |
|---|---|
| Strong gain | 1 |
| Weak gain | 0.541403 |

The individual use of each magnetorquer for each pair of gains is illustrated in Figures 43 and 49. For these initial conditions, none of the gains created a moment of saturation. This might indicate that the magnetorquer model chosen could be adequate for this model of Cubesat. Also, since the faster result came from the Strong gain, a control gain that reaches the desired attitude within a period of 24 orbits and lower energy consumption should be found closer to that value.

Figure 43 – Magnetoquer use for Weak gain - Upside Down initial condition - 1U CubeSat.

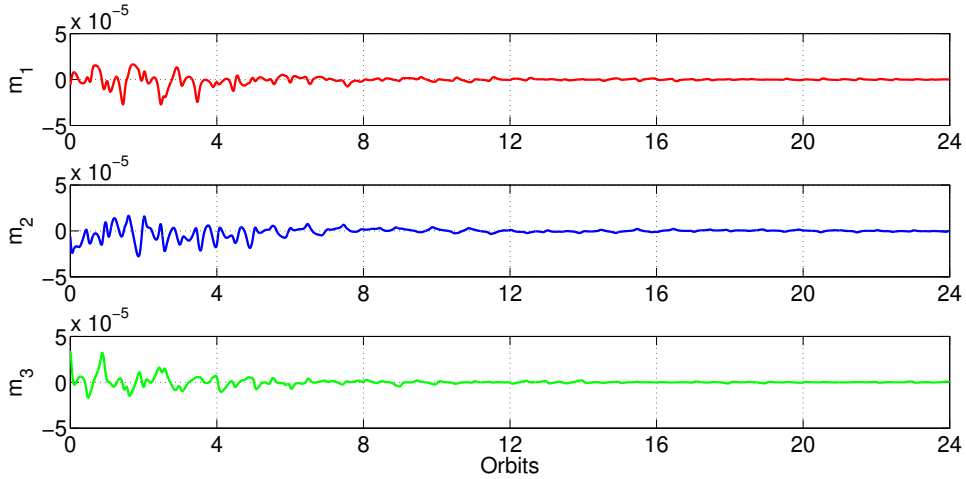


Source: The author.

Figure 44 – Magnetoquer use for Strong gain - Upside Down initial condition - 1U CubeSat.

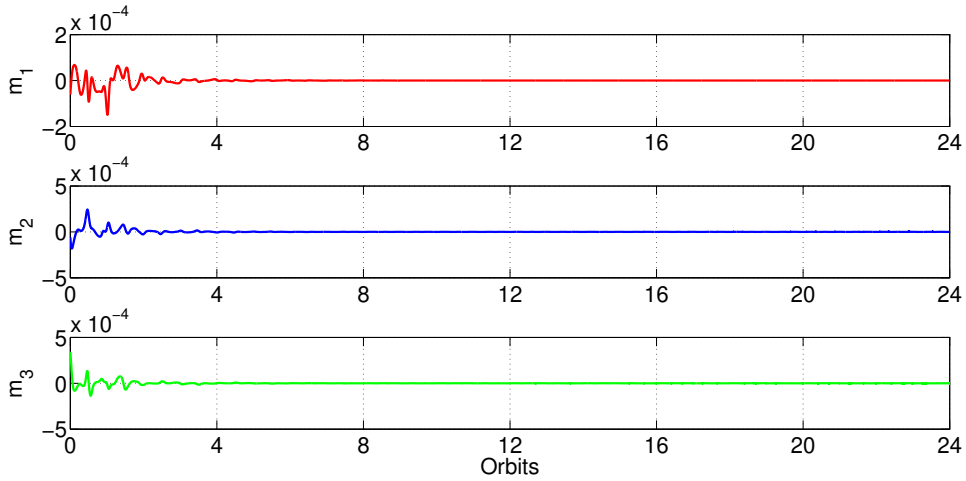


Source: The author.

#### *4.2.2.2 Random Initial Condition*

For the second simulation of the 1U CubeSat model, the Random initial condition given by Table 2 was used. The model was also simulated for a total of eight orbits for each pair of gains state in Table 10. Figures 45 and 46 show the results obtained for this initial condition.

Figure 45 – Error Quaternion - Random initial condition - 1U CubeSat: Weak gain (blue solid line) and Strong gain (red dashed line).

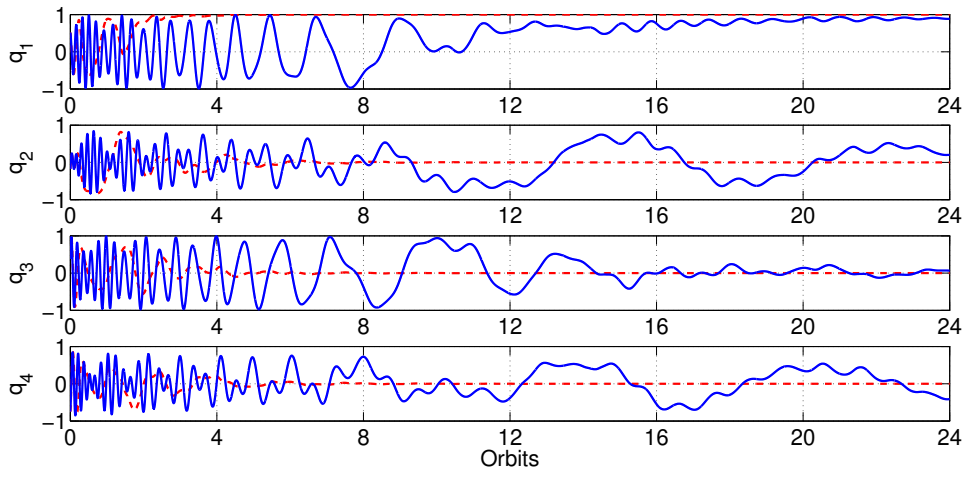


Source: The author.

Once again, the Strong gain seems to achieve the objective in about eight orbits while the Weak gain does not seem to be able to do it in the whole 24 orbits. The higher initial angular velocity in the Random initial condition demands more from the controller. For this reason, the Weak gain configuration is not capable of reducing the satellite angular velocity as fast as the Strong gain. This reflects directly on the attitude variations.

Figure 46 – Angular velocity error - Random initial condition - 1U CubeSat: Weak gain (blue solid line) and Strong gain (red dashed line).

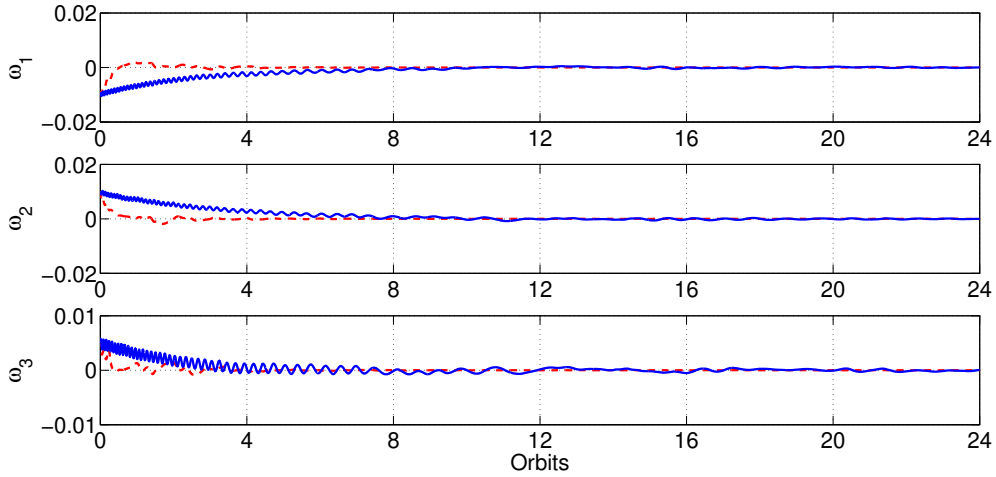


Source: The author.

Considerable attitude oscillations can still be seen in the Weak gain results till the eighth orbits.

Table 12 and Figure 47 present the energy used results. The Strong gain used more energy again but but the difference has considerably decreased. When the objective is taken into account, this greater use of energy might not be a problem. Since the Weak gain did not end its effort, the energy required to get to the objective will increase, reducing the usage difference between them and might even surpassing the Strong gain use.

Figure 47 – Energy used - Random initial condition - 1U CubeSat: Weak gain (blue solid line) and Strong gain (red dashed line).

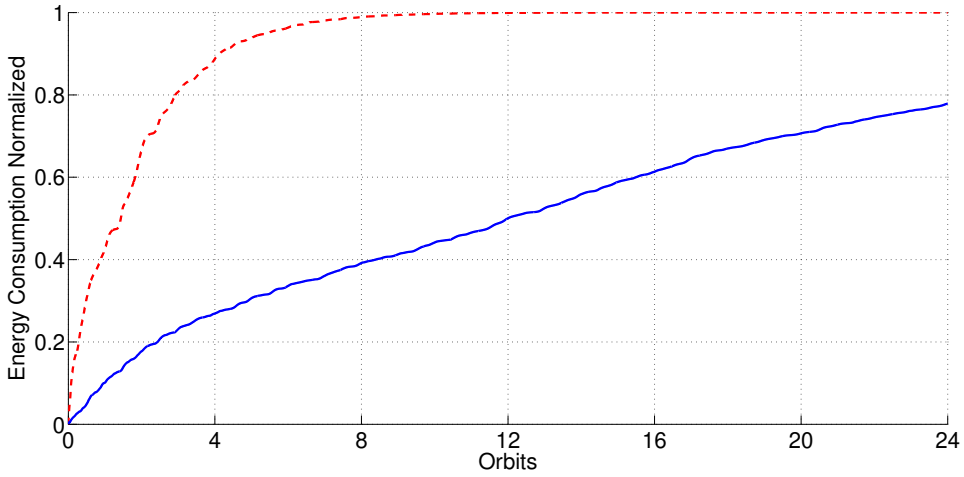


Source: The author.

Table 12 – Energy used on 1U CubeSat - Random initial condition.

| Controller | Energy (normalized) |
|---|---|
| Strong gain | 1 |
| Weak gain | 0.778782 |

The individual use of each magnetorquer for each pair of gains is illustrated in Figures 48 and 49. Despite demanding more effort from the controller, the Random initial condition did not produce saturation for these controller gains. This reinforces that the magnetorquer model chosen would satisfy any controller input demand if it was used. Again, since the objective was achieved by the Strong gain configuration, the optimized control gain should be found closer to this value.

Figure 48 – Magnetoquer use for Weak gain - Random initial condition - 1U CubeSat.

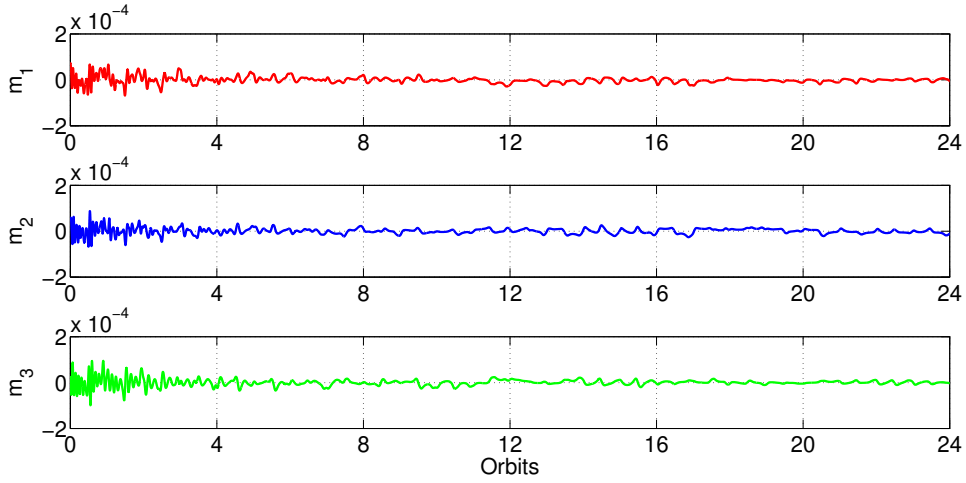


Source: The author.

Figure 49 – Magnetoquer use for Strong gain - Random initial condition - 1U CubeSat.

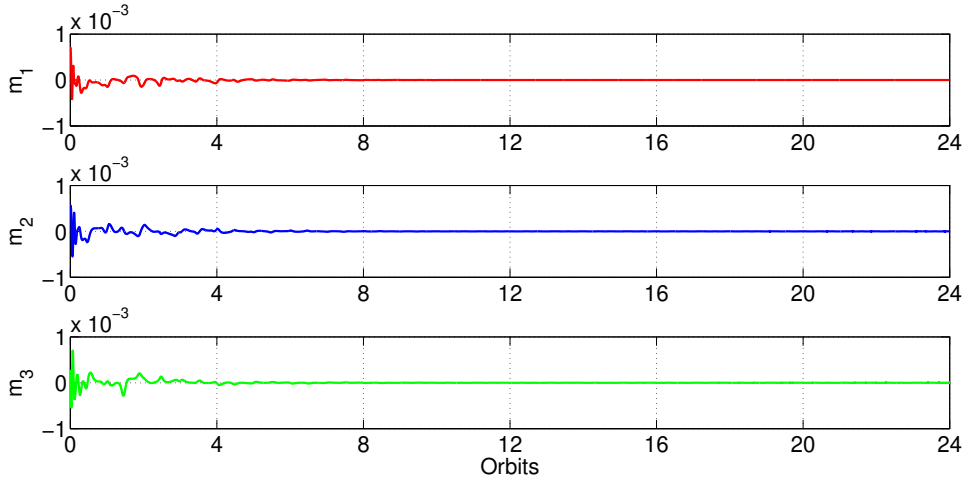


Source: The author.

# 5 CONCLUSIONS

This Master's dissertation presented a new effective approach to an active attitude control strategy using magnetorquers as actuators for nanosatellites. The proposed control law makes use of Earth's magnetic field interaction with the orbiting satellite to determine a fixed gain $\bar{\Gamma}$ to the system, counterpointing an adaptive control gain $\Gamma_{av}(t)$ describe previously in the literature. The control system not only keeps the stability of the system but is also able to bring the satellite to its correct attitude despite the magnetorquer dynamic of producing only torques orthogonal to the magnetic field. The periodicity of the magnetic field allows the use of average theory to deal with the problem that its skew-symmetric matrix cannot be inverted.

Simulation results showed that this fixed gain approach reduces energy use by the attitude control system, reaching $70\%$ economy in some cases. This, in turn, allows the spacecraft to utilize this power for other mission purposes. Moreover, by fixing the gain, this approach also removes the computational effort needed by an adaptive gain.

Among the key takeaways obtained from the simulation results, it can be mentioned that spherical top bodies with small inertia matrices - a common configuration among 1U CubeSats - might require further attention in the control design since the magnetic torque does not have to deal with all the terms of the dynamic since the inertia matrix configuration removes one of the terms. Also, the controller gains $K_p$ and $K_v$ could be chosen through an optimized method in order to improve the performance and energy economy even more.

CubeSat satellite missions started as university *hands-on* projects but have since expanded, with components being commercially manufactured nowadays. Nevertheless, the missions continue to have restricted capacities due to their size and overall project budgets. By reducing energy consumption as well as processing demands, the fixed gain brings important benefits for spacecraft planning and operation. Beyond that, the fixed controller was able to be used with different satellite inertia matrices.

The fixed gain $\bar{\Gamma}$ was determined based on the orbital path, which is determined in the mission objectives, in the planning phase. Since the targeted orbit and reference attitude are necessary aspects of the mission, accurate magnetic field models can be used to accu-

rately estimate the magnetic field that will interact with the satellite at the chosen orbit, and consequently, the fixed gain. This gain is independent of the satellite characteristics such as size, inertia matrix, and shape. Throughout this dissertation, the environmental aspect of the magnetic field was modeled through two different methods present in the literature: a simpler model to verify the controller approach and a more complex one to assess the controller performance. The proposed fixed controller produced a reduction in energy consumption when both models were used to determine and assess the fixed gain.

Further aspects, both internal and external to the satellite, should be added in future analysis for a more complete assessment of a proposed satellite. Among these aspects, it can be mentioned the reduction of actuator saturation, the inclusion of battery use restrictions, a more accurately determined inertia matrix, the inclusion of disturbance torques (aerodynamic drag, solar pressure, gravity gradient, dipole), and a more accurate orbit path for the satellite. Even though saturation did not pose a problem for the simulated scenarios because it was considered only the magnetorquer nominal operation value, it might occur due to other restrictions, such as battery capacity or mission tasks prioritization, and should be taken into account while planning an active system.

Finally, other alternative approaches to the problem of invertibility of the skew symmetric matrix for the magnetic field $S(B(t))$ could be explored. For instance, the strongest component of the magnetic field could be a factor used to define the controller gains. As the magnetic field on the satellite varies, the component determining the gains is switched in a way that the strongest component always contributes the most. Preliminary results for situations similar to the ones presented in Chapter 4 are encouraging but further development is still needed. This idea and its first results are shown in the appendix C.

# REFERENCES

ALKEN, P. *et al.* International Geomagnetic Reference Field: the thirteenth generation. **Earth, Planets and Space**, [S.l.], v. 73, n. 1, 2021.

ALKEN, P.; THéBAULT, E.; BEGGAN, C. International Geomagnetic Reference Field: the thirteenth generation. **Earth Planets Space**, [S.l.], v. 73, n. 49, 2021.

BANGERT, P. **Magnetic Attitude Control of Miniature Satellites and its Extension towards Orbit Control using an Electric Propulsion System**. 2019. PhD Thesis — Universität Würzburg, 2019.

BAUER, R. Attitude Dynamics Model Of A Cubesat With Reaction Wheels For An Extended Kalman Filter. *In*: CSME CONGRESS 2021, 2021. **Proceedings [...]** [S.l.: s.n.], 2021.

BOMANI, B. **CubeSat Technology Past and Present: Current State-of-the-Art Survey**. Cleveland, Ohio: Glenn Research Center, National Aeronautics and Space Administration, 2021. 74 p.

BORGES, R. A. *et al.* The AlfaCrux CubeSat Mission Description and Early Results. **Applied Sciences**, [S.l.], v. 12, n. 19, 2022.

CLINE, D. **Variational Principles In Classical Mechanics**. 755 Library Road, Rochester, NY: River Campus Libraries, 2021.

F. LANDIS MARKLEY, J. L. C. **Fundamentals of Spacecraft Attitude Determination Control**. New York, New York: Springer, 2014. v. 1, p. 486.

HELMY, M.; HAFEZ, A. T.; ASHRY, M. CubeSat Reaction Wheels Attitude Control Via Modified PI-D Controller. *In*: INTERNATIONAL TELECOMMUNICATIONS CONFERENCE (ITC-EGYPT), 2022., 2022. **Proceedings [...]** [S.l.: s.n.], 2022. p. 1–6.

JOHNSTONE, A. CubeSat design specification Rev. 14.1 the CubeSat program. **Cal Poly SLO**, [S.l.], p. 1–34, 2022.

JOVANOVIC, N. *et al.* Design of Magnetorquer-Based Attitude Control Subsystem for FORESAIL-1 Satellite. **IEEE Journal on Miniaturization for Air and Space Systems**, [S.l.], v. PP, p. 1–1, 06 2021.

KAPLAN, C. **LEO Satellites: attitude determination and control components**. 2006. 174 p. Master's Thesis — , 2006.

KASIRI, A.; SABERI, F. Adaptive Feedback-Linearization Attitude Tracking Control of a Spacecraft. *In*: 2022 , 2019. **Proceedings [...]** [S.l.: s.n.], 2019.

KHALIL, H. K. **Nonlinear Systems**. 3nd. ed. Upper Saddle River, New Jersey: Prentcie Hall, 2002.

LI, J.; POST, M.; LEE, R. Real-Time Nonlinear Attitude Control System for Nanosatellite Applications. **Journal of Guidance, Control, and Dynamics**, [S.l.], v. 36, n. 6, p. 1661–1671, 2013.

LING, W. Y. L. *et al.* A brief review of alternative propellants and requirements for pulsed plasma thrusters in micropropulsion applications. **Chinese Journal of Aeronautics**, [S.l.], v. 33, n. 12, p. 2999–3010, 2020.

LOVERA, M. Magnetic satellite detumbling: the b-dot algorithm revisited. *In*: AMERICAN CONTROL CONFERENCE (ACC), 2015., 2015. **Proceedings [...]** [S.l.: s.n.], 2015. p. 1867–1872.

LOVERA, M.; ASTOLFI, A. Global magnetic attitude control of spacecraft in the presence of gravity gradient. **IEEE Transactions on Aerospace and Electronic Systems**, [S.l.], v. 42, n. 3, p. 796–805, 2006.

MARCELINO, G. M. *et al.* A Critical Embedded System Challenge: the floripasat-1 mission. **IEEE Latin America Transactions**, [S.l.], v. 18, n. 02, p. 249–256, 2020.

MT01: compact magnetorquer. [S.l.]: Agencia Espacial Civil Ecuatoriana, 2023. https://www.cubesat.market/_files/ugd/4249fe_3156dce9495c43ba87ce4146552f68b2.pdf.

MURCIA PIñEROS, J.; DOS SANTOS, W.; PRADO, A. Analysis of the orbit lifetime of CubeSats in low Earth orbits including periodic variation in drag due to attitude motion. **Advances in Space Research**, [S.l.], v. 67, 11 2020.

NALLAPU, R. T.; TALLAPRAGADA, A.; THANGAVELAUTHAM, J. Radiometric actuators for spacecraft attitude control. *In*: IEEE AEROSPACE CONFERENCE, 2017., 2017. **Proceedings [...]** [S.l.: s.n.], 2017. p. 1–7.

NASA. **State-of-the-Art**: Small Spacecraft Technology. Ames Research Center, Moffett Field, California: Small Spacecraft Systems Virtual Institute, National Aeronautics and Space Administration, 2023. 407 p.

National Centers for Environmental Information (NCEI). **Geomagnetic Calculators, Maps, Models and Software**. `https://www.ngdc.noaa.gov/geomag/models.shtml`, Last accessed on 2023-03-01.

PANG, W. *et al.* Boom of the CubeSat: a statistic survey of cubesats launch in 2003–2015. *In*: INTERNATIONAL ASTRONAUTICAL CONGRESS (IAC), GUADALAJARA, MEXICO, 67., 2016. **Proceedings [...]** [S.l.: s.n.], 2016. p. 26–30.

RAYBURN, C. *et al.* Development of a micro pulsed plasma thruster for the Dawgstar nanosatellite. *In*: AIAA/ASME/SAE/ASEE JOINT PROPULSION CONFERENCE AND EXHIBIT, 36., 2000. **Proceedings [...]** [S.l.: s.n.], 2000.

RUKHAIYAR, A. *et al.* **Design and Assembly of a Prototype 6U Solar Sail CubeSat for Debris Capture Operations in LEO**. 2021.

SALTON, A. *et al.* Semidefinite Programming Solution to the Spacecraft Analysis and Control Problem. **IFAC-PapersOnLine**, [S.l.], v. 50, p. 3959–3964, 07 2017.

SCHUCH, N. *et al.* The Present  Future of the Brazilian INPE-UFSM NANOSATC-BR, CubeSats Development Program. **Annales Geophysicae Discussions**, [S.l.], p. 1–16, 05 2019.

SINCLAIR, D.; GRANT, C.; ZEE, R. E. Enabling Reaction Wheel Technology for High Performance Nanosatellite Attitude Control. *In*: ANNUAL AIAA/USE CONFERENCE ON SMALL SATELLITES, 21., 2007. **Proceedings [...]** [S.l.: s.n.], 2007.

STRAY, F. **Attitude Control of a Nano Satellite**. 2010. 107 p. Master's Thesis — , 2010.

SUTHERLAND, R.; KOLMANOVSKY, I.; GIRARD, A. R. Attitude Control of a 2U Cubesat by Magnetic and Air Drag Torques. **IEEE Transactions on Control Systems Technology**, [S.l.], v. 27, n. 3, p. 1047–1059, 2019.

TORCZYNSKI, D.; AMINI, R.; MASSIONI, P. Magnetorquer Based Attitude Control for a Nanosatellite Testplatform. *In*: AIAA INFOTECH@AEROSPACE 2010, 2010. **Proceedings [...]** [S.l.: s.n.], 2010.

VAN DE HENGEL, A. **Magnetorquer Design and Attitude Control for SHAPE**. 2018. 88 p. Master's Thesis — , 2018.

VÁZQUEZ, A. L. R. **Purely Magnetic Attitude Control Algorithm for Low Earth Orbit Satellites**. 2013. 113 p. PhD Thesis — , 2013.

WISNIEWSKI, R. **Satellite Attitude Control Using Only Electromagnetic Actuation**. 1997. 147 p. PhD Thesis — , 1997.

YANG, Y. *et al.* Study of a low-power micro coaxial pulsed plasma thruster with axial applied magnetic field. **Vacuum**, [S.l.], v. 210, p. 111719, 2023.

YANG ZHONG YAN-WU GUAN, J.-Q. S. F. X. The calculation method of full tensor geomagnetic gradient based on IGRF model. **Geophysical and Geochemical Exploration**, [S.l.], v. 44, n. 3, p. 582, 2020.

ZHAO, S. **Time Derivative of Rotation Matrices**: a tutorial. [S.l.]: arXiv, 2016.

# APPENDIX A VECTOR MANIPULATION

## Cross product

Take two generic 3-dimensional vectors $a$ and $b$ given by

$$a = \begin{bmatrix} a_1 \\ a_2 \\ a_3 \end{bmatrix}, \quad b = \begin{bmatrix} b_1 \\ b_2 \\ b_3 \end{bmatrix}$$

The cross product between $a$ and $b$ can be described as:

$$a \times b = \begin{bmatrix} a_2b_3 - a_3b_2 \\ a_3b_1 - a_1b_3 \\ a_1b_2 - a_2b_1 \end{bmatrix} = \begin{bmatrix} c_1 \\ c_2 \\ c_3 \end{bmatrix} \tag{88}$$

The resultant vector $c$ will be perpendicular to both $a$ and $b$. If vectors $A$ and $B$ are parallel, i.e., if $a = kb$, $k \in \mathbb{R}$, then

$$a \times b = 0 \tag{89}$$

It is possible to arrive at this result using the skew-symmetric matrix.

$$a \times b = S(a)b = \begin{bmatrix} 0 & -a_3 & a_2 \\ a_3 & 0 & -a_1 \\ -a_2 & a_1 & 0 \end{bmatrix} \begin{bmatrix} b_1 \\ b_2 \\ b_3 \end{bmatrix} = \begin{bmatrix} a_2b_3 - a_3b_2 \\ a_3b_1 - a_1b_3 \\ a_1b_2 - a_2b_1 \end{bmatrix} = \begin{bmatrix} c_1 \\ c_2 \\ c_3 \end{bmatrix}, \tag{90}$$

## Scalar product

Take the same generic 3-dimensional vectors $a$ and $b$ as described before. The scalar product (sometimes called dot product) of $a$ and $b$ can be calculated by

$$a \cdot b = a^T b = a_1b_1 + a_2b_2 + a_3b_3 = d \tag{91}$$

# Vector decomposition

Consider the two generic 3-dimensional vectors $a$ and $b$ as described before. It is possible to break up vector $b$ into two vectors: a parallel to vector $a$ called $b_{||}$; and a perpendicular to vector $a$ called $b_{\perp}$.

The parallel vector can be obtained by:

$$b_{||} = \frac{(b \cdot a)}{||a||^2} a \tag{92}$$

where $\cdot$ is the dot product between vectors.

Once calculated the parallel vector, the perpendicular vector can be calculated using the difference

$$b_{\perp} = b - b_{||} \tag{93}$$

# Skew Symmetric product

Consider a generic angular velocity vector $W$ given by

$$W = \begin{bmatrix} W_1 & W_2 & W_3 \end{bmatrix}^T$$

and a spherical top inertia matrix given by

$$J = \begin{bmatrix} \kappa & 0 & 0 \\ 0 & \kappa & 0 \\ 0 & 0 & \kappa \end{bmatrix} \tag{94}$$

where $\kappa > 0$. For any value of $W$ and $\kappa$, the product $S(W)JW = 0$.

$$\begin{aligned} S(W)JW &= \begin{bmatrix} 0 & -W_3 & W_2 \\ W_3 & 0 & -W_1 \\ -W_2 & W_1 & 0 \end{bmatrix} \begin{bmatrix} \kappa & 0 & 0 \\ 0 & \kappa & 0 \\ 0 & 0 & \kappa \end{bmatrix} \begin{bmatrix} W_1 \\ W_2 \\ W_3 \end{bmatrix} \\ S(W)JW &= \kappa \begin{bmatrix} 0 & -W_3 & W_2 \\ W_3 & 0 & -W_1 \\ -W_2 & W_1 & 0 \end{bmatrix} \begin{bmatrix} W_1 \\ W_2 \\ W_3 \end{bmatrix} = \kappa \begin{bmatrix} -W_3W_2 + W_2W_3 \\ W_3W_1 - W_1W_3 \\ -W_2W_1 + W_1W_2 \end{bmatrix} \\ S(W)JW &= \kappa \begin{bmatrix} 0 \\ 0 \\ 0 \end{bmatrix} = \begin{bmatrix} 0 \\ 0 \\ 0 \end{bmatrix} \end{aligned} \tag{95}$$

This result is also valid if $W$ has only one of its elements different from zero.

# Attitude Matrix properties

For a given quaternion $q = \begin{bmatrix}\eta & \epsilon_1 & \epsilon_2 & \epsilon_3\end{bmatrix}^{\mathsf{T}}$, its attitude matrix is defined by:

$$
\begin{aligned}
R(q) &= (\eta^2 - \epsilon^T\epsilon)I_3 + 2\epsilon\epsilon^T - 2\eta S(\epsilon) \\
R(q) &= \begin{bmatrix}\eta^2 - \epsilon^T\epsilon & 0 & 0 \\ 0 & \eta^2 - \epsilon^T\epsilon & 0 \\ 0 & 0 & \eta^2 - \epsilon^T\epsilon\end{bmatrix} + 2\begin{bmatrix}\epsilon_1^2 & \epsilon_1\epsilon_2 & \epsilon_1\epsilon_3 \\ \epsilon_1\epsilon_2 & \epsilon_2^2 & \epsilon_2\epsilon_3 \\ \epsilon_1\epsilon_3 & \epsilon_2\epsilon_3 & \epsilon_3^2\end{bmatrix} - 2\eta\begin{bmatrix}0 & -\epsilon_3 & \epsilon_2 \\ \epsilon_3 & 0 & -\epsilon_1 \\ -\epsilon_2 & \epsilon_1 & 0\end{bmatrix} \\
R(q) &= \begin{bmatrix}\eta^2 + \epsilon_1^2 - \epsilon_2^2 - \epsilon_3^2 & 2\epsilon_1\epsilon_2 + 2\eta\epsilon_3 & 2\epsilon_1\epsilon_3 - 2\eta\epsilon_2 \\ 2\epsilon_1\epsilon_2 - 2\eta\epsilon_3 & \eta^2 - \epsilon_1^2 + \epsilon_2^2 - \epsilon_3^2 & 2\epsilon_2\epsilon_3 + 2\eta\epsilon_1 \\ 2\epsilon_1\epsilon_3 + 2\eta\epsilon_2 & 2\epsilon_2\epsilon_3 - 2\eta\epsilon_1 & \eta^2 - \epsilon_1^2 - \epsilon_2^2 + \epsilon_3^2\end{bmatrix}.
\end{aligned}
\tag{96}
$$

Thus, when taking into account the property

$$\eta^2 + \epsilon_1^2 + \epsilon_2^2 + \epsilon_3^2 = 1 \tag{97}$$

it follows that

$$R(q)R(q)^T = I. \tag{98}$$

Therefore,

$$R(q)^{-1} = R(q)^T \tag{99}$$

and that

$$det\big(R(q)\big) = 1. \tag{100}$$

It can be seen from (96) that $R(q) = I$ when $q = \begin{bmatrix}1 & 0 & 0 & 0\end{bmatrix}^{\mathsf{T}}$. Thus, when the quaternion $q$ describes no rotations, then its attitude matrix $R(q)$ will be $I$. Also, as presented by (ZHAO, 2016), the time derivative of the attitude matrix $R(q)$ is given by:

$$\dot{R}(q) = S(\omega)R(q), \tag{101}$$

where $\omega$ is the angular velocity within which the quaternion is rotating.

# APPENDIX B MATLAB CODES

The following diagram illustrates how the MATLAB codes were organized in order to create the simulations for this dissertation. The codes for each function are presented after the diagram.

Figure 50 – MATLAB codes Diagram.

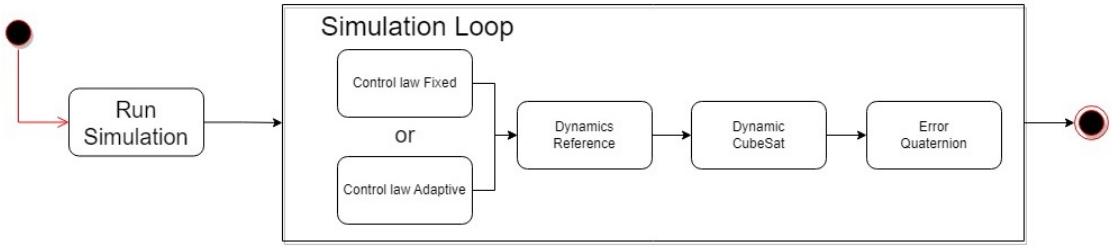


Source: The author.

**Run simulation**

```
%% 04/2023 Initial dynamic environment for orbit control
clc
clear all
close all

%% Constants
J = 0.002*eye(3) % kg m^2 - 1U

%% Earth
r_earth = 6.37; % Thousand of km

%% Reference satellite
orbit_angle = 0; % initial position in the orbit

%% Dynamics
```

```
% Simulation parameters
global T T_orbit
T_orbit = 5760;              % Seconds per orbit
T = 1/5;                     % Seconds sim step
N_orbit = 8;                 % Number of orbits
steps = T_orbit*N_orbit/T;   % Number of simulation steps
tspan = [0 T];               % for ode23 simulation
k = 1;                       % Counter
options = odeset('RelTol',1e-3,'MaxStep',T);


%% Satellite and Reference attitude parameters
% Euler Angles Initial values
o_sat = [0; pi; pi/2];  % Upside down initial condition
o_ref = [0; 0; pi/2];


% Quaternion Initial values
q_sat = ea2q(o_sat); % Euler Angle to quaternion
q_ref = ea2q(o_ref); % Euler Angle to quaternion
q_er = zeros(4,steps);
q_er(:,1) = ErrorQuaternion(q_sat, q_ref);
n = q_er(1,1);
e = q_er(2:4,1);

% Angular velocity Initial values - rad/second
w_ref = 2*pi/T_orbit;
w_sat = zeros(3,steps);
w_sat(:,1) = [1 1 1]'*w_ref;  % Upside down

% Angular velocity error
w_er_recording = zeros(3,steps);
w_er = w_sat(:,1) - ( (n^2 - e'*e)*eye(3) + 2*e*e' - 2*n*SS
   (e) )*[0; w_ref; 0; ];
w_er_recording(:,1) = w_er;

% Satellite state vector
IC = [ q_sat(:,1) ; w_sat(:,1)];
xsat = zeros(7,steps);
```

```
xsat(:,1:2) = [IC IC];

% Reference state vector
IR = q_ref;
REFq = zeros(4,steps);
REFq(:,1:2) = [IR IR];

% Control signal initial value
m = zeros(3,steps);
m1 = zeros(3,steps);

% Gamma Average initial value
Gama_av = zeros(3,3,steps);
Gama_av(:,:,1) = Gama(0, q_sat);
Eigen = zeros(3,steps);
Eigen(:,1) = eig(Gama_av(:,:,1));

% Magnetic Field
B_recording = zeros(3, steps);
B_on_sat_recording = zeros(3, steps);

% Energy
energy = 0;
Energy_used = zeros(1,steps);

% Ploting Error Quaternion
figure(1)
PlotDATA1 = plot(subplot(4,1,1), nan,nan);
set(PlotDATA1,'YData',q_er(1,1:100:end),'XData',(1:100:
   steps)*T/T_orbit)

PlotDATA2 = plot(subplot(4,1,2), nan,nan);
set(PlotDATA2,'YData',q_er(2,1:100:end),'XData',(1:100:
   steps)*T/T_orbit)

PlotDATA3 = plot(subplot(4,1,3), nan,nan);
set(PlotDATA3,'YData',q_er(3,1:100:end),'XData',(1:100:
   steps)*T/T_orbit)
```

```
PlotDATA4 = plot(subplot(4,1,4), nan,nan);
set(PlotDATA4,'YData',q_er(4,1:100:end),'XData',(1:100:
   steps)*T/T_orbit)

%% Simulation loop
N = 1;
N2= 1; % extra counter
for k=1:steps

    % Control Law
%    [m1(:,k), Gama_av(:,:,k+1), Btil_0, Btil] =
   Control_law_Adaptive(k, q_er(:,k), w_er, Gama_av(:,:,k))
   ;
   [m1(:,k), Btil_0, Btil] = Control_law_Fixed(k, q_er(:,k)
      , w_er);

    % Energy used
    energy = energy + sqrt(m1(:,k)'*m1(:,k));
    Energy_used(k) = energy;

    m(:,k) = m1(:,k);
    % Saturation - Normalized % MT01 AECE
    if m1(1,k) > 0.0019
        m(1,k) = 0.0019;
    else
        if m1(1,k) < -0.0019
            m(1,k) = -0.0019;
        else
            m(1,k) = m1(1,k);
        end
    end
    if m1(2,k) > 0.0019
        m(2,k) = 0.0019;
    else
        if m1(2,k) < -0.0019
            m(2,k) = -0.0019;
        else
            m(2,k) = m1(2,k);
        end
```

```
end
if m1(3,k) > 0.0019
    m(3,k) = 0.0019;
else
    if m1(3,k) < -0.0019
        m(3,k) = -0.0019;
    else
        m(3,k) = m1(3,k);
    end
end

% Eigen value for Gama
Eigen(:,k) = eig(Gama_av(:,:,k));

% Update Reference state
[t,x_ref] = ode45(@dyn_rigid_body_ref, tspan, REFq(:,k)
   , options, [0; w_ref; 0; ]);
REFq(:,k+1) = x_ref(end,:)';
q_ref = REFq(1:4,k+1);

% Update Satellite state
[t,xq] = ode45(@dyn_cube_sat, tspan, xsat(:,k), options
   , J, m(:,k), Btil);
xsat(:,k+1) = xq(end,:)';
q_sat = xsat(1:4,k+1);
w_sat(:,k+1) = xsat(5:7, k+1);

% Update Quaternion error
q_er(:,k) = ErrorQuaternion(q_sat, q_ref);
n = q_er(1,k);
e = q_er(2:4,k);

% Update Angular Velocity error
w_er = w_sat(:,k+1) - ( (n^2 - e'*e)*eye(3) + 2*e*e' -
   2*n*SS(e) )*[0; w_ref; 0; ];
w_er_recording(:,k) = w_er;

% Record magnetic field
B_on_sat_recording(:, k) = Btil;
```

```
    B_recording(:, k) = Btil_0;

    % Loop progress checkpoint
    if(k==T_orbit*N/T/100)
        clc;
        disp(N)

      if(k==T_orbit*N2/T/10)
        set(PlotDATA1,'YData',q_er(1,1:100:end),'XData'
           ,(1:100:steps)*T/T_orbit)
        set(PlotDATA2,'YData',q_er(2,1:100:end),'XData'
           ,(1:100:steps)*T/T_orbit)
        set(PlotDATA3,'YData',q_er(3,1:100:end),'XData'
           ,(1:100:steps)*T/T_orbit)
        set(PlotDATA4,'YData',q_er(4,1:100:end),'XData'
           ,(1:100:steps)*T/T_orbit)
        drawnow
        N2 = N2+1;
      end
     N = N + 1;
    end

    % Update Orbit Angular Position
    orbit_angle = orbit_angle + w_ref*T;

end
```

**Euler angles to quaternion**

```
function [ q ] = ea2q( ea )
    % Convert Euler angles to quaternion
    cang = cos( ea/2 );
    sang = sin( ea/2 );

    q = [-sang(1,:).*sang(2,:).*sang(3,:) + cang(1,:).*cang
       (2,:).*cang(3,:);
    sang(1,:).*cang(2,:).*cang(3,:) + sang(2,:).*sang(3,:)
       .*cang(1,:);
    -sang(1,:).*sang(3,:).*cang(2,:) + sang(2,:).*cang(1,:)
```

```
        .*cang(3,:);
    sang(1,:).*sang(2,:).*cang(3,:) + sang(3,:).*cang(1,:)
        .*cang(2,:);];

end
```

**Error quaternion**

```
function q_error = ErrorQuaternion(q_sat, q_ref)

    % Calculates error quaternion
    q0  = q_sat(1);
    q0d = q_ref(1);

    qv  = [q_sat(2) q_sat(3) q_sat(4)]';
    qvd = [q_ref(2) q_ref(3) q_ref(4)]';

    q0_error = q0*q0d + qv'*qvd;
    qv_error = q0d*qv - q0*qvd + SS(qv)*qvd;

    q_error = [q0_error; qv_error];

end
```

**Skew Symmetric**

```
function [ S ] = SS( x )
    % Skew-symmetric matrix
    S = [    0, -x(3),  x(2);
           x(3),     0, -x(1);
          -x(2),  x(1),     0;];
end
```

**Control law Fixed**

```
function [m, Btil_0, Btil] = Control_law_Fixed(k, q_ref,
   q_sat, w_er)
    % Fixed Control Law function for run_sim
```

```
    global T_orbit T;

    % Gains - 1 U CubeSat
    varepsilon = 0.001;
    Kp = 500*0.00001;
    Kv = 200*0.00001;

    % Error Quaternion
    q_er = ErrorQuaternion(q_sat, q_ref);

    mu_f = 7.9*10^15;          % Wb*m
    i_m = 87*pi/180;           % Inclination (rad)
    a = 6820000;               % Semi-major axis (m)
    we = 2*pi/T_orbit;         % Angular velocity

    Btil_0 = mu_f/a^3*[2*sin(we*k*T)*sin(i_m);
                       cos(we*k*T)*sin(i_m);
                       cos(i_m);];

    % Fixed Gain
    inv_K = [ 1.4393, 0.0997, 0.0681;
              0.0997, 1.2874, 0.0794;
              0.0681, 0.0794, 1.9383;];

    % Magnetic Field on satellite
    Btil = q2R(q_sat)*Btil_0;
    B = 1/norm(Btil)*Btil;
    MagField = Btil_0;

    G = - varepsilon^2 * Kp * inv_K * q_er(2:4) -
       varepsilon * Kv * w_er;

    % Magnetic Moment
    m = -vpa(cross(Btil/norm(Btil), G/norm(Btil)));

end
```

**Control law Adaptive**

```
function [m, Gama_av, Btil_0, Btil] = Control_law_Adaptive(
   k, q_ref, q_sat, w_r, Gama_av)
    % Adaptive Control law function for run_sim

    % update Gamma_av
    [temp, Btil_0, Btil] = Gama(k, q_sat);
    if k<2
        Gama_av = temp;
    else
        Gama_av = 1/k*temp + (1-1/k)*Gama_av;
    end

    % Error Quaternion
    q_er = ErrorQuaternion(q_sat, q_ref);

    % Eigenvalue criteria
    if (rank(Gama_av)<3 || min(eig(Gama_av))< 0.1)
        u = -0.2 * w_r ;
    else
        u = -inv(Gama_av)*(0.0005 * q_er(2:4) + 0.2 * w_r);
    end

    % Magnetic moment
    m = 1/norm(Btil)^2*SS(Btil)'*u;

end
```

**Gama**

```
function [Gama, Btil_0, Btil] = Gama(k, q_sat)
    % Calculates Gamma for Simple Model

    global T T_orbit

    mu_f = 7.9*10^15;        % Wb*m
    i_m = 87*pi/180;         % Inclination (rad)
    a = 6820000;             % Semi-major axis (m)
    we = 2*pi/T_orbit;       % Angular velocity
```

```
    Btil_0 = mu_f/a^3*[2*sin(we*k*T)*sin(i_m);
                       cos(we*k*T)*sin(i_m);
                       cos(i_m);];


    Btil = q2R(q_sat)*Btil_0;
    B = 1/norm(Btil)*Btil;

    Gama = SS(B)*SS(B)';
end
```

**Attitude matrix - quaternion**

```
function [ R ] = q2R( q )
    % Create attitude matrix for quaternion q

    q1 = q(1);
    q2 = q(2);
    q3 = q(3);
    q4 = q(4);
    R = [ q1^2+q2^2-q3^2-q4^2,  2*(q2*q3-q1*q4),      2*(q2
       *q4+q1*q3);
          2*(q2*q3+q1*q4),      q1^2-q2^2+q3^2-q4^2,  2*(q3
             *q4-q1*q2);
          2*(q2*q4-q1*q3),      2*(q3*q4+q1*q2),      q1^2-
             q2^2-q3^2+q4^2;];

end
```

**Dynamics Reference**

```
function dx = dyn_rigid_body_ref(t, x, w_ref)
    %DYNAMIC EQUATIONS of the reference, x \in R^7

    n = x(1);
    e = x(2:4);

    dx = zeros(4,1);
    dn = -0.5*(e'*w_ref);
```

```
    de = 0.5*(n*eye(3) + SS(e))*w_ref;

    dx(1) = dn;
    dx(2) = de(1);
    dx(3) = de(2);
    dx(4) = de(3);

end
```

**Dynamics CubeSat**

```
function dx = dyn_cube_sat(t, x, J, m, Btil)
    %DYNAMIC EQUATIONS OF A rigid body, x \in R^7

    n = x(1);
    e = x(2:4);
    w = x(5:7);
    q_sat = [x(1); x(2); x(3); x(4)];

    dn = -0.5*(e'*w);
    de = 0.5*(n*eye(3) + SS(e))*w;
    dw = J\(SS(w)*J*w + SS(Btil)*m);

    dx = zeros(7,1);
    dx(1) = dn;
    dx(2) = de(1);
    dx(3) = de(2);
    dx(4) = de(3);
    dx(5) = dw(1);
    dx(6) = dw(2);
    dx(7) = dw(3);

end
```

# APPENDIX C FUTURE PERSPECTIVES

Considering that the main aspects of an active attitude control system that uses magnetorquers are the variation of the magnetic field seen on the satellite $B(t)$ and the torque created through the cross product between $B(t)$ and the magnetic moment $m(t)$ generated by the magnetorquers, a possible control approach is to determine the strongest magnetic field component acting over the satellite and switches the control signal applied over the magnetorquers based on that factor. The rationale behind this idea is to avoid unnecessary control efforts while keeping the system controllable.

The cross-product used to calculate the magnetic torque makes it possible to control two axes in the satellite's frame at a time while nullifying one direction. Due to this restriction, a control strategy could be set to identify and focus the control efforts on the axes that can be controlled. By measuring the axis with the most prominent value from the magnetic field $B(t)$, three possible auxiliary vectors $\hat{B}_i$ can be written, each created with one of the three components of $B(t)$:

$$\begin{aligned} \hat{B}_1 &= \begin{bmatrix} -1/B_X(t) & 0 & 0 \end{bmatrix} \\ \hat{B}_2 &= \begin{bmatrix} 0 & -1/B_Y(t) & 0 \end{bmatrix} \\ \hat{B}_3 &= \begin{bmatrix} 0 & 0 & -1/B_Z(t) \end{bmatrix} \end{aligned} \tag{102}$$

These three vectors can be converted into matrices by applying the skew-symmetric

matrix to them. The results are the matrices $S(\hat{B}_i)$:

$$
\begin{aligned}
S(\hat{B}_1) &= \begin{bmatrix} 0 & 0 & 0 \\ 0 & 0 & 1/B_X \\ 0 & -1/B_X & 0 \end{bmatrix}, \\
S(\hat{B}_2) &= \begin{bmatrix} 0 & 0 & -1/B_Y \\ 0 & 0 & 0 \\ 1/B_Y & 0 & 0 \end{bmatrix}, \\
S(\hat{B}_3) &= \begin{bmatrix} 0 & 1/B_Z & 0 \\ -1/B_Z & 0 & 0 \\ 0 & 0 & 0 \end{bmatrix}.
\end{aligned} \tag{103}
$$

The purpose of these auxiliary matrices is to generate a magnetic moment $m_s(t)$ in the form

$$
m_s(t) = -S(\hat{B}_i(t))\bar{\Gamma}\big(K_p\epsilon(t) + K_v\omega(t)\big) \tag{104}
$$

such that, for a full orbit, the control input obtains

$$
\lim_{t\to\infty} S(\tilde{B}(t))S(\hat{B}_i(t)) = I \tag{105}
$$

The product $S(B(t))S(\hat{B}_i(t))$ results in three possible matrices:

$$
\begin{aligned}
S(B(t))S(\hat{B}_1(t)) &= \begin{bmatrix} 0 & -\frac{B_Y(t)}{B_X(t)} & -\frac{B_Z(t)}{B_X(t)} \\ 0 & 1 & 0 \\ 0 & 0 & 1 \end{bmatrix}, \\
S(B(t))S(\hat{B}_2(t)) &= \begin{bmatrix} 1 & 0 & 0 \\ -\frac{B_X(t)}{B_Y(t)} & 0 & -\frac{B_Z(t)}{B_Y(t)} \\ 0 & 0 & 1 \end{bmatrix}, \\
S(B(t))S(\hat{B}_3(t)) &= \begin{bmatrix} 1 & 0 & 0 \\ 0 & 1 & 0 \\ -\frac{B_X(t)}{B_Z(t)} & -\frac{B_Y(t)}{B_Z(t)} & 0 \end{bmatrix}.
\end{aligned} \tag{106}
$$

The resulting matrices are not an identity matrix as desired but by analyzing the variation of the chosen $B_i(t)$ parameter through a satellite following the reference in the same polar orbit described in this dissertation, using the Simple model for the magnetic field, it is possible to see that there is a periodic alternation between chosen parameters $\hat{B}_i$. Figure 51 illustrates this variation for five orbits.

Considering the same inertia matrix $J = diag(\begin{bmatrix} 50 & 5 & 60 \end{bmatrix})$ used before (even though the elements of the diagonal do not respect the triangular inequality), and the same random

Figure 51 – Chosen parameter $\hat{B}_i$.

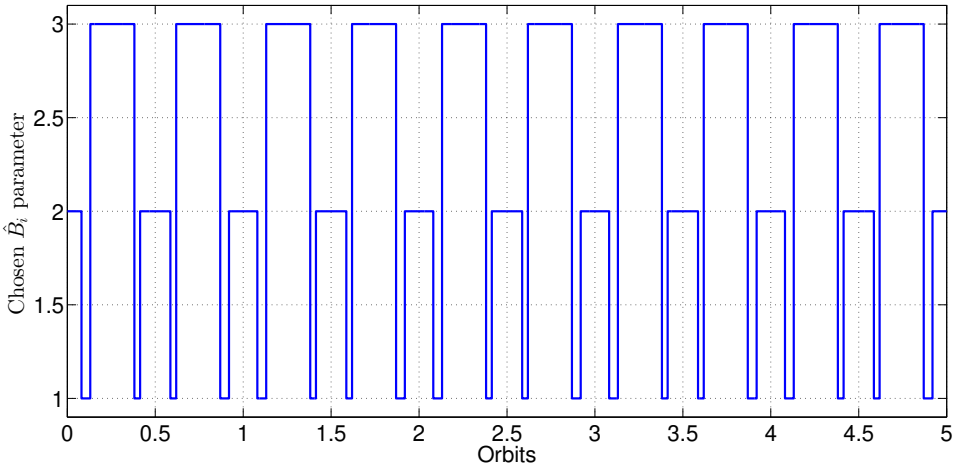


Source: The author.

initial condition, the results obtained by this switching strategy are quite promising. This control approach needed a similar time to achieve the attitude objective but required less energy than both the adaptive and the fixed controllers, as illustrated in Figures 52 and 53.

Figure 52 – Comparison of Error Quaternion for different controllers - Random Initial condition.

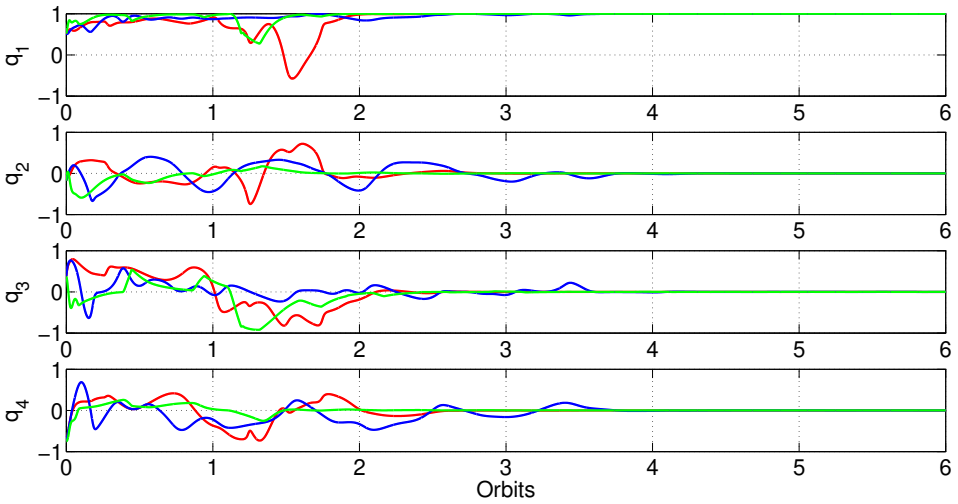


Source: The author.

The downside of this approach is that it wastes some energy by producing a magnetic moment $m_s(t)$ that is not completely perpendicular to the magnetic field $B(t)$. The amount of energy wasted is considerable, as shown in Figure 53. Despite this considerable waste of the effort, the switched approach obtained the lowest energy use among the three controllers compared. Table 13 summarizes these results.

Figure 53 – Comparison of Energy used by controllers - Random initial condition.

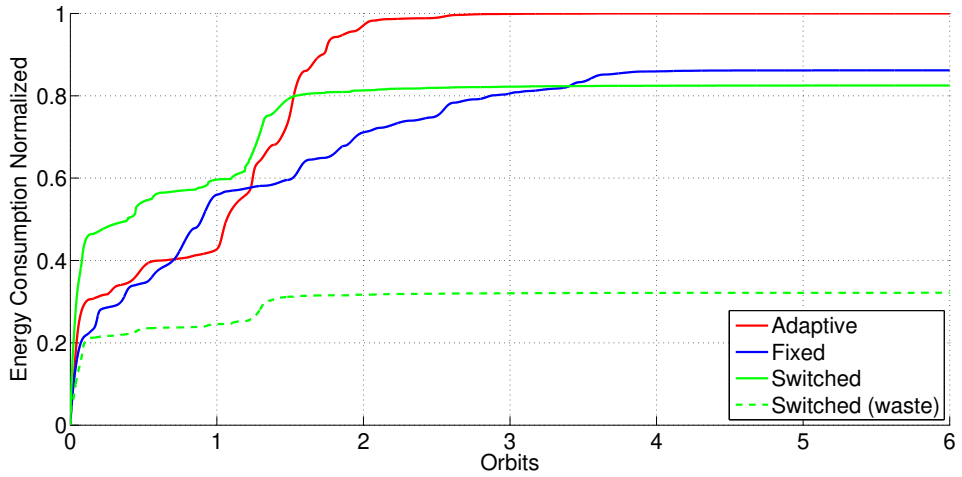


Source: The author.

Table 13 – Energy used by controllers - Random initial condition.

| Controller | Energy (normalized) |
|---|---|
| Adaptive | 1 |
| Fixed | 0.8618 |
| Switched | 0.8250 |
| Switched (waste) | 0.3215 |

Despite the promising result, further development should be made into this switching strategy to extend this result to other initial conditions and to improve its energy efficiency.